ABSTRACT

Title of Document:	VARIABILITY OF TERRESTRIAL CARBON CYCLE AND ITS INTERACTION WITH CLIMATE UNDER GLOBAL WARMING
	Haifeng Qian, Doctor of Philosophy, 2008
Directed By:	Professor Ning Zeng Department of Atmospheric and Oceanic Science

Land-atmosphere carbon exchange makes a significant contribution to the variability of atmospheric CO_2 concentration on time scales of seasons to centuries. In this thesis, a terrestrial vegetation and carbon model, VEgetation-Global-Atmosphere-Soil (VEGAS), is used to study the interactions between the terrestrial carbon cycle and climate over a wide-range of temporal and spatial scales.

The VEGAS model was first evaluated by comparison with FLUXNET observations. One primary focus of the thesis was to investigate the interannual variability of terrestrial carbon cycle related to climate variations, in particular to El Niño-Southern Oscillation (ENSO). Our analysis indicates that VEGAS can properly capture the response of terrestrial carbon cycle to ENSO: suppression of vegetative activity coupled with enhancement of soil decomposition, due to predominant warmer and drier climate patterns over tropical land associated with El Niño. The combined affect of these forcings causes substantial carbon flux into the atmosphere. A unique

aspect of this work is to quantify the direct and indirect effects of soil wetness vegetation activities and consequently on land-atmosphere carbon fluxes. Besides this canonic dominance of the tropical response to ENSO, our modeling study simulated a large carbon flux from the northern mid-latitudes, triggered by the 1998-2002 drought and warming in the region. Our modeling indicates that this drought could be responsible for the abnormally high increase in atmospheric CO_2 growth rate (2 ppm/yr) during 2002-2003.

We then investigated the carbon cycle-climate feedback in the 21st century. A modest feedback was identified, and the result was incorporated into the Coupled Carbon Cycle Climate Model Inter-comparison Project (C4MIP). Using the fully coupled carbon cycle-climate simulations from C4MIP, we examined the carbon uptake in the Northern High Latitudes poleward of 60˚N (NHL) in the 21st century. C4MIP model results project that the NHL will be a carbon sink by 2100, as CO_2 fertilization and warming stimulate vegetation growth, canceling the effect of enhancement of soil decomposition by warming. However, such competing mechanisms may lead to a switch of NHL from a net carbon sink to source after 2100. All these effects are enhanced as a result of positive carbon cycle-climate feedbacks.

VARIBILITY OF TERRESTRIAL CARBON CYCLE AND ITS INTERACTION WITH CLIMATE UNDER GLOBAL WARMING

By

Haifeng Qian

Dissertation submitted to the Faculty of the Graduate School of the
University of Maryland, College Park, in partial fulfillment
of the requirements for the degree of
Doctor of Philosophy
2008

Advisory Committee:
Professor Ning Zeng, Chair
Professor Eugenia Kalnay
Dr. G. James Collatz
Professor Raghu Murtugudde
Professor Christopher Justice

Preface

This dissertation has a seven-chapter layout. Chapter 1: Introduction; Chapter 2: Evaluation of VEGAS against Observations; Chapter 3: Response of the Terrestrial Carbon Cycle to the El Niño-Southern Oscillation; Chapter 4: Impact of 1998–2002 Midlatitude Drought and Warming on Terrestrial Ecosystem and the Global Carbon Cycle; Chapter 5: How Strong is Carbon Cycle-Climate Feedback under Global Warming? Chapter 6: Enhanced Terrestrial Carbon uptake in the Northern High Latitudes under Climate Change in the 21st Century from C4MIP Models Projections; Chapter 7: Conclusion and Future Directions. Finally, Appendices containing the description of VEGAS and a glossary of the thesis follow. In the interest of future usability and readability of this dissertation, each of the main chapters may include its own introductory remarks, literature survey, data and methodology descriptions, and a short summary.

Some chapters of this dissertation have been individually submitted, or published in scientific journals:

- Qian, H., R. Joseph, and N. Zeng, 2008: Enhanced terrestrial carbon uptake in the Northern High Latitudes in the 21st century from the C4MIP model projections. *Submitted to Global Change Biol.*
- Qian, H., R. Joseph, and N. Zeng, 2008: Response of the terrestrial carbon cycle to the El Niño-Southern Oscillation, *Tellus B,* doi: 10.1111/j.1600-0889.2008.00360.x.
- Zeng, N., H. Qian, C. Rödenbeck, and M. Heimann, 2005: Impact of 1998-2002 Midlatitude drought and warming on terrestrial ecosystem and the global carbon cycle. *Geophys. Res. Lett.* **32**, L2270910.1029/2005GL024607.

✧ Zeng, N., H. Qian, E. Munoz, and R. Iacono, 2004: How strong is carbon cycle-climate feedback under global warming? *Geophys. Res. Lett.* **31**, L20203, doi:10.1029/2004GL020904.

Acknowledgements

First of all, I would like to express my gratitude to my advisor Professor Ning Zeng for his valuable support, guidance, and patience over years. His optimism, patience and scientific supervision have fostered my enthusiasm for the research presented here. I would like to thank my committee members: Professor Eugenia Kalnay, Raghu Murtugudde, Christopher Justice, and Dr. G. James Collatz. I owe a great deal of gratitude to Dr. Jin-ho Yoon, Dr. Renu Joseph, and Brian Cook, with whom I have had very productive scientific discussions and collaborations.

I want to extend thanks to all members of the Department of Atmospheric and Oceanic Science. Special thank goes to the staff in our department and the International Education Service of University of Maryland for providing help and solving my VISA related problems when I was delayed in China for half a year. I am also thankful to my friends at University of Maryland for the learning and personal experiences we have shared during all this time, especially to my classmates: Dr. Junjie Liu, Dr. Hong Li, Emily Becker etc. for our enjoyable lunchtime discussions, and Bin Guan, Can Li, Feng Niu etc. for their helpful discussions on coursework initially and research afterwards.

Finally, I dedicate this dissertation to my beloved parents and my wife Fang Zhang for everything they did for me throughout the years. It is their love, support and encouragement that provided me with the opportunity to pursue higher education and shape my life here.

Table of Contents

This Table of Contents is automatically generated by MS Word, linked to the Heading formats used within the Chapter text.

List of Tables

List of Figures

Chapter 1: Introduction

1.1 Importance of terrestrial carbon cycle in climate systems

Carbon cycle is one of the most important biogeochemical cycles in the climate system because carbon dioxide (CO_2) is a principal greenhouse gas that contributes significantly to global warming. Since the beginning of the industrial era, around 1750, the CO_2 concentration in the atmosphere has risen, at an increasing rate, from around 280 ppm to nearly 387 ppm in 2007 at Mauna Loa Observatory (MLO) (Figure 1.1). Ice core record reveals that current CO_2 level is already 27% higher than its highest recorded level during the past 650,000 years before the Industrial Revolution (Siegenthaler et al., 2005; Spahni et al., 2005). Over the 20th century the global average surface temperature resultantly has risen by 0.65±0.2˚C (IPCC, 2007).

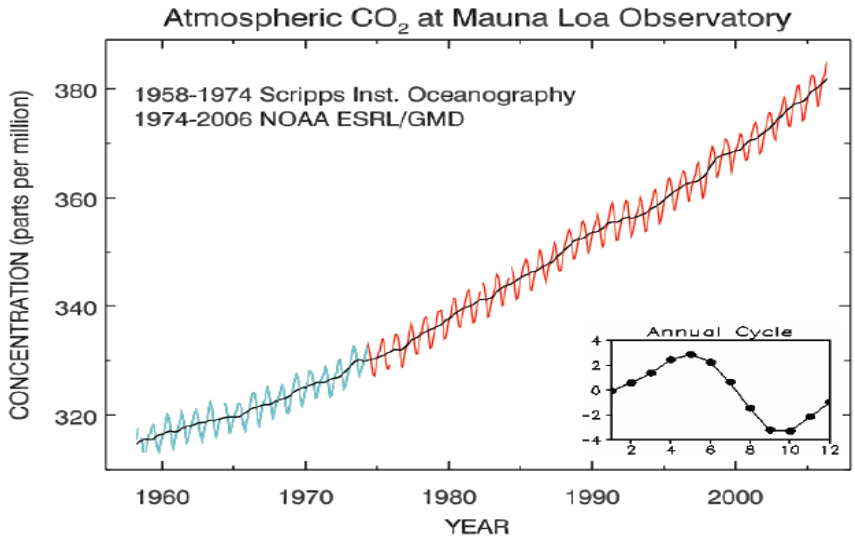

Figure 1.1 Atmospheric carbon dioxide monthly mean mixing ratios in Mauna Loa Observatory. Data prior to 1974 is from the Scripps Institution of Oceanography (SIO, blue), data since 1974 is from the National Oceanic and Atmospheric Administration (NOAA, red) (source from www.cmdl.noaa.gov). The annual cycle of CO_2 concentration is shown at bottom right for reference, which is based on the period of 1960-2005 after long-term increasing trend is removed.

The amount of carbon dioxide in the atmosphere is highly dependent on the carbon exchange between the atmosphere and ecosystem, anthropogenic fossil fuel emission and land use change (Figure 1.2). Although recent estimates of fossil fuel burning and atmospheric CO_2 concentration are quite precise, there is a discrepancy in estimates of land/ocean uptake and land use change (Thompson et al., 1996; Rayner et al., 1999; Bousquet et al., 2000; McGuire et al., 2001; Gurney et al., 2002; Le Quere et al., 2002; DeFries et al., 2002; Houghton, 2003a, b; Rödenbeck et al., 2003; Baker et al., 2006). For instance, one recent estimate (House et al., 2003) indicated that in the 1990s the ocean and land carbon fluxes were −2.1 ± 0.7 PgC/yr and −1.0 ± 0.8 PgC/yr respectively, compared with −1.7 ± 0.5 PgC/yr for ocean and −1.4 ± 0.7 PgC/yr for land according to Prentice et al. (2001) (Table 1.1).

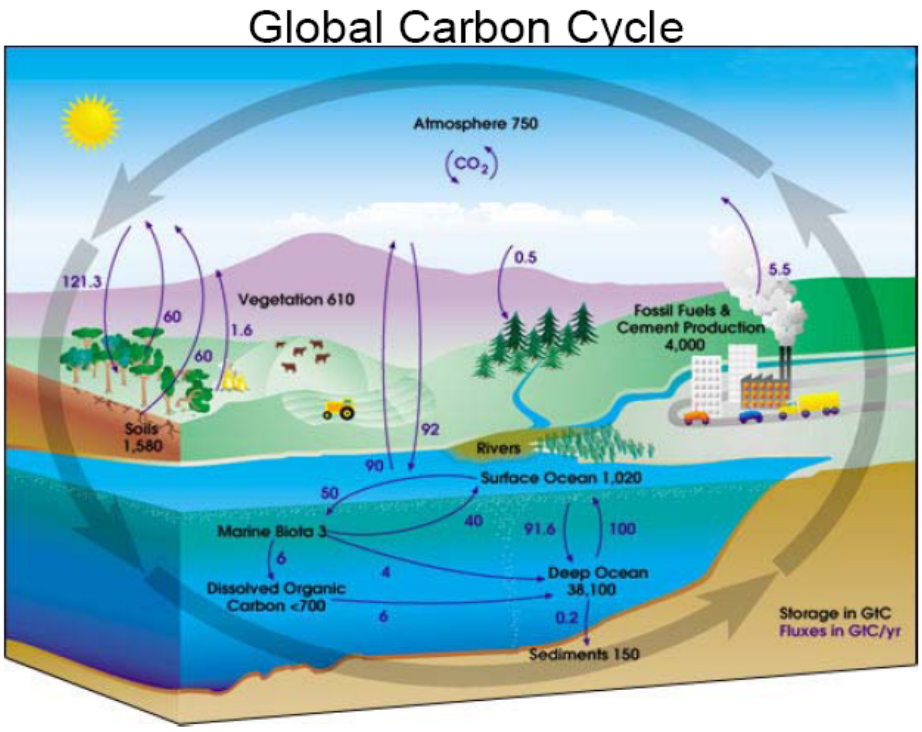

Figure 1.2 Global carbon cycle diagram. The illustration above shows total amounts of stored carbon in black and annual carbon fluxes in purple. Unit for carbon storage is PgC and PgC/yr for fluxes. Source from http://earthobservatory.nasa.gov.

Table 1.1 The global carbon budget (adapted from House et al., 2003). Positive values represent atmospheric CO_2 increase (or ocean/land sources); negative numbers represent atmospheric CO_2 decrease (ocean/land sinks). Unit in PgC/yr.

	IPCC[1]		Update	
	1980s	1990s	1980s	1990s
Atmospheric increase	3.3 ± 0.1	3.2 ± 0.1		
Emissions (fossil fuel, cement)	5.4 ± 0.3	6.3 ± 0.4		
Ocean–atmosphere flux	−1.9 ± 0.6	−1.7 ± 0.5	−1.8 ± 0.8	−2.1 ± 0.7
Land–atmosphere flux[2]	−0.2 ± 0.7	−1.4 ± 0.7	−0.3 ± 0.9	−1.0 ± 0.8
–Land-use change[3]	*1.7 (0.6 to 2.5)*	*Incomplete*	*0.9 to 2.8*	*1.4 to 3.0*
–Residual terrestrial sink	*−1.9 (−3.8 to 0.3)*	*Incomplete*	*−4.0 to –0.3*	*−4.8 to −1.6*

[1] Prentice et al., 2001, IPCC Third Assessment Report.

[2] The net land atmosphere flux consists of emissions due to land-use change as estimated by models, and sinks due to other processes, calculated as a residual.

[3] The IPCC estimated range for the land use change flux is based on the full range of Houghton's book-keeping model approach (Houghton, 1999; Houghton et al., 1999; Houghton et al., 2000) and the Carbon Cycle Model Linkage Project (CCMLP) (McGuire et al., 2001). In the update, the 1980s estimate is the full range of Houghton updated (Houghton, 2003a) and CCMLP; while the 1990s flux is based on Houghton (2003a) only as the CCMLP analysis stopped at 1995.

Furthermore, year-to-year variations of the atmospheric CO_2 growth rate (gCO_2: time derivative of the CO_2 concentration of Mauna Loa Observatory in this thesis) are still imperfectly understood. Such interannual variability of CO_2 growth rate can be up to 4-5 PgC/yr during El Niño years (Figure 1.3). Because fossil fuel emissions and land use change increase slowly with small year-to-year variation, the interannual variability of CO_2 growth rate in the atmosphere lies in the changing absorption capacity of the land and ocean and is related to climate variation. Bousquet et al. (2000) applied an inversion model to 20 years of atmospheric CO_2 measurements and reported that global terrestrial carbon flux was approximately twice as variable as ocean fluxes between 1980 and 1998, and that the tropical land contributes most of the interannual changes in global carbon balance.

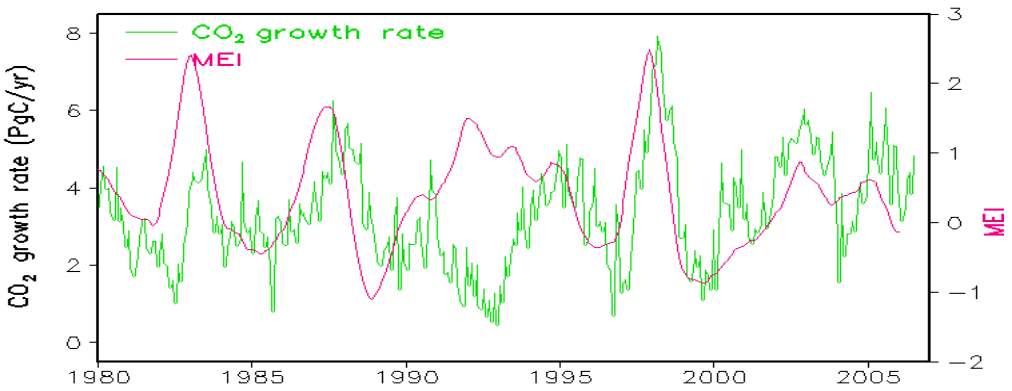

Figure 1.3 Time-series indicating the correspondence of the CO_2 growth rate (gCO_2) at Mauna Loa Observatory, Hawaii with the ENSO signal (Multivariate ENSO Index: MEI; units dimensionless). The seasonal cycle has been removed with a filter of 12-month running mean for both. The exception during 1992-1993 is caused by the eruption of Mount Pinatubo, which is discussed in the text.

These studies of global carbon cycle on interannual and decadal timescale have advanced our understanding of terrestrial ecosystem in response to climate change (Keeling et al., 1985; Thompson et al., 1996; Bousquet et al., 2000; Gurney et al., 2002; Defries et al., 2002; Houghton, 2003b; Rödenbeck et al., 2003). Some important unanswered questions are: How will the terrestrial biosphere respond to global warming (Figure 1.4), and how will this affect the climate in the future? Fully coupled three-dimensional carbon cycle-climate models recently have been used to study the interaction between the global carbon cycle and the climate (Cox et al., 2000; Friedlingstein et al., 2001; Joos et al., 2001; Zeng et al., 2004; Matthews et al., 2005; Friedlingstein et al., 2006;). Based on simulations from 11 modeling groups in the Coupled Carbon Cycle Climate Model Inter-comparison Project (C4MIP), Friedlingstein et al. (2006) concluded that there was a positive carbon cycle-climate feedback in all C4MIP models, albeit of different magnitudes. Due to this positive feedback, there will be an additional 20-200 ppm CO_2 in the atmosphere, leading to

temperature 0.1-1.5˚C warmer by 2100. Most C4MIP models simulate a robust reduction of global terrestrial carbon uptake by 2100, dominated by the tropics. This may cause the tropical forest vulnerable to decay under future global warming, such as a dieback of Amazon rainforest (e.g., Cox et al., 2000; Betts et al., 2004; Cox et al., 2004). All of these studies disclose the crucial role of terrestrial ecosystems in the climate system. Understanding the uptake of atmospheric CO_2 by the land surface is of significance in projecting future climate.

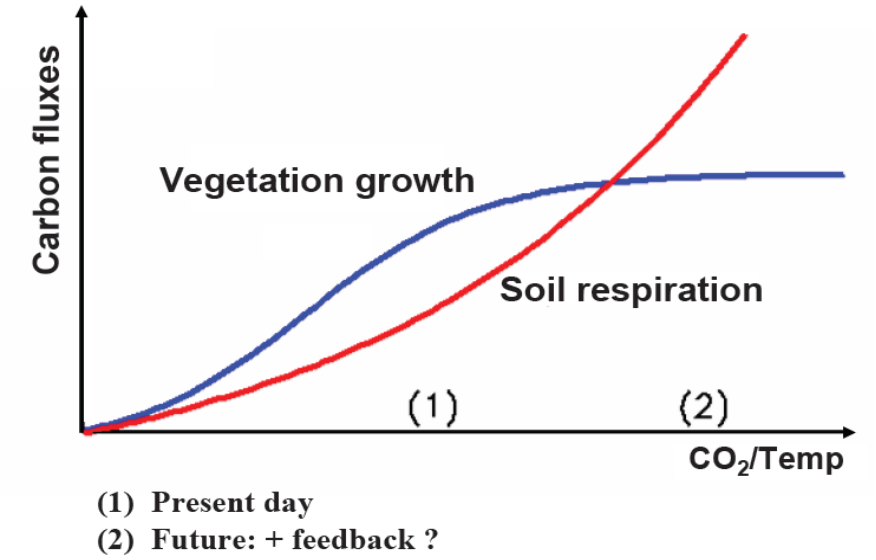

Figure 1.4 A conceptual diagram shows the competition between the vegetation growth and soil respiration, which determines whether and when the land will become a carbon sink or source in the future. Increasing CO_2 and temperature labeled in X-axis is only for reference purpose.

1.2 The interaction between the terrestrial carbon cycle and climate

The terrestrial biosphere gains carbon from the atmosphere through photosynthesis and loses it primarily through respiration (autotrophic and heterotrophic). This land-atmosphere carbon exchange is, in principle, governed by the prevailing physical (incoming solar radiation), climatic (temperature and

precipitation), and edaphic (e.g., nutrients and soil texture) conditions leading to the notion of a biome equilibrium distribution (Budyko, 1974). On the other hand, changes in the vegetation type, structure and physiology of terrestrial ecosystems can feedback to climate via changes in the partitioning of energy between latent and sensible heat, albedo, and roughness, etc.

In this thesis, I will present a study of the interactions between the terrestrial carbon ecosystem and climate over a wide-range of temporal and spatial scales, based on a terrestrial vegetation carbon model, VEgetation-Global-Atmosphere-Soil (VEGAS) (Zeng, 2003; Zeng et al. 2005a). Several sensitivity simulations have been designed to diagnose and understand the variability of the carbon cycle at different temporal scales. A focus is the response of the terrestrial carbon ecosystem to climate change, particularly to El Niño-Southern Oscillation (ENSO) and Midlatitude droughts. This helps to understand how terrestrial carbon cycle influences the atmospheric CO_2 growth rate. The carbon cycle-climate feedback and carbon uptake by the Northern High Latitudes terrestrial biosphere in the 21st century also have been studied.

1.2.1 Modeling the seasonal cycles of terrestrial carbon ecosystem

Modeling a "correct" seasonal cycle is critical for terrestrial vegetation and carbon cycle model to quantify the phenology and biochemical processes. Heimann et al. (1998) evaluated 6 terrestrial carbon cycle models on their capability to capture the seasonal cycle of atmospheric CO_2. Their results showed that, in the tropics, the prognostic models generally tended to over-predict the net seasonal exchanges of carbon fluxes and had stronger seasonal cycles than indicated from observations.

Wittenberg et al. (1998) suggested that this was possibly due to the influence of biomass burning on the seasonal CO_2 signal as observed at monitoring stations. Cramer et al. (1999) pointed out large differences in the simulated seasonal changes among models, both globally and locally. Presumably the differences are due to distinct representation in the models. Randerson et al. (1999) found that an increase in early season ecosystem uptake could explain recent changes in the seasonal cycle of atmospheric CO_2 at high northern latitudes. This was in line with what Keeling et al. (1996) anticipated - since1960s the biosphere activity in the northern latitudes may have changed strongly, producing a longer vegetation growing period. Myneni et al. (1997) confirmed this with Advanced Very High Resolution Radiometer (AVHRR) satellite records. With modeling developments, current terrestrial vegetation and carbon models generally agree on the phase of the terrestrial seasonal cycle in the high northern latitudes (Nemry et al., 1999; Cramer et al., 1999; Zhuang et al., 2001; Dargaville et al., 2002).

However, models and observations exhibited oppositely phased seasonal cycles for tree growth at measurement site in the Amazon basin (e.g., Saleska et al., 2003). Saleska et al. (2003) proposed that seasonally moist tropical evergreen forests might have evolved two adaptive mechanisms in an environment with strong seasonal variations of light and water: deep roots for access to water in deep soils and leaf phenology for access to light. Xiao et al. (2005) simulated high GPP (Gross Primary Productivity) in the late dry seasons in Amazon basin, consistent with the estimated GPP from the CO_2 eddy flux tower there. Huete et al. (2006) found MODIS Enhanced Vegetation Index (EVI, an index of canopy photosynthetic capacity)

increased by 25% with sunlight during the dry season across Amazon forests. Oliveira et al. (2005) suggested that in addition to soil water uptake by deep root, the process of hydraulic redistribution could be another contributing factor explaining the absence of plant water stress during drought. Their proposed mechanism for this redistribution is the nocturnal transfer of water by roots from moist to dry regions of the soil profile.

Eddy covariance observation stations, which characterize fluxes and energy exchange at the surface and provide useful parameters to global and regional climate modelers, are still limited. Although the micro-meteorological flux measurements at FLUXNET sites are building up coverage with more sites across the globe in North, Central and South America, Europe, Scandinavia, Siberia, Asia, and Africa, they are still very sparse, especially in tropical forests. Observations and recent improvements of carbon cycle modeling have advanced our understanding of the seasonal dynamics of the terrestrial carbon cycle, particularly in different regions, such as the tropical and boreal forest. In Chapter 2, I will discuss the model comparison of VEGAS against FLUXNET observations. A brief description of physical processes of VEGAS will be also provided firstly in that chapter.

1.2.2 Modeling the interannual variability of terrestrial carbon cycle

The records of atmospheric CO_2 at Mauna Loa Observatory (MLO) since 1958 indicate that besides the seasonal cycle, substantial interannual variability of atmospheric CO_2 is superimposed on the ongoing increasing atmospheric CO_2 concentration. The association between CO_2 growth rate and ENSO (Figure 1.3) was initially reported in the 1970's and has been confirmed by recent studies (Bacastow,

1976; Keeling and Revelle, 1985; Braswell et al., 1997; Rayner et al., 1999; Jones et al., 2001; Zeng et al., 2005a). It was noticed that during El Niño (La Niña) events, the atmospheric CO_2 growth rate increased (decreased) at Mauna Loa Observatory with a 5-month lag of ENSO peak.

Different climatic responses have been suggested in previous studies to explain the ENSO-related terrestrial carbon cycle variation. For example, Kindermann et al. (1996) suggested that the temperature dependence of Net Primary Production (NPP, a variable usually used to indicate vegetation growth) is the most important factor in determining land-atmosphere carbon flux. However, precipitation has been suggested alternatively as the dominant factor for variation of terrestrial carbon cycle (Tian et al., 1998; Zeng et al., 2005a). Nemani et al. (2003) and Ichii et al. (2005) indicated that in tropical terrestrial ecosystems, variations in solar radiation and, to a lesser extent, temperature and precipitation, explained most interannual variation in the Gross Primary Production (GPP). Hashimoto et al. (2004) confirmed the dependence of global heterotrophic respiration and fire carbon fluxes on interannual temperature variability and strongly suggested that ENSO-mediated NPP variability influenced the atmospheric CO_2 growth rate. Besides these direct biological responses, biomass burning due to climate change might as well play an important role on the variation of total land-atmosphere carbon flux (Page et al., 2002; Langenfelds et al., 2002; Van der Werf et al., 2004). Van der Werf et al. (2004) estimated that during the 1997-98 El Niño, the anomalous carbon emission due to fires were 2.1 ± 0.8 PgC, or $66 \pm 24\%$ of the atmospheric CO_2 growth rate anomaly in that period.

These studies emphasized various factors related to the interannual variability of the terrestrial carbon flux; they have provided insight and opportunities to explore the underlying physical and biological mechanisms of the interannual variability of atmospheric CO_2 growth rate. Most of the studies cited above, however, have primarily focused on the effect of the climatic factors on photosynthetic processes (GPP, NPP), or the land-atmosphere carbon flux with respect to biomass burning. To date, few studies have been conducted to understand the underlying physical processes through which soil moisture affects the interannual variability of the terrestrial carbon flux. For instance, temperature has a direct impact on vegetation photosynthesis and soil respiration On the other hand; the temperature regulates evapotranspiration, and thus influences the variation of soil moisture, which is an important factor for vegetation growth and soil respiration. Through this process, the temperature thus has an indirect impact on the vegetation growth and soil respiration. This indirect influence has not yet been studied.

In Chapter 3, I will present an investigation of the response of the terrestrial carbon ecosystem to ENSO for the period of 1980-2004, based on the simulations of VEGAS. A detailed investigation of soil moisture effect on terrestrial carbon exchange is of interest. Besides the canonic tropical response to ENSO, in Chapter 4, a modeling study of the impact of the 1998-2002 Midlatitude drought on terrestrial ecosystem and the global carbon cycle will serve as a clue regarding why the atmospheric CO_2 growth rate was over 2 ppm/yr during 2002–2003, an unusual 2-year increase like no other during the course of the Mauna Loa Observatory station record.

1.2.3 Modeling the terrestrial carbon uptake under global warming

The future CO_2 concentration in the atmosphere is not straightforward to predict since it depends critically on the capacity of the land and ocean carbon absorption, which, in turn, is sensitive to the future climate change. If the Earth ecosystem reduces the capacity to take up the anthropogenic emissions, more CO_2 will stay in the atmosphere, accelerating global warming. This will trigger a further robust reduction of carbon uptake by ecosystems, and provide a positive feedback to atmospheric CO_2 increase. Understanding the carbon cycle-climate feedback is thus of importance for the projection of future climate.

Early general circulation models generally excluded the interactions between climate and the biosphere, using static vegetation distributions and CO_2 concentrations from simple carbon-cycle models that did not include climate change. Betts et al. (1997) attempted to quantify the effects of both physiological and structural vegetation feedbacks on a doubled-CO_2 climate, with a general circulation model iteratively coupled to an equilibrium vegetation model. Using a terrestrial biogeochemical model, forced by simulations of transient climate change with a general circulation model, Cao et al. (1998) predicted that terrestrial ecosystem carbon fluxes responded to and strongly influence the atmospheric CO_2 increase and climate change. Cox et al. (2000) used a fully coupled three-dimensional carbon-climate model and reported that carbon-cycle feedbacks could significantly accelerate climate change during the 21^{th} century. In their study, the atmospheric CO_2 concentration could be 250 ppm higher by 2100 due to a positive carbon-climate feedback, causing an additional 1.5˚C warming. The Amazon rainforest was even

projected to have a dieback towards the end of this century. However, the experiments by Institute Pierre Simon Laplace (IPSL) (Friedlingstein et al., 2001; Dufresne et al., 2002; Berthelot et al., 2002) suggested that the amplitude of positive feedback was three times smaller than that simulated by Cox et al. (2000). Fung et al. (2005) indicated that the amplification of climate change by the additional CO_2 could be small at the end of the 21st century. Quantifying and predicting this carbon cycle-climate feedback is thus extremely difficult because of the limited understanding of the processes by which carbon and the associated nutrients are transformed or recycled within ecosystems, and exchanged with the overlying atmosphere (Heimann et al., 2008).

During the past decades, Northern High Latitudes (NHL: poleward of 60°N) have witnessed dramatic changes, where the annual average temperatures increased by 1-2˚C in northern Eurasia and northwestern North America (Arctic Climate Impact Assessment, 2005), much larger than the of 0.65±0.2˚C increase of global average surface temperature over the 20th century (IPCC, 2007). Accompanying the accelerating climate changes in the NHL, a vegetation "greening" trend has been observed in the boreal forests with satellite data and phenology studies (Keeling et al., 1996; Myneni et al., 1997; Zhou et al., 2001; Tucker et al., 2001; Lucht et al., 2002). The enhancement in photosynthetic activity, associated with the persistent increase in the length of the growing season, may be leading to long-term increase in carbon storage and changes in vegetation cover, which in turn affects the climate system. However, warming accelerates decomposition of dead organic matter, thus losing soil carbon to the atmosphere. Reichstein et al. (2007) analyzed the European eddy

covariance fluxes and reported that water availability was a significant modulator of Net Ecosystem Productivity (NEP) on these sites, while the multivariate effect of mean annual temperature was small and not significant. However, Piao et al. (2008) found that there was a net carbon dioxide loss of northern ecosystems in response to autumn warming, because the increase in respiration was greater than photosynthesis during autumn warming. NHL contains a large amount of carbon in frozen soil, which is vulnerable to decay under global warming (Davidson et al., 2006). To date, such processes in particular are poorly understood (Melillo et al., 2002; Bond-Lamberty et al., 2004; Lawrence and Slater, 2005; Bronson et al., 2008). The competition between the absorption of carbon by boreal forests and the release of carbon from soil therefore is important for future carbon-cycle climate feedback and the degree of climate change. Previous projection of carbon uptake in the NHL under global warming scenario was mostly based on offline simulations of vegetation-carbon models, which were forced by the IPCC climate projection (McGuire et al., 2000; Cramer et al., 2001; Schaphoff et al., 2006; Lucht el al. 2006; Sitch et al., 2007). However, fewer studies have considered the carbon cycle-climate coupling in the NHL (McGuire et al., 2006). With the positive carbon cycle-climate feedback included, the NHL may undergo more intense warming than expected. Consequently, the frozen soil may emit carbon and NHL can become a carbon source of the atmosphere.

In Chapter 5, using a fully coupled carbon cycle–climate model (UMD), we have investigated the carbon cycle-climate feedback on the future climate system.

Chapter 6 will focus on the study of carbon uptake in NHL terrestrial biosphere under climate change in the 21st century, based on simulations of C4MIP.

Chapter 2: Evaluation of VEGAS against Observations

2.1 Introduction

This chapter provides a description of VEGAS and focuses on the evaluation of the model against the observations. This helps to measure the ability of VEGAS in capturing some of the physical processes of the biosphere, and also gives some insight into the further improvement for the VEGAS model. A detailed description of the processes in VEGAS can be found in the Appendices. Seasonal and interannual variability of modeled carbon fluxes from VEGAS have been compared across many sites of FLUXNET in North and South America. Two suites of comparisons will be discussed here: Station Km67 in Tapajos National Forest in Brazil, and Old Black Spruce in Canada. A lot of attention has been paid to the Amazon forest basin recently (e.g., Cox et al., 2000; Friedlingstein et al., 2001; Zeng et al., 2004; Cook et al., 2008). The Amazon forest plays an important role in the global carbon cycle because of deforestation, and could be subject to a recession in the future. In Chapter 3, we will look into the response of the terrestrial carbon ecosystem to ENSO, highlighting the importance of the variability of the tropical terrestrial ecosystem. The Old Black Spruce site in Canada is a typical boreal forest type, which is an important carbon reservoir. Accompanying the accelerating climate changes during the past decades, a "greening" trend with vegetation growth has been observed in the boreal forests (Keeling et al., 1996; Myneni et al., 1997; Zhou et al., 2001; Tucker et al., 2001; Lucht et al., 2002); however, the frozen soil carbon in the NHL is vulnerable to

decay due to warming there, leading NHL to be a significant carbon source in the future. In Chapter 6, we will investigate the future carbon uptake of the NHL in the 21th century. After the comparison with the FLUXNET at the local scale, we then provide an independent evaluation of the interannual variability of VEGAS against observations by comparing its simulated Leaf Area Index (LAI) to observed NDVI.

2.2 Model description and setup

Figure 2.1 is a conceptual diagram indicating the important processes of terrestrial carbon cycle in VEGAS (see details of its dynamics in Appendices). Briefly, VEGAS simulates vegetation growth and competition among four different Plant Functional Types (PFTs): broadleaf tree, needle leaf tree, cold grass and warm grass (Zeng, 2003; Zeng et al., 2005a). In VEGAS, the photosynthetic pathways for these 4 types are distinguished as C3 (the first three PFTs above) or C4 (warm grass). The difference between C3 and C4 is the way in which they accept CO_2 from the air. C3 plants use the enzyme ribulosodiphosphatcarboxylase while C4 plants use phosphoenolpyruvatcarboxylase. C3 plants include more than 95 percent of the plant species on earth, including crops such as wheat, barley, potatoes and sugar beet. C4 plants also include crop plants, such as corn and sugar cane. Phenology (or the life cycle of plants) is simulated dynamically as the balance between growth and respiration/turnover. Competition between growths for the different PFTs is determined by climatic constraints and resource allocation strategy such as temperature tolerance and height. The relative competitive advantage then determines fractional coverage of each PFT with possibility of coexistence. Accompanying the vegetation dynamics is a full terrestrial carbon ecosystem, starting from

photosynthetic carbon assimilation in the leaves and the allocation of this carbon into three vegetation carbon pools: leaf, root and wood. After accounting for respiration, the biomass turnover from these three vegetation carbon pools cascades into a fast soil carbon pool, an intermediate and finally a slow soil pool. Temperature and moisture dependent decomposition, as well as occurrence of fires, of these fuel loads returns carbon back into the atmosphere, thus closing the terrestrial carbon cycle. In VEGAS, the carbon flux associated with biomass burning of vegetation is included in the respiration of vegetation and the rest is included in soil decomposition. The key carbon flux outputs from VEGAS are related as follows:

$$NPP = GPP - R_a \tag{2.1}$$

$$NEP = NPP - R_h \tag{2.2}$$

$$F_{ta} = -NEP \tag{2.3}$$

Here GPP, Gross Primary Production is the total amount of carbon fixed by the photosynthesis of the terrestrial ecosystem from the atmosphere. NPP denotes Net Primary Production, which is the amount of carbon fixed after subtracting the respiration of vegetation, called Autotrophic Respiration (R_a), from GPP. The difference between Heterotrophic Respiration (R_h), which is the carbon released due to decomposition of soil organic matter, and NPP, is the Net Ecosystem Production (NEP) of the terrestrial ecosystem. F_{ta} is the land-atmosphere carbon flux, otherwise referred to as the Net Ecosystem Exchange (NEE).

VEGAS was coupled with a simple land surface model SLand (Zeng et al., 1999). SLand is an intermediate-complexity model which consists of two soil layers of temperature and one layer for soil moisture. It includes subgrid-scale

parameterizations of the major processes of evapotranspiration, interception loss, surface and subsurface runoff. The validation of modeled soil moisture by SLand on seasonal, interannual and longer timescales can be found in Zeng et al. (2008). In this paper, basin-scale terrestrial water storage for the Amazon and Mississippi, diagnosed using the Precipitation-Evaporation-and-Runoff (PER) method from SLand, was compared with those from other land surface models, the reanalysis, and NASA's Gravity Recovery and Climate Experiment (GRACE) satellite gravity data. The results indicate that SLand is reliable on seasonal and interannual time scales. In this thesis, soil wetness (Swet) is used to indicate the relative soil water saturation. It is defined as a ratio of modeled soil moisture (mm) to the maximum value of 500 mm. Swet varies from 0 to 1.

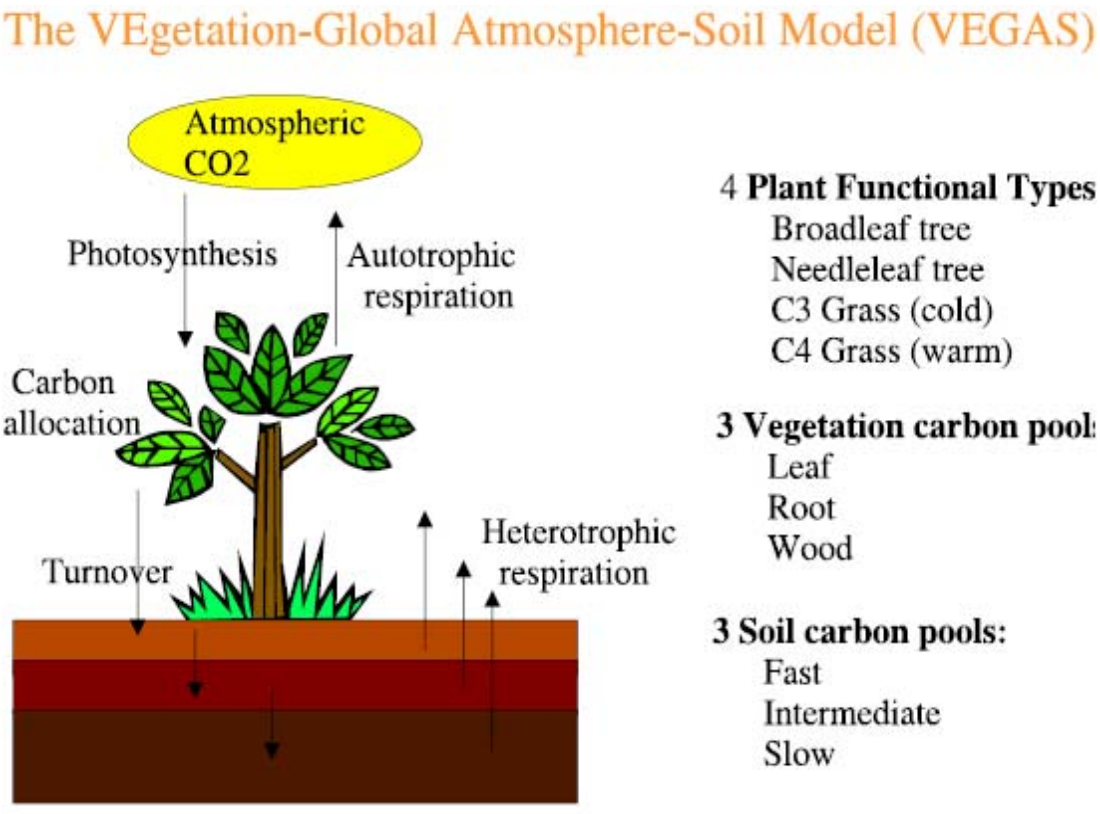

Figure 2.1 Concept of the VEgetation-Global-Atmosphere-Soil (VEGAS) model.

In this chapter and Chapter 3 and 4, an offline simulation, which is forced by observed climate variables, is used to evaluate VEGAS and investigate the variability of the terrestrial carbon ecosystem in response to climate variation. The physical climate forcing for this offline simulation includes surface temperature, precipitation, atmospheric humidity, radiation forcing, and surface wind. The driving data of precipitation for VEGAS was a combination of the Climate Research Unit (CRU: New et al., 1999; Mitchell and Jones, 2005) dataset for the period of 1901–1979, and the Xie and Arkin (1996) dataset of 1980-2006 (which has been adjusted with the 1981-2000 climatology of CRU dataset). The surface air temperature driving data was from the National Aeronautics and Space Administration (NASA) Goddard Institute for Space Studies (GISS) by Hansen et al. (1999) and CRU. We created a new temperature dataset using the anomaly of GISS temperature and CRU climatology of 1961-1990, in light of the climatology of precipitation from CRU. Seasonal climatology of radiation, humidity and wind speed were used to eliminate the potential CO_2 variability related to these climate fields. Humidity and wind speed are important terms in the land surface energy budget; however, their variations have second order effects on vegetation growth and soil decomposition. There is a large discrepancy as to the role of radiation in the terrestrial carbon flux, even the sign of the effect is uncertain. For instance, reduced direct solar radiation during wet periods would reduce photosynthesis (e.g., Knorr, 2000) while increased diffuse light under cloudy conditions (e.g., Gu et al., 2003) increases photosynthesis leading to a carbon uptake. We thus chose to use the climatology of light, humidity and wind speed, in order to focus on the effects of the interannual variability of precipitation and

temperature in this study. The atmospheric CO_2 concentration was kept constant at pre-industrial level of 280 ppm since the year-to-year variation of CO_2 level has a small impact on photosynthesis. The advantage of this offline simulation is that it gives prominence to the terrestrial responses to observed climate more directly than a fully coupled ecosystem model with model can, by eliminating model biases which would in turn affect the carbon model. The resolution of VEGAS is 1.0° x 1.0°. The steady state of model was reached by repeatedly using 1901 climate forcing. At this state, the global total GPP is 124 PgC/yr with NPP of 61 PgC/yr, and vegetation and soil carbon pools are 641 PgC, 1848 PgC, respectively. These are within the range of observationally based estimates (Schlesinger, 1991). This state was then used as the initial condition for the 1901-2006 run. We compare the results to an inversion model result by Rödenbeck et al. (2003), which estimated CO_2 fluxes by using a time-dependent Bayesian inversion technique, based on 11, 16, 19, 26 and 35 observation sites of atmospheric CO_2 concentration data from NOAA Climate Monitoring and Diagnostics Laboratory (CMDL) and a global atmospheric tracer transport model.

2.3 Seasonal and interannual variability of terrestrial carbon fluxes in the Amazon Basin

Station Km67 of FLUXNET is located in Tapajos National Forest in Brazil (2.8˚S, 55.0˚W). This important site is one of the few ones in the region to monitor and understand the characteristics of primary forest in Amazon basin. VEGAS modeled Net Ecosystem Production (NEE), Gross Primary Production (GPP), and Total Respiration ($R_e=R_a+R_h$) are compared with those from the observation.

Temperature and precipitation forcing VEGAS have been compared with those from the FLUXNET site and found to be in general agreement with them.

Though the magnitude of VEGAS NEE and the FLUXNET observations are similar, it is notable that the phase of the seasonal cycle is opposite (Figure 2.2a). The inversion result by Rödenbeck et al. (2003) shows a similar seasonal cycle to VEGAS. During the wet season (Jan-Aug), VEGAS simulates that land absorbs carbon because the modeled photosynthesis (GPP) is larger than the total respiration (R_e) (Figure 2.2b), and results in negative NEE, implying carbon uptake by the land. During the dry season, vegetation activity is suppressed a lot by water supply in VEGAS, while respiration increases a bit with high temperature. As a result, a net loss of carbon is seen in the dry season. However, the observation indicates that high respiration can be maintained in the wet cool season and the vegetation growth is not suppressed in dry season.

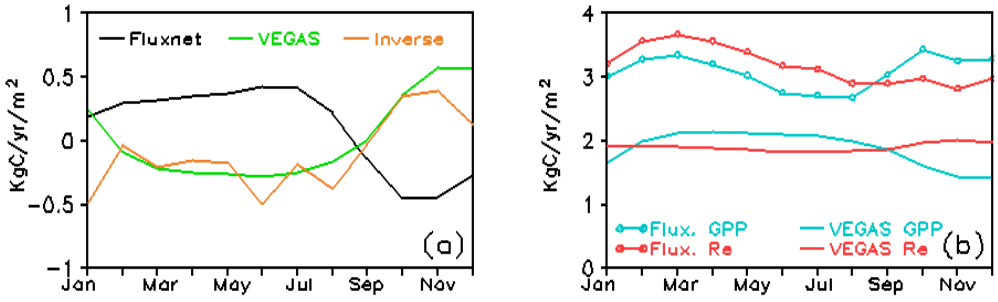

Figure 2.2 Seasonal cycles of carbon fluxes from VEGAS simulation and on-site observation in Tapajos National Forest (Km67: 2.8˚S, 55.0˚W), Brazil. (a) Land-atmosphere carbon flux (NEE) from VEGAS (climatology of 1991-2004), FLUXNET (climatology of 2002 -2004), and inversion (climatology of 1992 -2001); (b) GPP and R_e from VEGAS with FLUXNET. Unit in $KgC/m^2/yr$.

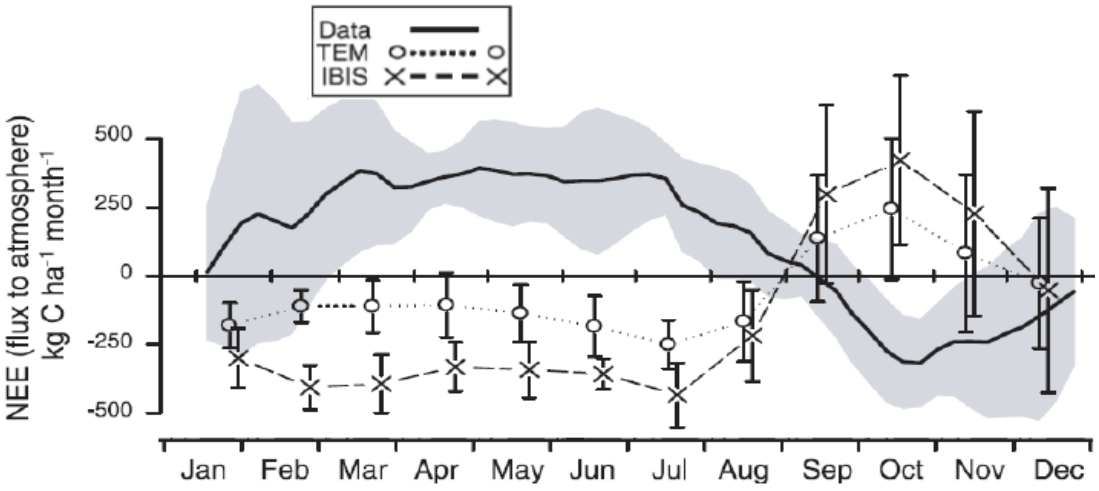

Figure 2.3 Seasonal cycle of land-atmosphere carbon flux from FLUXNET and two vegetation and carbon models: TEM (dotted curve) and IBIS (dashed curve) at Tapajos National Forest (adapted from Saleska et al., 2003).

Saleska et al. (2003) compared the same FLUXNET observation with the modeling results from TEM (Terrestrial Ecosystem Model) and IBIS (Integrated Biosphere Simulator). These two terrestrial carbon models simulated a seasonal cycle of NEE similar to VEGAS (Figure 2.3). Saleska et al. (2003) suggested that the old-grown trees in the Tapajos had access to deep soil water during the dry periods and show little evidence of water stress. Wood increment rates declined a little in the beginning of dry season, but maintained substantial increase just before the rains return, suggesting an adaptive mechanism of vegetation rather than a response to the seasonal climate forcing. This "hydraulic" adaptive behavior of tropical big trees has not been considered in terrestrial carbon models before. In principle, terrestrial carbon models usually parameterize tropical vegetation dynamics based on the assumption that the tropics are a water-limited area. Furthermore, Saleska et al. (2003) proposed that respiration in soils, litter, and coarse wood debris is concentrated near the surface

and inhibited by desiccation during the dry season. This implies that soil moisture, rather than temperature, may control soil decomposition.

However, it is of interest that VEGAS modeled NEE anomaly generally agrees with the observations after the seasonal cycle is removed (Figure 2.4). Why does VEGAS simulate "right" interannual variability of land-atmosphere carbon flux, while giving an "out-of-phase" seasonal cycle against the observations? Further analysis of interannual variability of GPP and R_e indicates that in Tapajos the models and the observation may have different mechanisms of controlling the carbon uptake with respect to the climate variation on interannual timescales. VEGAS determines its interannual variability of NEE by NPP, while the observations attribute it to the respiration (not shown). However, sparse sites and short-term coverage of the observations in the tropical forest limit the model evaluation in the Amazon basin. The discrepancies between terrestrial carbon models (e.g., VEGAS, TEM and IBIS) and observations, though not resolved, have advanced our understanding of physical processes in the tropical forest area. Additional observation sites in the tropical forest and improvement of terrestrial carbon models are both called for.

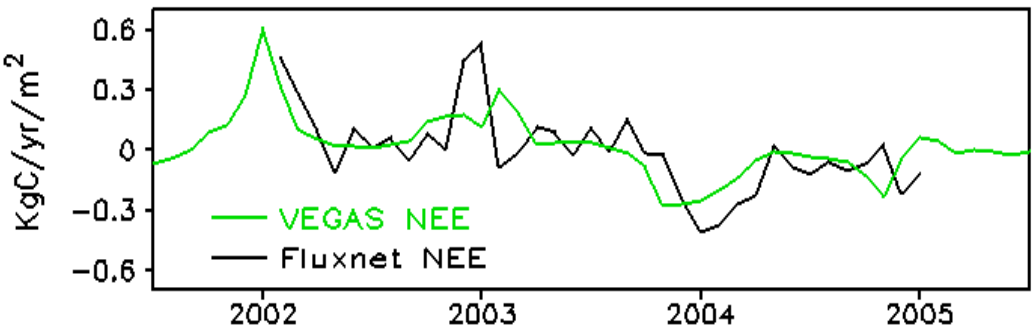

Figure 2.4 Anomaly of land-atmosphere carbon flux from VEGAS and FLUXNET after season cycle is removed in Tapajos National Forest; The inversion result is not plotted here because its simulation time coverage ends 2001. Unit in $KgC/m^2/yr$.

2.4 Seasonal and interannual variability of terrestrial carbon fluxes of boreal forest in Canada

The station site in Old Black Spruce, Manitoba, Canada (55.9˚N, 98.5˚W) is covered with boreal evergreen forests and has records dating back nearly 10 years. In this site, vegetation begins to grow when the temperature returns above 0˚C in VEGAS (GPP) (Figure 2. 5b). This matches the observations well. VEGAS tends to underestimate the amplitude of vegetation growth during summer time (75% of the observed GPP). After the summer season, VEGAS GPP and the observational GPP are comparable. Similar to GPP, VEGAS modeled R_e is also underestimated in summer season; but both agree with measurements in spring, fall and winter season. Although VEGAS GPP and R_e are both underestimated, their difference, NEE has a good agreement with the observational value in terms of seasonal phase (Figure 2.5a). The observations indicate that land takes up carbon from April to August, and the model extends this uptake to October but with low efficiency of carbon absorption. On the interannual time scale, there is an agreement of the NEE anomalies between VEGAS and the observations (Figure 2.6). The similarities of seasonality and interannual variability between VEGAS and the observations imply that VEGAS is able to reproduce the natural physical processes in the boreal forest.

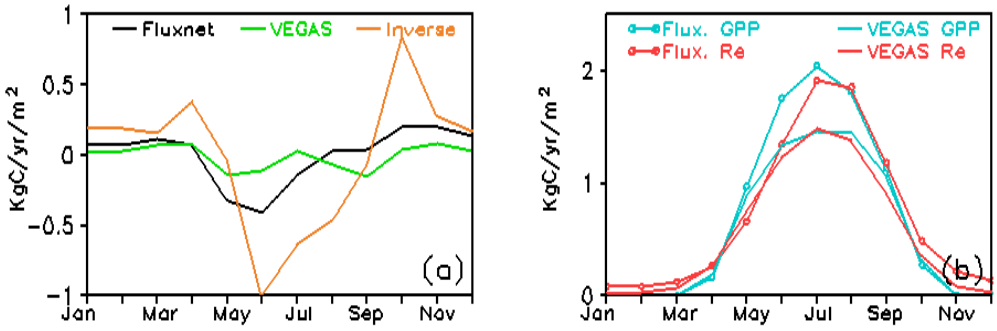

Figure 2.5 Same as Figure 2.2 but for Old Black Spruce, Manitoba, Canada (55.9˚N, 98.5˚W).

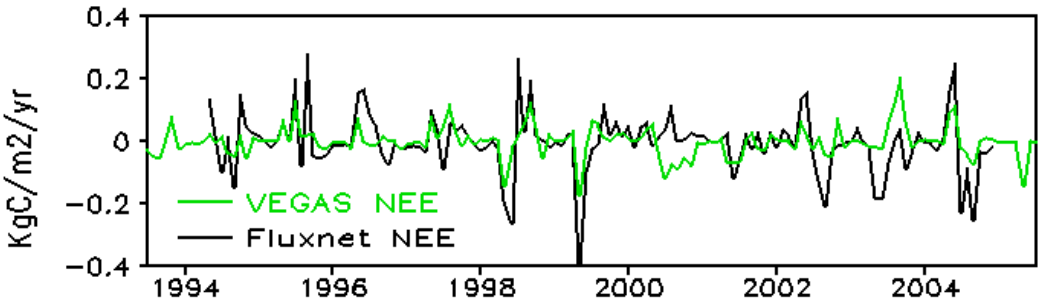

Figure 2.6 Same as Figure 2.4 but for Old Black Spruce, Manitoba, Canada (55.9˚N, 98.5˚W).

2.5 Evaluation of the interannual variability of VEGAS LAI with NDVI

Here, an independent evaluation of the interannual variability of VEGAS was performed by comparing its simulated Leaf Area Index (LAI) to satellite observed Normalized Difference Vegetation Index (NDVI) (Figure 2.7). The high resolution 1.0° x 1.0° satellite NDVI dataset of 1981-2004 comes from the Global Inventory Modeling and Mapping Studies (GIMMS) data set, which provides a 24-year satellite record of monthly changes in terrestrial vegetation (Tucker et al., 2001; Zhou et al., 2001; http://gimms.gsfc.nasa.gov/). NDVI is the difference between the Advanced Very High Resolution Radiometer (AVHRR) near-infrared and visible bands divided by the sum of these two bands and can be used to quantify the density of plant growth on the Earth. Many studies have used NDVI as an indicator of vegetation growth to address its interannual-to-decadal variability in the northern hemisphere (Myneni et al., 1998; Zhou et al., 2001; Tucker et al., 2001). LAI is defined as the total leaf area per unit ground area. It is an important canopy parameter for ecosystem studies (Nemani and Running, 1989). In general, there is a close relationship between NDVI and LAI (Wardley and Curran, 1984). The spatial pattern of the temporal correlation between the filtered LAI simulated by VEGAS and the NDVI is indicated in Figure

2.7 for the period of 1981-2004. The results indicate that the correlation is good in Northern and Southern Hemisphere extratropics, but poor in the tropics. As mentioned in the previous section, both the satellite observations and model simulation could have problems which could lead to the poor correlation in the tropics.

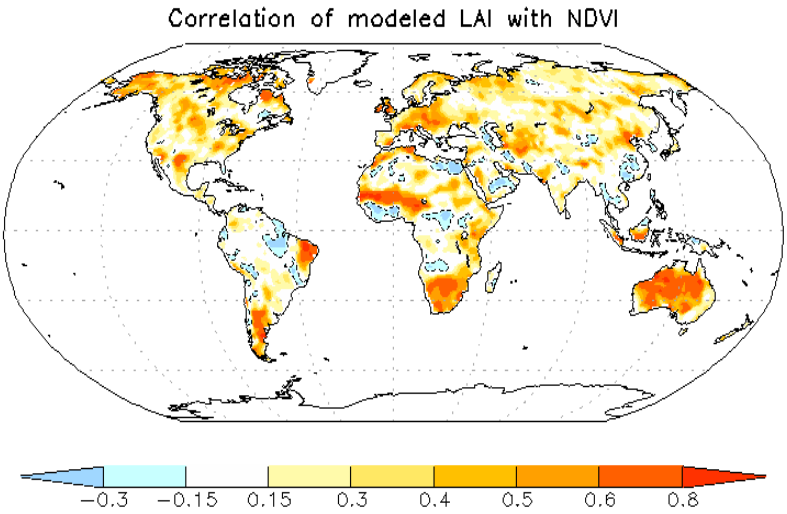

Figure 2.7 Evaluation of VEGAS: the spatial pattern of correlation between VEGAS simulated LAI and the satellite observed NDVI between 1981 and 2004. A contour is used for shaded areas with value smaller than -0.15. Value of 0.33 is statistically significant at the 90% level of Student's t-test.

2.6 Summary

In short, VEGAS is able to capture the interannual variation of the land-atmosphere carbon flux against the observations in both Tapajos and Old Black Spruce. At the Tapajos site, VEGAS simulates an "opposite" seasonal cycle of NEE as do other state-of-the-art vegetation models like TBM and IBIS. The reason is that the current terrestrial carbon models (VEGAS, TEM and IBIS) may not incorporate some important physical processes, such as a "hydraulic" adaptive process for trees

during the dry season as suggested by Saleska et al. (2003). But these processes are still poorly understood. The extent to which, soil moisture, temperature or both, control the heterotrophic respiration, is still subject to debate, and is in fact, even more poorly understood. The density of measurement stations in the tropics is still very sparse and the spatiotemporal patterns of carbon fluxes could vary with location or canopy type. The Tapajos site even only has a 3-year observational record. The similarity in the interannual variability of land-atmosphere carbon fluxes between VEGAS and observations is encouraging, and this provides an opportunity to investigate the response of terrestrial carbon ecosystem to climate variation (in Chapter 3, 4). In the boreal forest in North America, VEGAS is able to reproduce the vegetation growth, respiration, and land-atmosphere carbon flux seen at the station site. This agreement encourages the application of process-based modeling in studying the carbon absorption in the boreal forest.

The evaluation of the interannual variability of VEGAS LAI against satellite observed NDVI indicates higher correlation in extratropics, but lower correlation in the tropics. Note that the satellite NDVI data may be of limited value due to cloud contamination and saturation of satellite signals (Knyazikhin et al., 1998; Myneni et al., 2002).

Chapter 3: Response of the Terrestrial Carbon Cycle to the El Niño-Southern Oscillation

3.1 Introduction

An association between the CO_2 growth rate and ENSO (Figure 3.1) was initially reported in the 1970's and has been confirmed by recent statistical analysis (Bacastow, 1976; Keeling and Revelle, 1985; Braswell et al., 1997; Rayner et al., 1999; Jones et al., 2001; Zeng et al., 2005a). Climate driven variations in the global carbon cycle have been attributed as the primary cause of the interannual variability of atmospheric CO_2 growth rate after accounting for long-term trends of fossil fuel emission and land use change. The typical El Niño events are characterized by changes in atmospheric circulation and precipitation patterns (Ropelewski and Halpert, 1987) that give rise to warmer and drier conditions in the tropical land regions. Such a pervasive influence is likely to exert an impact on the land-atmosphere carbon exchange. Those physical and biological responses of the terrestrial ecosystem to climate variation, especially to ENSO cycle, however, are not well known.

Several studies have addressed the primary cause of ENSO-related terrestrial carbon cycle variation from different climatic points of view. For example, Kindermann et al. (1996) suggested that the temperature dependence of NPP is the most important factor in determining land-atmosphere carbon flux. However, precipitation has alternatively been suggested as the dominant factor for variation of

terrestrial carbon cycle (Tian et al., 1998; Zeng et al., 2005a). Further, studies by Nemani et al. (2003) and Ichii et al. (2005) had indicated that in tropical terrestrial ecosystems, variations in solar radiation and, to a lesser extent, temperature and precipitation, explained most interannual variation in GPP. Besides these direct biological responses, fire due to climate change was also noted to play an important role in the variation of total land-atmosphere carbon flux (Page et al., 2002; Langenfelds et al., 2002; Hashimoto et al., 2004; Van der Werf et al., 2004). Hashimoto et al. (2004) confirmed the dependence of global fire carbon fluxes on interannual temperature variability. Van der Werf et al. (2004) estimated that during the 1997-98 El Niño, the anomalous carbon emission due to fire was 2.1 ± 0.8 PgC of carbon, or 66 ± 24% of the atmospheric CO_2 growth rate anomaly in that period.

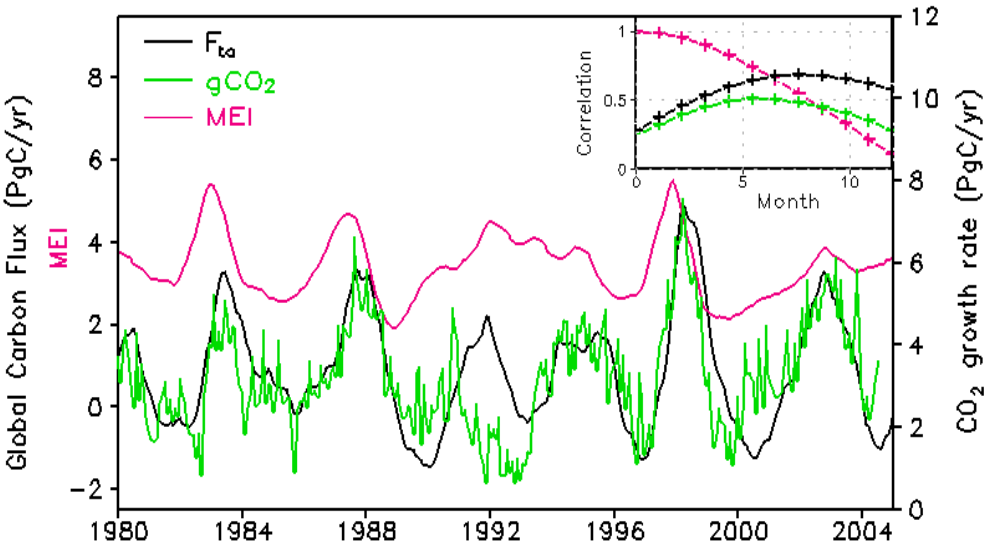

Figure 3.1 Time-series indicating the correspondence of the CO_2 growth rate (gCO_2) at Mauna Loa, Hawaii with global total land-atmosphere carbon flux simulated by VEGAS and their lag with the Multivariate ENSO Index (MEI; units dimensionless), which is shifted up by 3 units. The seasonal cycle has been removed with a filter of 12-month running mean. The right top panel is the lagged correlation of MEI, F_{ta} and atmospheric CO_2 growth rate with MEI where the X-axis indicates the time lag in months. Value of 0.33 is statistically significant at the 90% level of Student's t-test.

Zeng et al. (2005a) studied the interannual variability of the terrestrial carbon and have suggested that the tropical dominance is a result of a "conspiracy" between climate and plant/soil physiology. During ENSO warm events, less precipitation and higher temperature in the tropical land tended to suppress vegetation growth and enhance soil decomposition, both contributing to more land carbon release to the atmosphere in the same direction. Though the results of these studies emphasizing the dominant factors influencing the interannual variability of the terrestrial carbon flux vary a lot, they provided insight and opportunities to explore the underlying physical and biological mechanisms of the interannual variability of atmospheric CO_2 growth rate. Most of the studies cited above, however, have primarily focused on the effect of the climatic factors on photosynthetic processes (GPP, NPP). To date, few studies have been conducted on understanding the physical processes by which soil moisture affects the interannual variability of the terrestrial carbon flux. For instance, temperature has a direct impact on vegetation photosynthesis and soil decomposition. On the other hand, the temperature largely regulates the evapotranspiration, and thus influences the variation of soil moisture, which is an important factor for vegetation growth and soil decomposition. Through this, the temperature thus has an indirect impact on the vegetation growth and soil decomposition. This indirect influence has not yet been studied.

The primary purpose of this present study is to provide insight into the mechanism of how ENSO-related precipitation and temperature variations regulate vegetation growth, soil respiration and land-atmosphere carbon flux. The following specific scientific questions will be addressed with relevant data sets:

- What are the robust spatial and temporal features of the terrestrial carbon ecosystem in response to ENSO in observations and can it be simulated by a process-based model?
- How do the variations of physical climate (e.g., temperature, precipitation, etc.) associated with ENSO govern terrestrial biophysical processes, such as the vegetation activity and soil decomposition? What are their relative contributions? Can the direct and indirect effects of temperature on the terrestrial carbon flux be quantified?

To answer these questions, an offline simulation of VEGAS is used to investigate the response of the terrestrial carbon ecosystem to ENSO. The Multivariate ENSO Index (MEI) from NOAA is used as an indicator of ENSO signal. MEI is produced based on six observed variables over the tropical Pacific: sea-level pressure, zonal and meridional components of the surface wind, sea surface temperature, surface air temperature, and total cloudiness fraction of the sky (Wolter and Timlin, 1998; Markgraf and Diaz, 2000; http://www.cdc.noaa.gov/ENSO). The uninterrupted CO_2 record for 1965-2006 at Mauna Loa Observatory (MLO) is used to calculate the atmospheric CO_2 growth rate. Besides the inversion modeling of Rödenbeck et al. (2003), a high resolution 1.0° x 1.0° NDVI dataset of 1981-2004 was used. We will focus on the period 1980-2004 in view of the availability of observational NDVI dataset and the inversion model results. A caveat of the evaluation process is that the evaluating data themselves have limitations. For instance, inversion estimates themselves are based on transport models constrained by observational data. Gurney et al. (2003) have found significant differences in carbon

flux between different inversion models. Similarly, in the tropics, the satellite produced NDVI data may be deemed suspect because of cloud contamination and saturation of NDVI (Knyazikhin et al., 1998; Myneni et al., 2002) as mentioned before. On the other hand, Saleska et al. (2007) have suggested that many terrestrial vegetation and carbon models do not have roots deep enough to capture growth during short-term droughts in the tropics, consistent with observations as discussed in Chapter 2.

3.2 Interannual variability of terrestrial carbon flux

Interannual fluctuations in Sea Surface Temperature (SST) in the tropical Eastern and Central Pacific are linked to global climate anomalies. For example, the changes of SSTs in the eastern tropical Pacific Ocean and associated deep convection perturb the Hadley circulation and produce a wavetrain starting with anomalous upper troposphere divergence in the tropics (Trenberth et al., 1998). Ropelewski and Halpert (1987) examined the link between ENSO events and regional precipitation patterns around the globe and noted that Northeastern South America from Brazil up to Venezuela had 16 dry episodes during the past 17 ENSO events. Others areas in the tropics, such as Indonesia, Australia, India etc, also showed a strong tendency to be dry during ENSO events. These dry conditions are usually followed by forest fires and decline of crop yield. Thus the climate variations associated with ENSO cycle tend to have a strong impact on the terrestrial biosphere in the lower latitudes, especially in the tropical forest areas.

The global and regional F_{ta} simulated by VEGAS (The interannual variability of the time-series of VEGAS and the inversion model is calculated by removing the

seasonal cycle and then filtering the data using a 12-month running mean to remove short term fluctuations.) was compared with the corresponding fluxes from the inversion model by Rödenbeck et al. (2003), which conducted inversions using either inversion simulations with 11, 16, 19, 26 or 35 sites. We use the simulation of 11 sites for the following ENSO composite analysis because of its longest temporal coverage) (Figure 3.2). Overall, the interannual variability of F_{ta} by VEGAS and the inversion model show a good agreement globally with a correlation of 0.68 (11 sites). A major discrepancy between VEGAS and inversion is the period after the 1991 Mount Pinatubo eruption (Figure 3.2a). The relatively low atmospheric CO_2 growth rate after Mount Pinatubo eruption has been discussed in the past but a consensus about the underlying mechanism has not yet been reached (Jones and Cox, 2001; Lucht et al., 2002; Gu et al., 2003; Angert et al., 2004). The climatic suppression of respiration by the observed cooling after the eruption, and the enhancement of productivity by changes in diffuse light due to aerosols, have been suggested as possible reasons for this discrepancy. Most of the contribution to the global flux comes from the tropics (Figure 3.2b). The consistency of VEGAS and the inversion model in the tropics is reflected in the correlation value of 0.55 (11 sites). In contrast to the tropics, the interannual variation in the extratropics is smaller. The terrestrial carbon flux from the Northern Hemisphere extratropics by VEGAS lies within the range of the inversion results (Figure 3.2c).

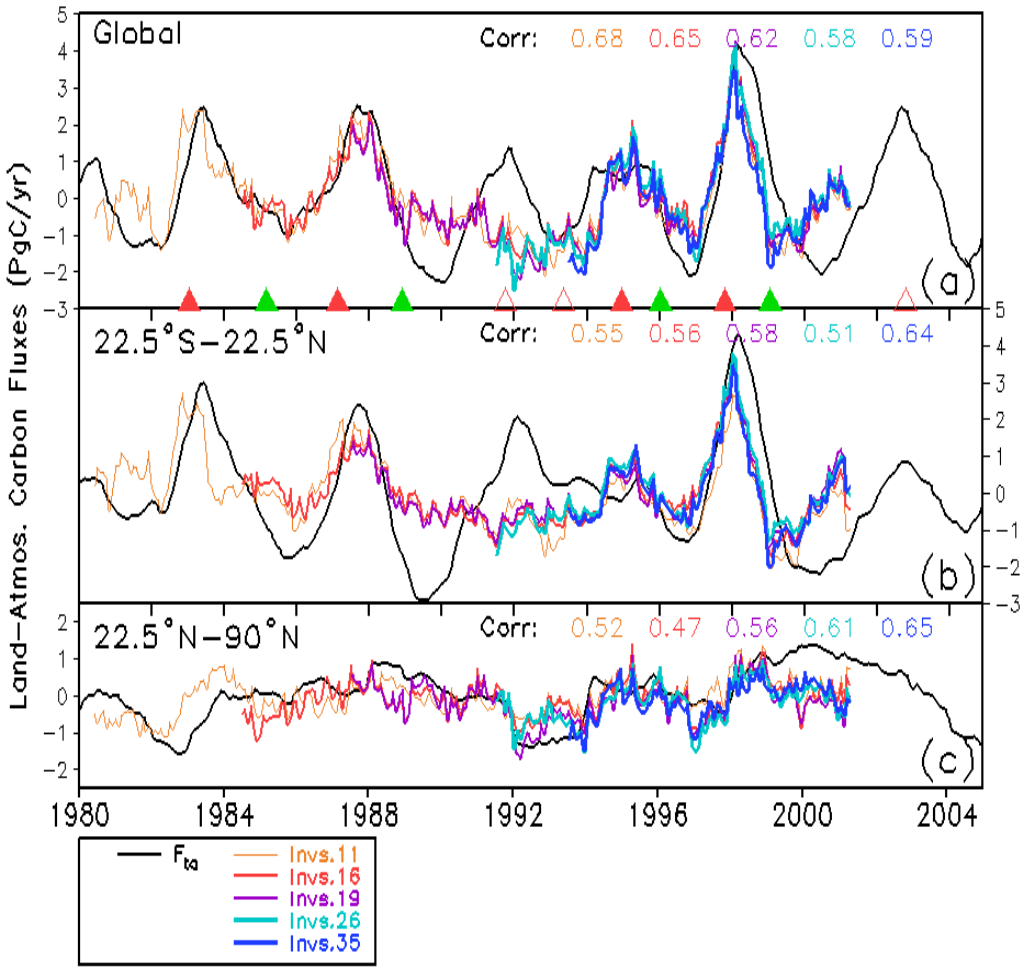

Figure 3.2 Interannual variability of land-atmosphere carbon fluxes (F_{ta}) by VEGAS and inversion from Rödenbeck et al. (2003) (lines for the inversion modeling with the CO_2 measurements from 11, 16, 19, 26 and 35 sites) for various regions: (a) Global; (b) Tropics between 22.5°S and 22.5°N; (c) Northern Hemispheric extratropics between 22.5°N and 90°N. Seasonal climatology is calculated based on the 1981-1999 time period for VEGAS and the inversion model with 11 observational sites; The climatology of the other inversion simulations are calculated with their respective time coverage. The filled triangles represent the ENSO events which have been selected in the composite analysis that follows in the text, with red triangles for El Niño events and green for La Niña events. The individual correlation of the land-atmosphere carbon fluxes between VEGAS and the inversion simulation with different number of stations is indicated in the 3 panels. The figure legend refers to the number of stations used in the inversion modeling calculations. All these correlation values are statistically significant at the 90% level of Student's t-test.

3.3 Robust features of the terrestrial response to ENSO

Composite analysis is a useful method in climate studies to highlight the canonical features of a given type of variability without focusing on the differences between individual events (Rasmusson and Carpenter, 1982). Here similar events are averaged to emphasize the general aspects related to the growth and decay of the event. We used this method to investigate the robust response of the terrestrial ecosystem and associated climate variables during the ENSO cycle. El Niño and La Niña events used in this analysis have values that exceed a standard deviation of 0.75 based on the MEI. These events are consistent with the analysis of Trenberth (1997). El Niño occurred in 1982-83, 1986-1987, 1991-92, 1993, 1994-95 and 1997-98 and La Niña occurred in 1984-85, 1988-89, 1995-96, and 1998-99. Because of the 1991 Pinatubo eruption, 1991-92 and 1993 were not included in the following composite analysis. La Niña events were essentially treated as negative El Niño events, and combined to investigate the terrestrial response of ENSO. The composite analysis is similar to that of Rasmusson and Carpenter (1982). To highlight features related to the interannual variability, the composites used in this study were made after the seasonal cycle was removed and a filter was used to smooth the data. Figure 3.3 shows a composite of the 2.5-year time evolution of ENSO events of the observational climate fields and simulated terrestrial responses for the whole globe (left panel), the tropics (central panel) and the Northern Hemisphere extratropics (the right panel). The global total land-atmosphere carbon fluxes from VEGAS (F_{ta}), the inversion model, and the atmospheric CO_2 growth rate resemble each other closely during the initiation phase of ENSO and exhibit a 6-month lag with the MEI index

(Figure 3.3a). The maturity of El Niño occurs in November of "year 0" of the ENSO event and the peak of the inversion flux anomaly lags by 4-5 months, followed by F_{ta} and CO_2 growth rate by 1-2 months later. The tropical land-atmosphere carbon flux anomalies have a similar magnitude and phase as the global fluxes, not only in VEGAS simulation but also in the inversion model (Figure 3.3b). In the tropics, the composite phase of the precipitation anomaly has nearly the same phase as MEI, but the response of modeled soil moisture is delayed because of its memory (Figure 3.3h). The simulated vegetation activity (NPP) peaks 6 months after the MEI (Figure 3.3e), more close to the phase of soil wetness rather than to precipitation. On the other hand, modeled soil decomposition R_h also peaks at about a 6-month lag with MEI. As a result, in the model, the decrease of NPP anomaly and increase of R_h anomaly contributes in the same direction and dramatically increase the F_{ta} anomaly during the ENSO warm events. In the middle and high latitudes of Northern Hemisphere, VEGAS F_{ta} anomaly phase is in general agreement with inversion flux model results. The response to ENSO is much weaker (Figure 3.3c). The variation of precipitation and temperature are in phase there, which is different from the out-of-phase relationship between precipitation and temperature in the tropics.

To better understand the response of the terrestrial ecosystem to ENSO, lead-lag correlations of tropical temperature, precipitation, simulated soil wetness and CO_2 growth rate, as well as terrestrial carbon fluxes with MEI during 1980-2004 were calculated (Figure 3.4). In this analysis, only the seasonal cycle was removed from data and no smoothing of the data was performed. This highlights the findings in the central panels of Figure 3.3 and gives the exact phase relationship. The peak of the

atmospheric CO_2 growth lags MEI about 5-6 months (R=0.45), similar to Zeng et al. (2005a). In the tropics, observed precipitation closely follows the MEI peak with about 1-month lag (R=-0.83), while temperature lags by 5-6 months (R=0.43). These climate patterns were suggested to be associated with the changes in atmospheric circulation during ENSO event (Ropelewski and Halpert, 1987). Because of the soil memory of water recharge, modeled soil wetness has a 5-month lag. Modeled NPP lags MEI by about 6 months (R=-0.8), with a 11-month lag for LAI by VEGAS, which suggests that vegetation does not show an immediate response to precipitation but rather responds to soil wetness more closely. On the other hand, R_h follows observed temperature closely and peaks with about a 6-month lag with the MEI. Thus, NPP and R_h simultaneously contribute to the F_{ta} lag of 6 months with the MEI (R=0.83) in the tropics in VEGAS. The "perfect" out of phase relationship of NPP and R_h in the tropics is determined by the anti-correlation of precipitation and temperature pattern associated with ENSO events.

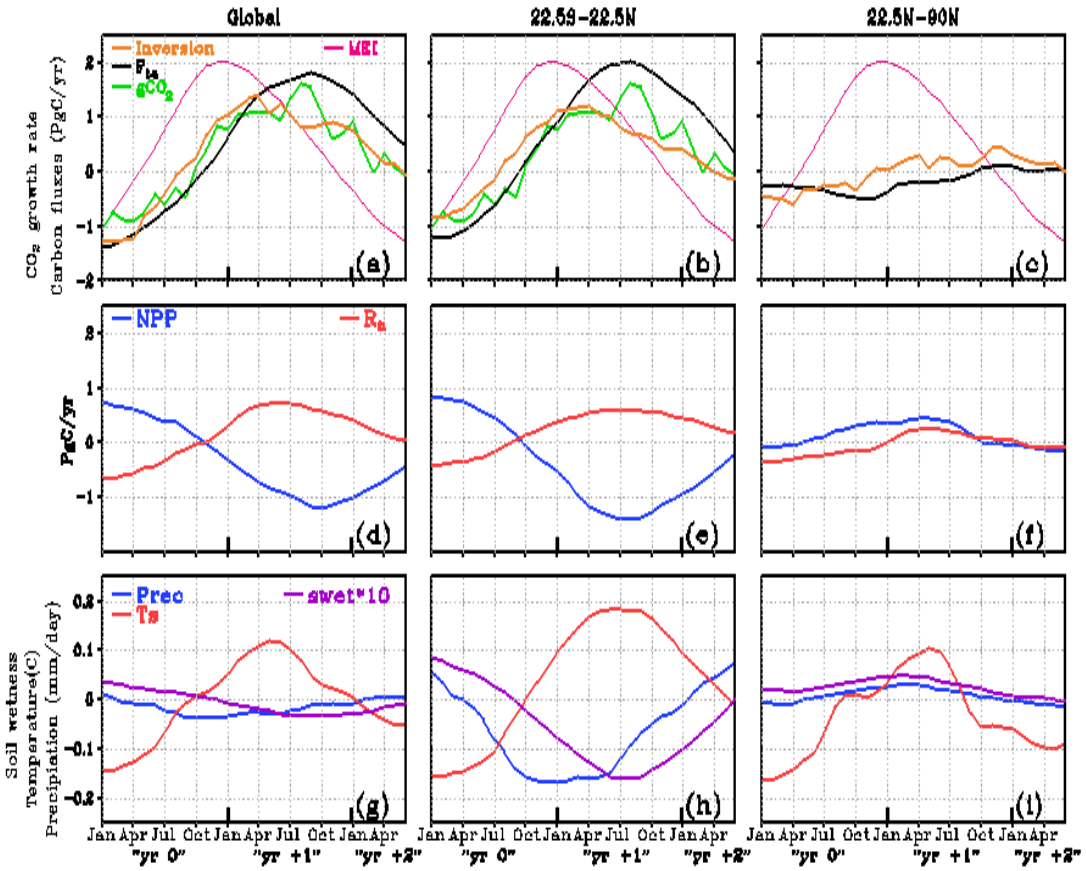

Figure 3.3 Composites of the carbon fluxes and the climatic field anomalies during the growth, mature, and decaying phases of ENSO: The left (a, d, g), central (b, e, h) and right (c, f, i) panels are the global, the tropical (22.5°S to 22.5°N) and Northern Hemispheric extratropics (22.5°N to 90°N) composites of the terrestrial fields. The top panels (a, b, c) are the terrestrial land-atmosphere carbon flux anomalies of VEGAS (F_{ta}) and inversion model, the atmospheric CO_2 growth rate (gCO_2) and the reference MEI; The middle panels (d, e, f) are the corresponding Net Primary Production (NPP), and heterotrophic transpiration (R_h), and the bottom panels (g, h, i) are the observed temperature, precipitation and modeled soil wetness (Swet). Units for carbon fluxes and CO_2 growth rate are PgC/yr; mm/day for precipitation, and ˚C for temperature, and MEI and soil wetness are non-dimensional. The notation of "yr 0", "yr +1", "yr +2" is the same as in Rassmusson and Carpenter (1982) in which "yr 0" is the mature phase of ENSO.

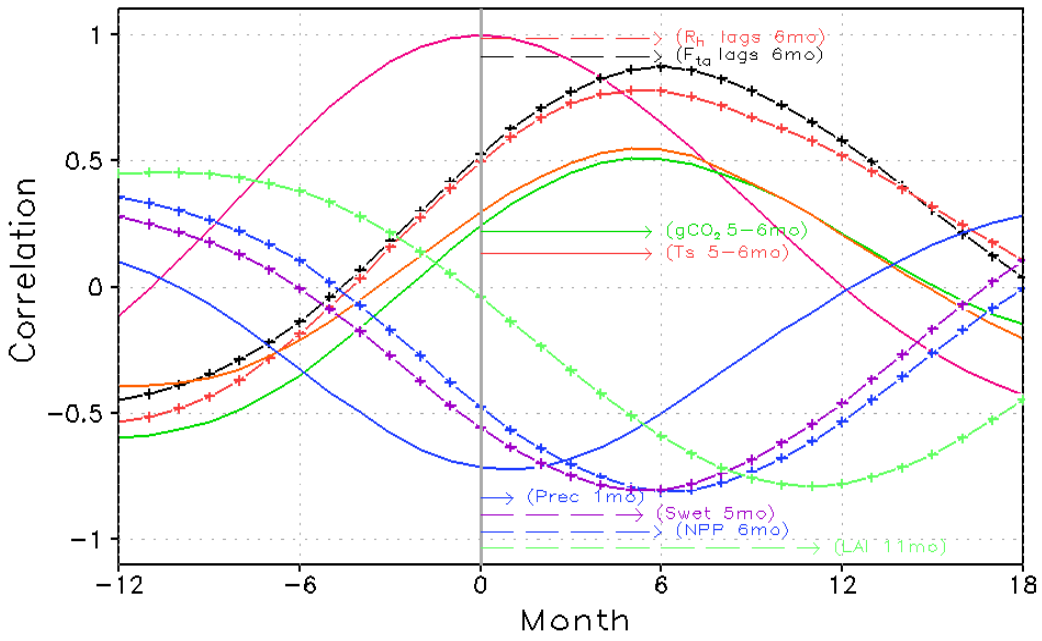

Figure 3.4 Lead-lag correlations of tropical terrestrial carbon fluxes and climatic fields with MEI. The observed CO_2 growth rate (gCO_2), temperature, precipitation, modeled NPP, Rh, LAI, F_{ta} and soil wetness are indicated; the solid magenta line is the autocorrelation of MEI with itself. Negative values in x-axis represent the number of months the corresponding variables lead the MEI and the positive values denote the number of months the variables lag by. Arrows indicate the peak response of each variable. A correlation value of 0.33 is statistically significant at the 90% level of Student's t-test.

Spatial patterns of the response of VEGAS 6 months after the peak of the ENSO phase are shown in Figure 3.5a, c, e, g. The tropical regions have robust positive anomalies of land-atmosphere carbon fluxes. The largest positive signals are located in eastern Brazil, and equatorial and southern Africa, consistent with the results of Jones et al. (2001). Southeast Asia and the east coast of Australia have sparse positive signals. Overall, the inversion model results (Figure 3.5b) and those of VEGAS agree well in the tropics though there are discrepancies in the extratropics. Modeled LAI from VEGAS and NDVI still show global agreement except in the tropics (Figure 3.5c, d). The regions associated with large positive anomalies of F_{ta}

regions consistently have large negative NPP anomalies in VEGAS (Figure 3.5e) and large positive R_h anomalies (Figure 3.5g) in the tropics, such as in the Amazon basin, consistent with the area averaged values in Figure 3.4b. These are also regions with correspondingly warm and dry conditions with negative signals of soil wetness (Figure 3.5g, h and Figure 3.4h). Zeng et al. (1999) proposed dynamical and hydrological mechanisms for anti-correlation between precipitation and temperature anomalies in the tropics. Decrease (increase) in precipitation tends to make the land surface dryer (wetter) and with less (more) evapotranspiration, less (more) evaporative cooling and then cause higher (lower) temperatures. Increase in absorption of solar radiation due to the absence of cloud during warm ENSO events is also likely to be a candidate for land surface warming.

In the Northern Hemisphere extratropics, temperature anomaly is positively correlated with precipitation anomaly. The response of vegetation to ENSO in the extratropics is small (as seen in Figure 3.2 and Figure 3.3) and does not correspond to the 6-month lag response of vegetation in the tropics. However, interesting features emerge in Figure 3.5. North America exhibits a zonal dipole mode of F_{ta} anomalies. In the southwest U.S. the negative F_{ta} anomaly results from NPP positive anomalies surpassing R_h positive anomalies in strength. In contrast, the F_{ta} anomaly in the Northeast is dominated by negative NPP anomaly and positive R_h anomaly. Over the Eurasian continent, weak positive signals exist in East Asia, Northwest China, South Europe and Northeast Russia. In western Asia the large negative F_{ta} anomaly is attributable to soil moisture, which stimulates the vegetation activities and leads to large positive NPP anomaly. The scenario in other regions is more complex. Other

modes of variability like the Arctic Oscillation (Buermann et al., 2003) may influence the high latitudes. It is interesting to note that the spatial pattern of NDVI anomalies generally match LAI anomaly in the middle and high latitudes except in Northeast of North America, which demonstrates the capability of VEGAS to generally reproduce the variability of vegetation activities.

The carbon flux associated biomass burning is an important fraction of the total terrestrial carbon flux (Page et al., 2002; Langenfelds et al., 2002; Hashimoto et al., 2004; Van der Werf et al., 2004). In VEGAS, the carbon flux associated with biomass burning of vegetation and fast soil pool is included in the respiration of vegetation (R_a) and in soil decomposition (R_h). When fire occurs in VEGAS, leaves burn completely, while in reality only part of the wood gets burnt and the rest is lumped into the soil carbon pool and biomass burning of surface soil. Our simulation shows that the biomass burning accounts for about 25% of the total flux anomalies in the tropics during ENSO events (Figure 3.6), consistent with Zeng et al. (2005a). About 83% of the fire-related carbon release is included in the R_a and the remaining 17% is included in R_h.

The composite analysis used above has treated La Niña events as the linearly "opposite" phase of El Niño events to capture the common features in the response of vegetation to the ENSO cycle and increase the number of events for statistical stability. To highlight the differences in the responses between the two phases of the ENSO, composites of El Niño and La Niña events are separately plotted in Figure 3.7, for the atmospheric growth rate of CO_2, the land-atmosphere carbon fluxes of VEGAS and inversion model. First of all, the land-atmosphere carbon fluxes of

VEGAS and inversion, CO_2 growth rate agree in phase both in El Niño and La Niña events (Figure 3.7a, b), respectively. However, the phase evolutions during El Niño and La Niña do differ. After La Niña matures, MEI decreases slowly and takes more than one and half years to decay. Though the lag time of F_{ta} anomaly increases with respect to MEI in La Niña cycles is at most 2 months more than for El Niño cycles, the maturity of La Niña carbon flux responses last many months longer. By examining the evolution of the two individual El Niño events from the 1980s, we find that El Niño events normally decayed quickly in the second year while La Niña events normally took longer to decay. For example, 1982 and 1997 events decayed quickly in July/August of the second year. This quick decay of El Niño normally accompanies a quick change of climate which determines the terrestrial carbon response. Similarly, during La Niña periods, the longer persistence of F_{ta}, inversion-calculated flux, and CO_2 growth rate anomaly is the result of the slower decay of La Niña cycle. Not surprisingly, the later maturity of global F_{ta} anomaly in the overall ENSO composite comes from the contribution of the La Niña events to the composite. This is also true for the inversion fluxes and the CO_2 growth rate anomalies. Although there are some phase differences of variables between El Niño and La Niña composites, the overall ENSO composite still highlights the most important features of terrestrial responses to ENSO cycle, while using all the data at hand.

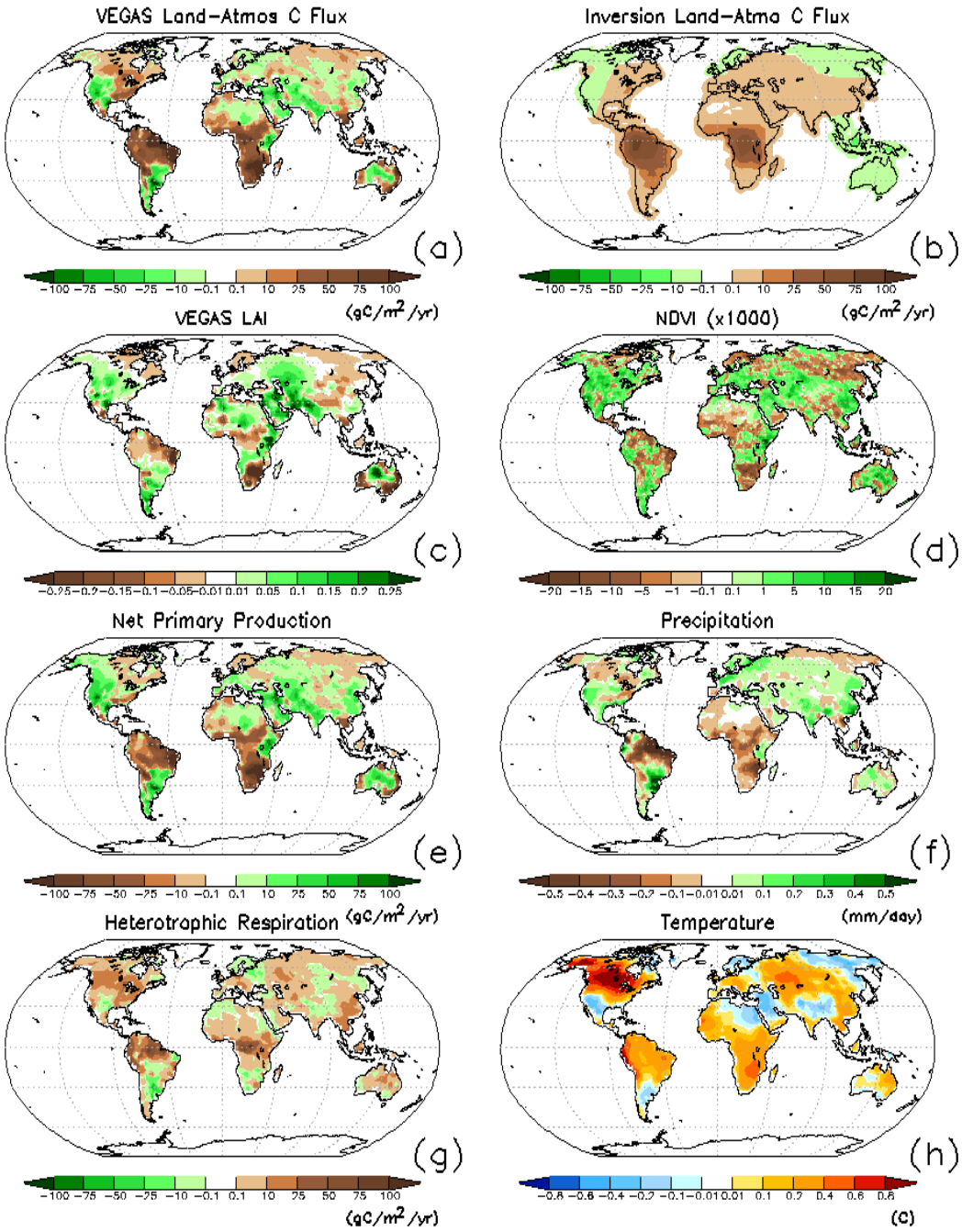

Figure 3.5 Spatial patterns of the anomalies of composite variables with 12-month averaging centered at the 6th month after MEI peak (as in Figure 3.3a) for: (a) Land-atmosphere carbon flux by VEGAS (F_{ta}) in unit of gC/m2/yr; (b) Land-atmosphere carbon flux by the inversion (gC/m2/yr). (c) LAI by VEGAS; (d) Satellite observed NDVI. (e) Net Primary Production (NPP) in gC/m2/yr; (f) Precipitation in mm/day; (g) Heterotrophic Respiration (R_h) in gC/m2/yr; (h) Surface air temperature in °C. Note: the shading for NPP is opposite to R_h and F_{ta}.

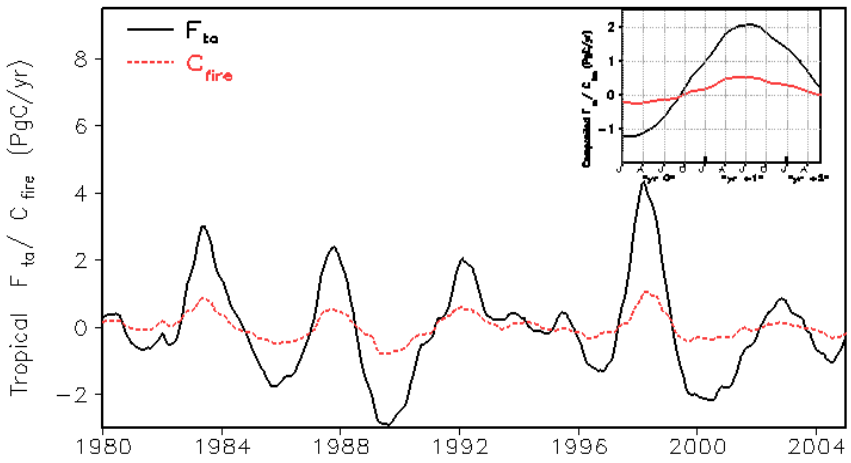

Figure 3.6 Time-series of the anomalies of modeled carbon flux due to biomass burning and total carbon flux in the tropics. The top right panel is the ENSO composites of these two variables, indicating the contribution of biomass burning to total carbon flux anomalies.

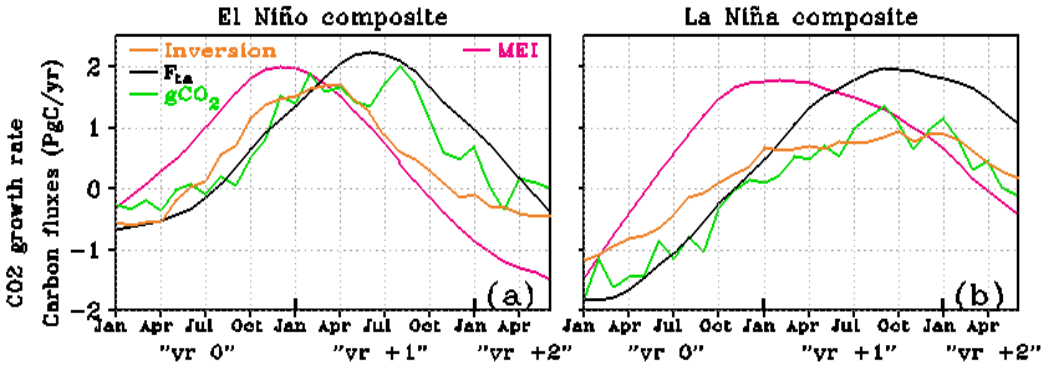

Figure 3.7 Tropical composites for (a) El Niño events only: 1982-83, 1986-87, 1994-95 and 1997-98; (b) La Niña events only: 1984-85, 1988-89, 1995-96, 1998-99. The selected variables are the same as Figure 3.3b.

3.4 Sensitivity Simulations to quantify the impact of climatic factors

Physical climatic factors like precipitation, temperature and soil moisture, etc. govern the terrestrial carbon cycle in the model. To elucidate and quantify the effects of individual climate forcing, we carefully designed 3 sensitivity simulations and compared them to the standard simulation (Table 3.1). The standard simulation is the

one in which temperature and precipitation are given from observations as discussed in the previous section. A "climatology" simulation in which the precipitation and temperature climatology is fixed provides input to one of the 3 sensitivity simulations. The sensitivity simulations are as follows: (1) "P-only" experiment, which uses the observed precipitation while using the climatology of temperature; (2) "T-only" experiment, which uses the observed temperature while using precipitation climatology; (3) "Swet-fixed" experiment, which is like "T-only", except soil moisture is also from climatology, not simulated by SLand model. Specifically, this soil moisture climatology comes from the "climatology" simulation described earlier. So, vegetation photosynthesis will see the variation of temperature; while the soil moisture changes due to evapotranspiration by temperature are excluded from vegetation photosynthesis in (3). This "Swet-fixed" simulation thus informs us of the indirect temperature effect on NPP through soil moisture, in contrast to the "T-only" simulation which includes both the direct effect of temperature and the indirect effect of temperature through soil moisture on NPP.

ENSO composites of these sensitivity simulations help quantify the effects of temperature, precipitation, and soil wetness on NPP/ R_h / F_{ta} and are shown in Figure 3.8 for the tropics. The period of maximum response (April to September of the "year +1") of the ENSO event is highlighted and the averaged values of those periods are calculated (Table 3.2). The percentage contribution of each climatic factor on F_{ta} is also provided (Figure 3.9). The period selected is based on the composite analysis and the lead-lag correlation in section 3.2.

Table 3.1 Changes in physical climate forcing (temperature/precipitation) in the sensitivity simulations. The same seasonal climatology of radiation, humidity and wind speed as well as constant CO_2 level for VEGAS, were used in all experiments listed.

Experiment	Physical climate forcing
Climatology	Climatology of temperature and precipitation, and soil moisture is simulated by SLand.
Standard	Observed temperature and precipitation, and soil moisture is simulated by SLand.
P-only	Observed precipitation while using the climatology of temperature, and soil moisture is simulated by SLand.
T-only	Observed temperature while using precipitation climatology and soil moisture is simulated by SLand.
Swet-fixed	In addition to "T-only", soil moisture is provided with the climatology from the "climatology" experiment rather than modeled by SLand in "T-only".

The mean global total of the F_{ta} anomaly for the selected period in the standard run is 1.68 PgC/yr, which is a little larger than that of the inversion model flux with 1.36 PgC/yr (Table 3.2). Both of them are larger than CO_2 growth rate which is 1.22 PgC/yr. This difference can be attributable to the net oceanic carbon uptake from the atmosphere during El Niño event and is within the range of previous estimates (Keeling and Revelle, 1985; Winguth et al., 1994; Feely et al., 2002; Bousquet et al., 2000, Plattner et al. 2002).

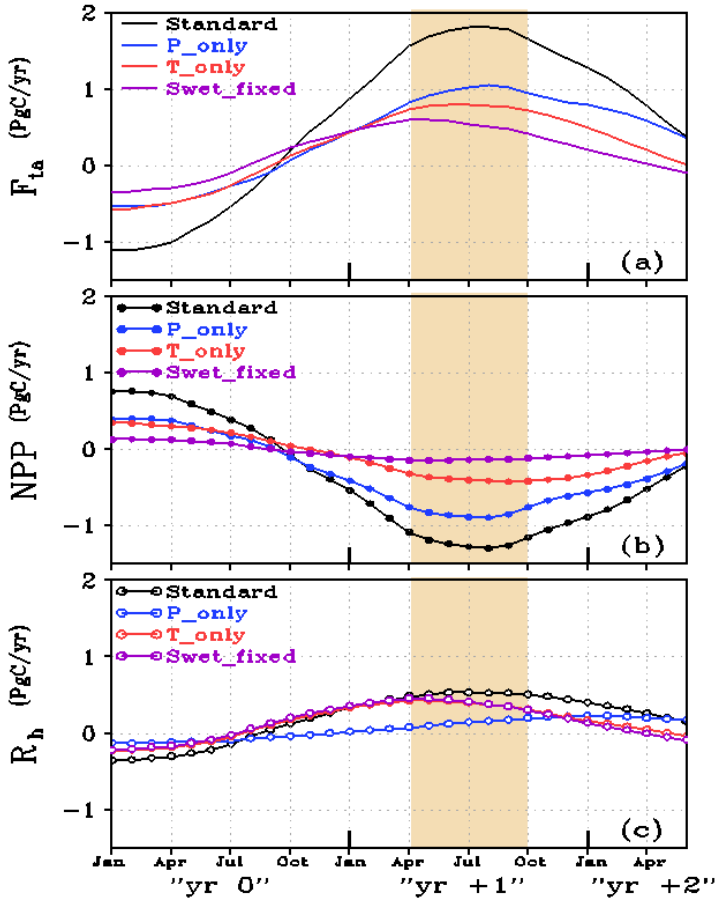

Figure 3.8 ENSO-composites of carbon fluxes for the sensitivity simulations: (a)VEGAS F_{ta} response in the tropics for the standard, "P-only", "T-only" and "Swet-fixed" sensitivity simulations; (b) the same as (a) except for NPP; (c) the same as (a) except for heterotrophic respiration. The shaded period of Apr.-Sep. of "yr +1" is the maximum regime of the response to the ENSO cycle. The carbon fluxes averaged in this regime are indicated in Table 3.2. Units in PgC/yr.

Table 3.2 Mean of composite global and tropical carbon fluxes during the peak response to ENSO (shaded area in Figure 3.8 corresponding to the 6-month average from April to September of "yr +1") for VEGAS standard, "P-only", "T-only", "Swet-fixed" experiments and CO_2 growth rate. Units in PgC/yr.

Region	Rödenbeck[a]	Standard	P-only	T-only	Swet-fixed
	RF	**F_{ta} (NPP/R_h)**	**F_{ta} (NPP/R_h)**	**F_{ta} (NPP/R_h)**	**F_{ta} (NPP/R_h)**
Global	1.36	1.68(-0.99/0.69)	0.74(-0.65/0.09)	0.95(-0.34/0.60)	0.79(-0.17/0.62)
Tropics	1.19	1.77(-1.21/0.56)	1.00(-0.86/0.14)	0.79(-0.34/0.44)	0.59(-0.13/0.46)
gCO_2	1.22				

[a] Rödenbeck et al. (2003) inversion modeling with 11 station measurements.

The tropical land-atmosphere carbon flux dominates the global total both in VEGAS and in the inversion model. However, in the standard VEGAS simulation, the extratropics acts as a relatively small carbon sink, while the inversion model indicates it as a small carbon source. In the tropics, out of the 1.77 PgC/yr F_{ta} variation, 1.21 PgC/yr comes from the suppression of vegetation (NPP) and the rest 0.56 PgC/yr from soil decomposition (Figure 3.8b, c). Our sensitivity simulations show a linear relationship of the effects of anomalous temperature and precipitation, on the terrestrial carbon cycle, particularly at the peak of the response. In reality, such effects, however, are extremely complicated and not well known. One possible reason is that the interannual variability can be considered as a small perturbation to the system (VEGAS), which itself is highly non-linear. Assuming an approximately linear relationship we can estimate that precipitation contributes about 1.0 PgC/yr, while temperature provides about 0.79 PgC/yr of the F_{ta} variation in the standard simulation. In the tropics, the "P-only" sensitivity experiment produced a change of -0.86 PgC/yr for the NPP anomaly, while soil decomposition decreases dramatically to 0.14 PgC/yr from 0.56 PgC/yr during this period. In the "T-only" simulation, the soil decomposition is remarkably enhanced due to warming, while less reduction of vegetation activity is seen. Spatially, the distribution of the regions with remarkable reduction of NPP in "P-only" is similar to the one in standard run, albeit with a smaller intensity (figures not shown). Compared to standard run, the regions with positive signal of soil decomposition shrink to encompass only Northern South America and Center Africa in the "P-only" run. The remarkable enhancements of soil decomposition due to warming and dramatic vegetation suppression due to drought

lie in the nature of the tropics, which are highly-decomposed and water-limited on the interannual timescale.

The absorption of water for vegetation depends on the water pressure level difference between the soil moisture and vegetation root. Thus vegetation activity closely follows soil moisture, rather than immediately responding to precipitation. However, soil moisture can be influenced by temperature through evapotranspiration. Thus precipitation affects NPP mainly through soil wetness, while temperature can influence NPP variation through soil moisture. In the "Swet-fixed" simulation, only -0.13 PgC/yr of NPP occurs compared to the -0.34 PgC/yr reduction in the "T-only" simulation, which reflect the indirect effect of temperature on the NPP through soil moisture. Spatially, the central Amazon basin and South Africa have much less vegetation suppression in the "Swet-fixed" run (spatial pattern not shown). The "Swet-fixed" sensitivity experiment indicates clearly that the indirect effect of temperature on the vegetation photosynthesis through soil wetness is significant, even a little larger than the direct temperature effect on the photosynthetic processes in the tropics in model. This is interesting because the tropics always has favorable temperature conditions for vegetation year-round, while the change in water supply during the ENSO period can drastically affect the vegetation growth.

Figrue 3.10 is a schematic diagram of the percentage of relative contribution of the individual and combined effects of precipitation and temperature on the variation of F_{ta} in the tropics during ENSO. Values used to calculate the percentages were obtained from Table 3.2 which correspond to a 6-month average (April to September) at the peak of the ENSO response. Some are obtained as a direct result of

the simulations, while the rest are obtained as residuals. The tropical ENSO response of the total carbon flux into the atmosphere is a result of 68% of photosynthesis and 32% of soil decomposition as obtained from the standard simulation. We estimated that out of the total land-atmosphere carbon flux, about 25% of that is due to biomass burning, which is accounted in the vegetation and soil respiration portion. Precipitation is the major contributor to photosynthesis variability while temperature controls soil decomposition. In terms relative to the variation of F_{ta}, precipitation contributes about 56% of the variation mainly through soil wetness in photosynthesis, while temperature accounts for 44%, as seen from the total flux of the "P-only" and "T-only" experiments. The total effect of temperature arises from direct and indirect effects. The direct effect is through a 26% influence on soil respiration and a 7% influence on respiration of vegetation as obtained from the "Swet-fixed experiment". The remaining contribution of temperature is through its indirect effect by which photosynthesis is affected by temperature changes affecting evaporation and thus changing soil moisture. This indirect effect of temperature is 12% of the total variation and is obtained as the difference between the "Swet-fixed" and "T-only" experiment. This indirect effect is highly complicated and has not been studied in the past. The total effect of soil wetness on the total flux into the atmosphere is obtained as a residual of the remaining terms, and 61% affects photosynthesis, while 6% affects soil decomposition.

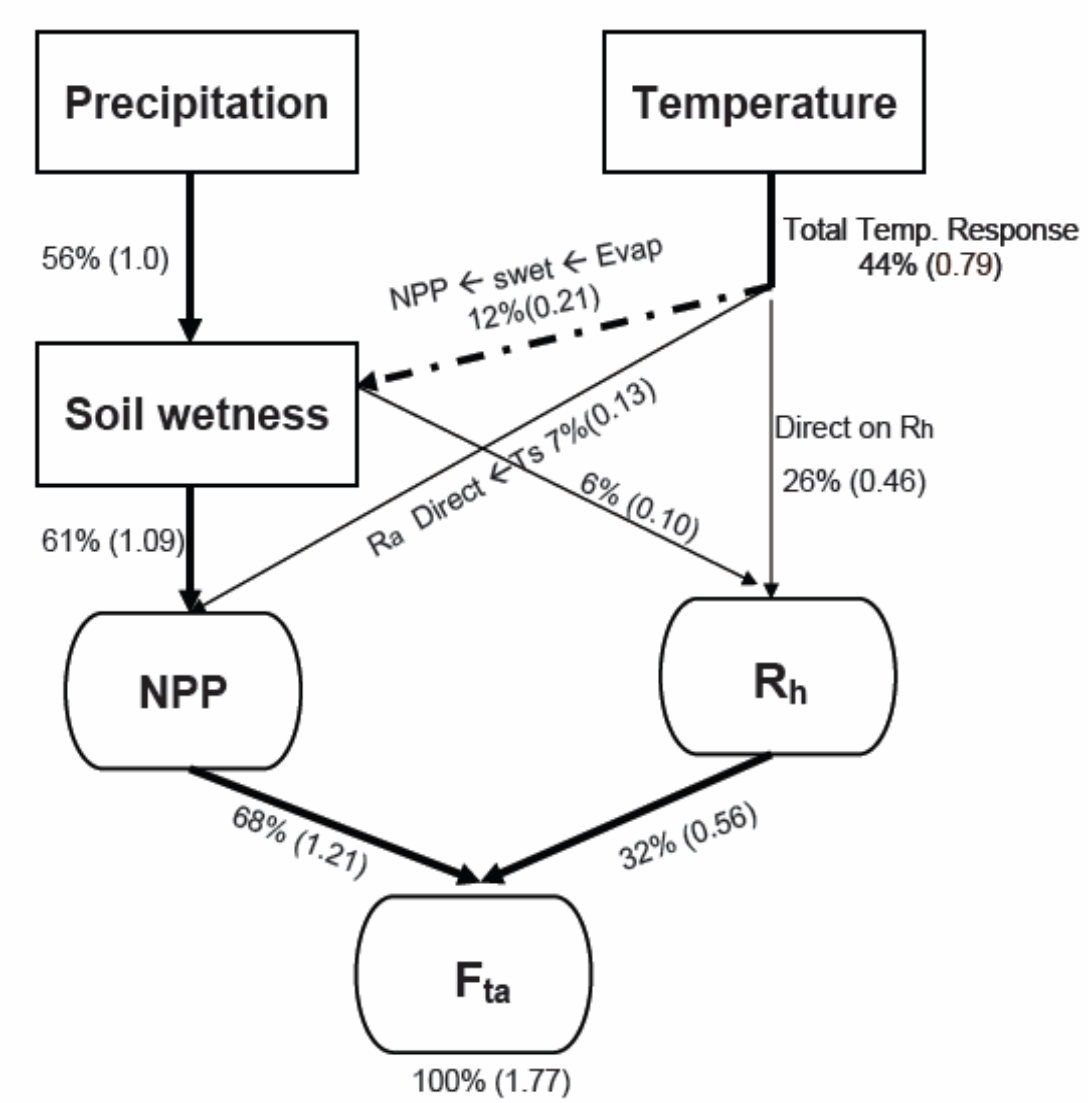

Figure 3.9 A conceptual diagram of the mechanism of tropical terrestrial carbon response to the ENSO cycle. The percentages refer to the contribution to F_{ta} variation (100%), with carbon flux anomalies in parenthesis (PgC/yr). These carbon fluxes are estimated from Table 3.2. The climate fields, such as precipitation, temperature and soil wetness are shown as rectangles and the corresponding NPP/Rh/ F_{ta} as rounded rectangle. The dashed arrow indicates the indirect effect of temperature on NPP through soil wetness. The solid lines in black from temperature are the direct effects of temperature on soil decomposition and on NPP. All processes are contributable to F_{ta} in the same direction (for example, increase of soil decomposition and decrease of vegetation growth during El Niño)

3.5 Conclusion and discussion

In this study, we have used VEGAS to investigate the response of the terrestrial carbon ecosystem to the physical climate variations and to isolate those effects, especially the ones associated with ENSO. The results of the model are first evaluated against observations to verify its capability in capturing the interannual variability. The simulated global total land-atmosphere carbon flux (F_{ta}) in our study agrees well with the results of inversion modeling based on the global observations on interannual timescales, especially in the tropics. Both of them are in agreement with the atmospheric CO_2 growth rate variation. The land-atmosphere carbon flux in the tropics has a similar magnitude as the global total, confirming the dominant role of the tropics on interannual timescale. This underscores the importance of extending the observational network in the tropics in the future.

Our analysis of ENSO composite and lead-lag correlation indicate that in the tropics VEGAS simulates a robust signal of F_{ta} with a 6-month lag of the ENSO cycle. This is largely caused by the suppression of vegetation and enhancement of soil decomposition, as suggested by the "conspiracy" theory of Zeng et al. (2005a). Though the anomalous precipitation lags the ENSO cycle by 1-2 months, the vegetation-dependent soil moisture takes about 5 months to respond due to soil memory. Less precipitation, with higher temperature drains the soil moisture and results in drought condition unfavorable for vegetation activities. This results in a 6-month lag of the NPP to ENSO. During El Niño, large areas of vegetation suppression occur in Brazil, equatorial Africa and South Africa. Simultaneously, higher temperature directly enhances soil decomposition in northern Brazil, equatorial

Africa. As a result, reduction of NPP and enhancement of R_h contributes in same direction and provide a large amount of carbon release to the atmosphere. The opposite is true for La Niña, although the time-dependence of the lags differs from El Niño.

Sensitivity simulations were performed to elucidate and quantify the effects of precipitation and temperature on the tropical terrestrial ecosystem. During ENSO events, the precipitation and temperature have very different mechanisms in regulating the above variation of vegetation growth and soil decomposition. A near linear relationship of terrestrial carbon response to the anomalous precipitation and temperature was found in model. In total, precipitation variation contributes to about 56% of F_{ta} variation, mostly through soil wetness in the photosynthesis process, while temperature accounts for 44%, which includes 25% from direct effect on the soil decomposition, 7% from its direct effect on vegetation respiration and 12% from its indirect effect on the photosynthesis through soil wetness. Such an indirect effect is significant, and has not been studied in the past. As a result, in the tropics vegetation activity suppression (effects on NPP) contributes 68% of variation of F_{ta}, with the remaining 32% coming from soil decomposition under a warmer and drier condition. Out of the total land-atmosphere carbon flux, about 25% is due to biomass burning, which is included in the vegetation and soil respiration.

Due to spatial cancellation and weak ENSO teleconnections, the response of the terrestrial system in middle and high latitudes is less robust and more complex. The interannual variability of the land-atmosphere carbon flux in the extratropics is complicated by other modes of climate variability, such as the Pacific North

American pattern of variability, the Atlantic Oscillation and Northern Annular Mode (Potter et al., 2003; Buermann et al., 2003; Russell and Wallace, 2004). Moreover, the role of solar radiation in control of vegetation activity is still in debate and has not been addressed in this study (Gu et al., 2003; Angert et al., 2004).

The results in this study are based on a single vegetation model and hence could be model dependent. Yet it has been useful in addressing the canonical response of the terrestrial carbon flux to ENSO. The linear response observed in the tropics helped quantify the mechanisms through which precipitation and temperature affect the carbon flux directly and indirectly, thus highlighting the importance of soil moisture on vegetation. Improved observations and advanced modeling studies are required to quantify exactly the terrestrial carbon cycle under changing climate.

Chapter 4: Impact of 1998–2002 Midlatitude Drought and Warming on Terrestrial Ecosystem and the Global Carbon Cycle

4.1 Introduction

The interannual variability in the atmospheric CO_2 growth rate is dominated by tropical land response to ENSO due to the constructive plant and soil physiology affected by patially coherent tropical climate anomalies (Bousquet et al., 2000; Zeng et al., 2005a; Qian et al., 2008). Changes in the carbon sources and sinks in Midlatitude regions, on the other hand, often tend to cancel each other, so the overall variability is weakly correlated with ENSO and it contributes only to a small fraction of the interannual variability in atmospheric CO_2.

A growth rate of over 2 ppm/yr during 2002–2003 was unprecedented from the MLO station record (Jones and Cox, 2005). Although the yearly growth rate was somewhat smaller than during the short-lived 1997–98 El Niño event, the 2001–2003 growth was sustained longer so that the bi-yearly peak is highest ever when the data is smoothed with 24 month running mean (Figure 4.1a). In the meantime, the 1998–2002 drought spanned much of the Northern Hemisphere Midlatitudes, with great severity in the regions of the western US, southern Europe, Southwest Asia, eastern Asia and Siberia (Waple et al., 2002; Hoerling and Kumar, 2003) (Figure 4.2a), with wide spread impacts such as wildfires in the western US.

In this section, we examine VEGAS offline simulation results to establish the relationship between the drought and the anomalous behavior in the carbon cycle,

which serves as the clue for determining the causes of such an anomalously higher CO_2 growth rate during 2002–2003. Atmospheric CO_2 inversion model results (Rödenbeck et al., 2003), and satellite observed vegetation index NDVI (Tucker et al., 2005) are used to compare with the VEGAS simulation.

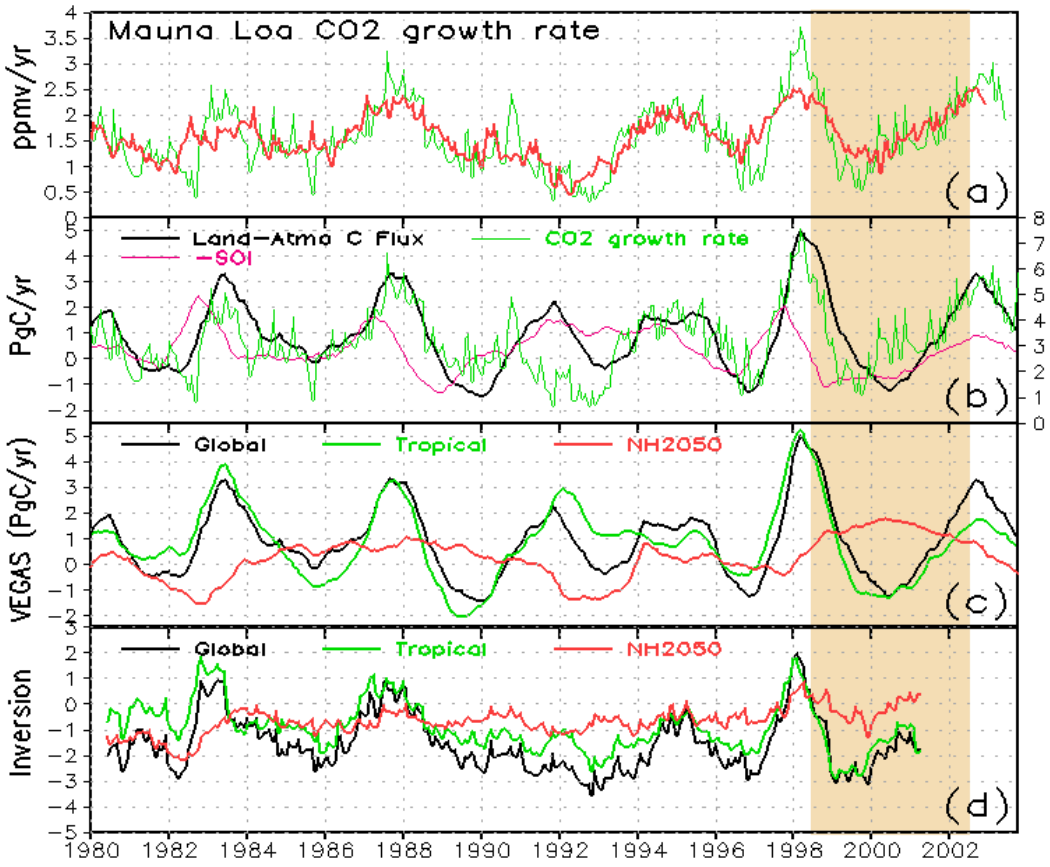

Figure 4.1 (a) Growth rate of atmospheric CO_2 observed at Mauna Loa, Hawaii from 1980 to 2003; a 12 month running mean (green) was used to remove the seasonal cycle, and 24 month running mean (red) was used to emphasize the lower frequency variability. (b) VEGAS simulated total land-atmosphere carbon flux (black), compared to Mauna Loa CO_2 growth rate (green, labeled on the right) and ENSO signal (the negative southern oscillation index: -SOI, in purple; mb labeled on the left). (c) VEGAS simulated global (black), tropics (20˚S-20˚N, in green) and Northern Hemisphere Midlatitude (20˚N-50˚N, in red). (d) Same as in (c) but from the atmospheric inversion of Rödenbeck et al. (2003). Seasonal cycle has been removed from all figures except where otherwise noted. Shading is for the June 1998–May 2002 period during which Northern Hemisphere Midlatitude released anomalously large amount of CO_2, modifying the normally tropically dominated ENSO response both in terms of amplitude and phasing.

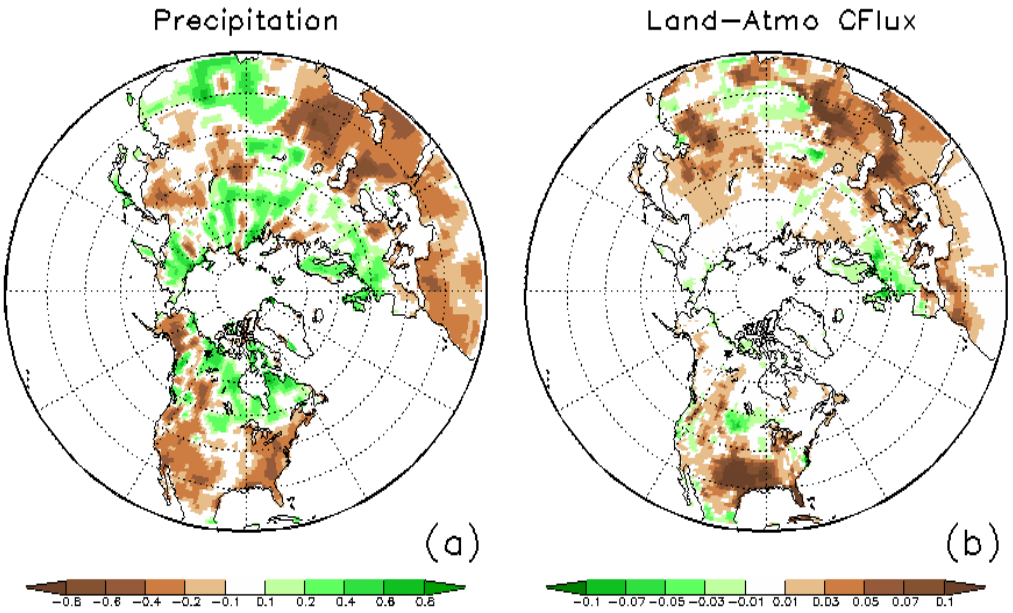

Figure 4.2 Anomalies for the period June 1998–May 2002 relative to the climatology of 1980–2003 for: (a) precipitation (Xie and Arkin, 1996) normalized by local standard deviation, (b) VEGAS modeled land-atmosphere CO_2 flux (kgC /m2/yr).

4.2 Drought and CO_2

VEGAS modeled global land-atmosphere carbon flux variability shows a general agreement with MLO CO_2 growth rate (Figure 4.1a, b), as well as with the global flux from an atmospheric inversion model study (Rödenbeck et al., 2003) (Figure 4.1d). On regional scale, both tropical and Northern Hemisphere Midlatitude show overall agreement with inversion results. However, in the drought period of 1998–2002, Midlatitude land regions are largely CO_2 sources to the atmosphere (Figure 4.2b). The most pronounced source anomalies are in the western US, Southwest Asia and Northeast Asia, while only small sinks are found in Canada and northern Europe. Although the detailed spatial pattern of these anomalies varied somewhat over time (not shown), the persistence of this Midlatitude drought and

carbon cycle response is striking, as during the same 4 year period, the tropics switched sign from the large 1997–98 El Niño to 1999–2001 La Niña and back to the modest 2002–2003 El Niño.

Over most of the period, the Northern Hemisphere land between 20˚N and 50˚N is a nearly constant source releasing 1.3 PgC/yr more than usual relative to the 1980-98 average. The inversion for the same region (Figure 4.1d) shows similar trend, with an anomalous flux from 1998-2001 larger than any other time during the 22 year period of the inversion. In particular, carbon flux changed from 1980–98 mean sink of 0.7 PgC/yr to nearly neutral for 1998–2001, with excursions as source in 1998 and 2001. Part of the difference between VEGAS and the inversion model may be that drought impact was partially alleviated by heavy land management such as irrigation in these regions. Since VEGAS did not include anthropogenic CO_2 emission, volcanic eruptions, or oceanic uptake effects, the modeled total land-atmosphere flux is overall shifted compared to inversion so that only the relative changes are comparable.

Another clue of the importance of the Midlatitude drought on the carbon cycle comes from the timing of the events. Typically, MLO CO_2 growth rate correlates well with ENSO signal with maximum correlation 0.59 at a lag of 5 months (here we use Southern Oscillation Index: SOI) (Zeng et al., 2005a, Qian et al., 2008). Though there is some difference between MEI and SOI (Wolter and Timlin, 1998), both of them are good ENSO phase indices with respect to the relationship to CO_2 growth rate. This lag is due to the delayed response in hydrology and biological activity to ENSO-related climate anomalies in the tropics. During 1998–2003, this normality was disrupted by the drought-related Midlatitude carbon release so that the CO_2 recovery

to higher post-ENSO event values after the 1999–2001 La Niña arrived several months earlier than usual. For instance, there is an early rise in MLO CO_2 growth rate in 2000, and the peak during 2002–2003 slightly leads SOI, rather than following the normal 5-month lag. If the Northern Hemisphere anomalies had been zero during 1998–2002, the tropical anomaly alone would have produced a significantly smaller CO_2 increase (Figure 4.1c), whereas observations shows a sustained and unprecedented 2–3 year period of fast growth in CO_2.

4.3 Regional contributions and mechanisms

The overall agreement between model simulated land-atmosphere carbon flux and MLO CO_2 growth rate suggests the usefulness of further analysis of regional characteristics and mechanisms. The modeled leaf area index (LAI; Figure 4.3a) follows precipitation closely with reduction in the western US and northern Mexico, Southwest Asia, and East Asia, while LAI increased in northeastern Canada and central Europe. The LAI increase in the latter two regions is partly due to warming (Figure 4.3f) because temperature is a limiting factor for growth, especially in northeastern Canada. The modeled LAI shows a generally good agreement with the satellite observed normalized difference vegetation index (NDVI), but some differences exist particularly in Southwest Asia where reduced NDVI is somewhat north of the modeled LAI. Because the spatial anomaly patterns varied over time (Lotsch et al., 2005), modeled LAI and NDVI may compare better on a year to year basis. More importantly, land use and management that was not included in the model likely have modified the natural response significantly. The general agreement in these regions is in some sense remarkable, suggesting natural climate variability

nonetheless manifests itself prominently.

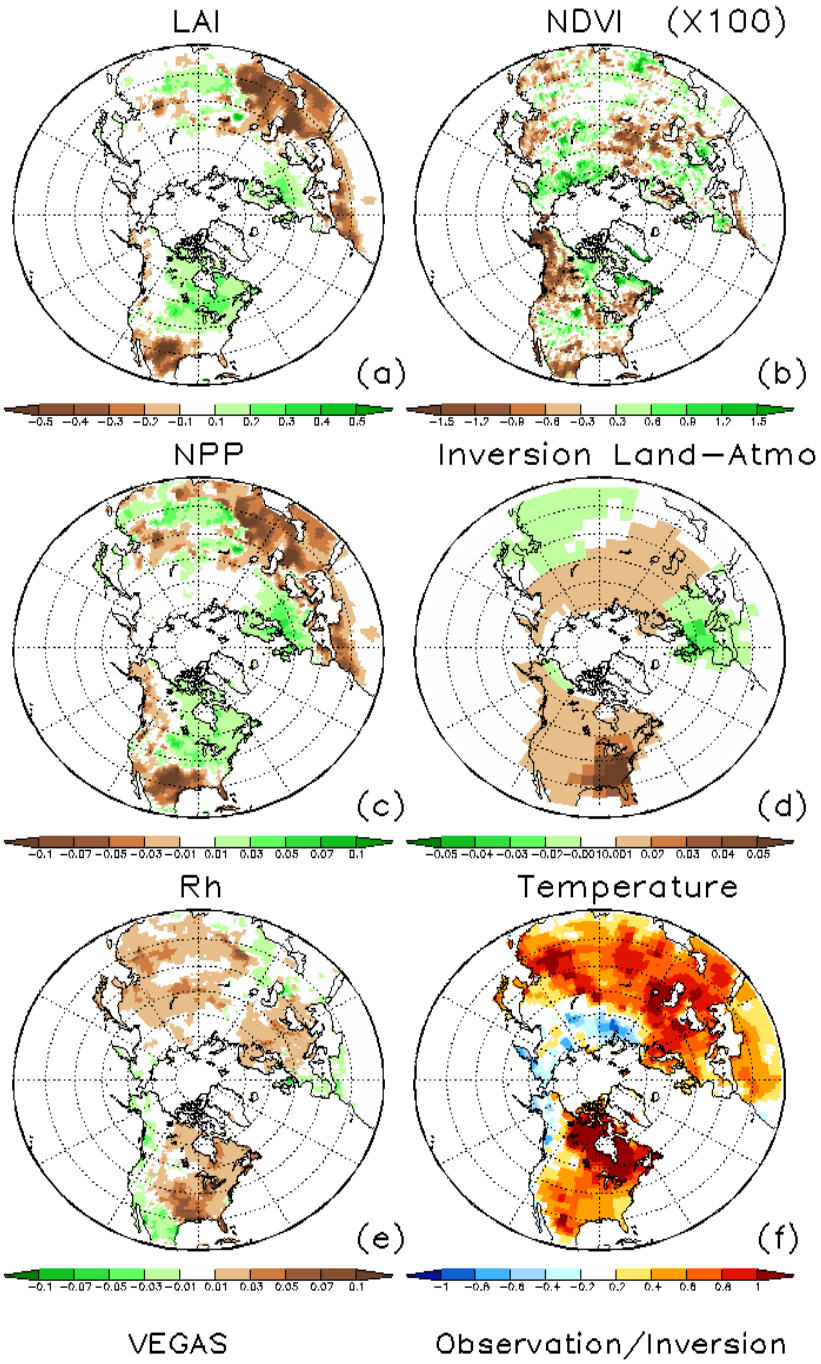

Figure 4.3 Anomalies of the period June 1998–May 2002 for (a) VEGAS modeled Leaf Area Index (LAI); (b) observed normalized difference vegetation index (NDVI); (c) modeled Net Primary Production (NPP, kgC/m^2/yr); (d) land-atmosphere flux from inversion of Rödenbeck et al. (2003) with 11 CO_2 stations (kgC/m^2/yr) for 1998–2001; (e) modeled soil respiration (R_h, kgC/m^2/yr); (f) observed surface air temperature (˚C).

The simulated anomalies in NPP in the Northern Hemisphere Midlatitude largely follow the precipitation change. However, the spatial extent of regions with reduced NPP is larger while the area with positive NPP anomalies shrank (see Figure 4.3c and 4.2a). This is mostly due to the enhanced autotrophic respiration in response to general warming over this period (Figure 4.3f). This tendency is further enhanced in the total land-atmosphere carbon flux (Figure 2b) because heterotrophic soil respiration (Figure 4.3e) also increased in response to the warming. As a result, the Northern Hemisphere Midlatitude was predominantly a CO_2 source to the atmosphere during 1998 –2002 with a spatial extent larger than the area affected by reduced precipitation.

Regional patterns from the inversion (Rödenbeck et al., 2003) (Figure 4.3d) indicate that from May 1998 to October 2001, most of North America is a carbon source especially in the US. There is a moderate carbon sink in central Europe, consistent with our forward model (Figure 4.2c). The inversion also shows a band of source areas covering southwest to central and East Asia, albeit very weak compared to modeled anomalies. The inversion may not resolve the sub-continental variations especially in Eurasia due to the lack of CO_2 station there.

From 1980 to 2003, VEGAS land-atmosphere carbon flux shows high correlation with precipitation (Figure 4.4a-c), and different regions differ in their detailed temporal evolutions. The drought in Eurasia (Figure 4.4c) started early and peaked in 1999–2000, with largest contribution from Southwest Asia for the first half, and significant contribution from Northeast Asia for the latter half (not shown). In contrast, drought in western US occurred between 2000 and 2003. Similar to the

forward model, the atmospheric inversion shows an anomalous increase early in 1998 from Eurasia and another increase from North America in 2000–2001. However, these two events are further apart in time in the inversion, so that the total flux has a minimum in 1999, while the forward model has a more sustained peak from 1998 to 2002.

Temperature also played an important role during 1998–2002 and in the overall evolution. For instance, the total Midlatitude carbon flux during 1998–2002 is 0.7 PgC/yr larger than the period 1984–1989, while precipitation is only modestly smaller (Figure 4.4a). This is partly because the recent drought hit the more sensitive semi-arid regions, and partly because the long-term warming trend leads to more respiration in the 1998–2002 period so that the net carbon flux is significantly higher. The importance of warming on carbon loss can be seen more clearly in two model sensitivity experiments in which either precipitation or temperature alone were used to force the physical land-surface and the carbon model (Figure 4.4e). During the 1998–2002 period, temperature-induced carbon release had somewhat smaller peak amplitude but lasted longer than the precipitation-induced anomalies. Interestingly, the temperature effect was significantly smaller during previous periods such as 1984–1989, another indication that the recent drought was unusual. The pathway by which warming influences carbon flux is through the direct effect of more respiration loss, and though an indirect effect as higher temperature leads to larger evaporation and also more severe drought (Wetherald and Manabe, 1995).

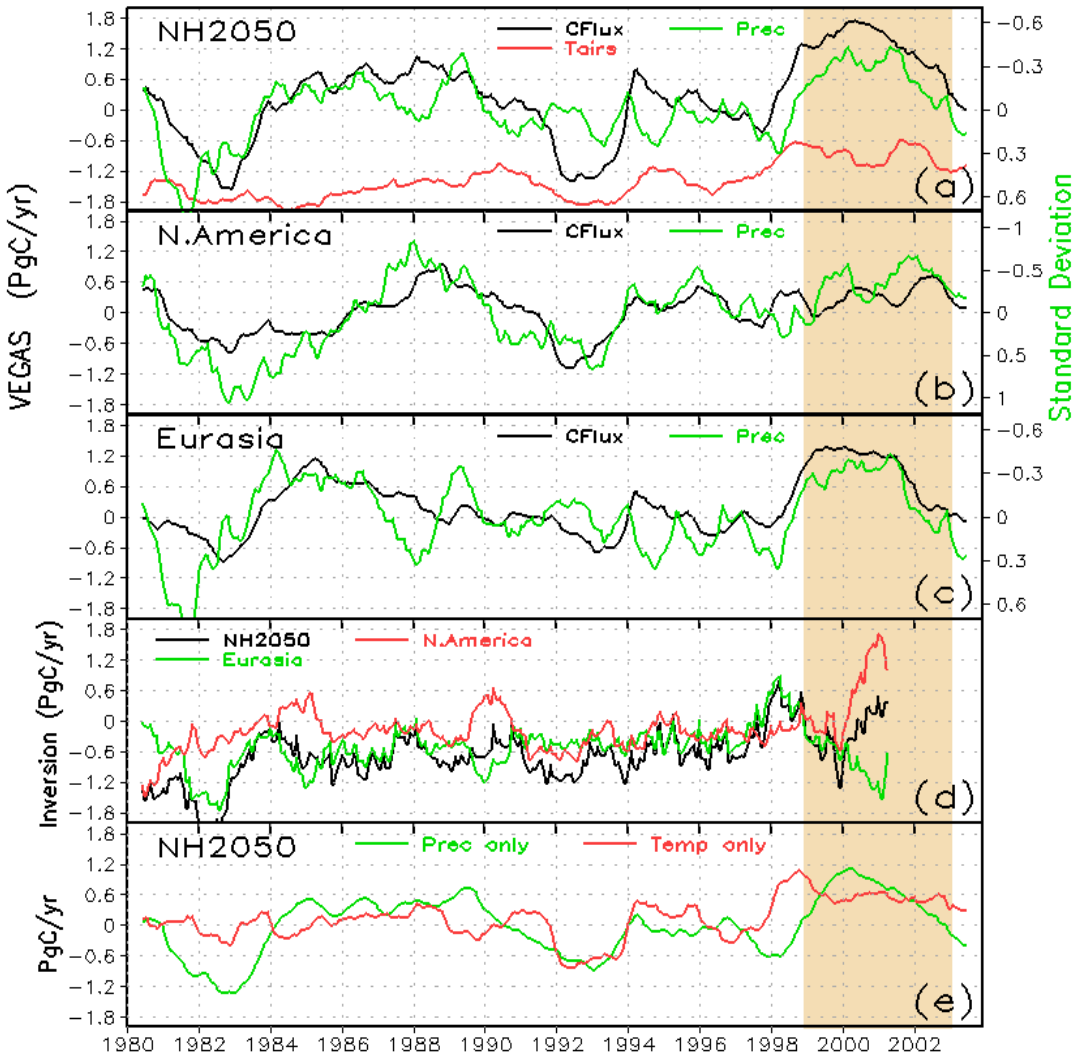

Figure 4.4 Observed precipitation (normalized by standard deviation; green) and temperature (red; not labeled: the range from minimum to maximum is 1.6 ˚C), and VEGAS modeled land-atmosphere carbon flux (black) for (a) Northern Hemisphere Midlatitude (20˚N–50˚N); (b) North America 20˚N–50˚N; (c) Eurasia 20˚N–50˚N. Also plotted in (d) is carbon flux for the same three regions from the inversion. (e) Modeled Northern Hemisphere Midlatitude carbon flux from two sensitivity experiments using "P-only" or "T-only" as forcing.

4.4 Conclusion and discussion

While climate models generally predict Midlatitude drying under global warming (Wetherald and Manabe, 1995), the changes in precipitation patterns and subsequent terrestrial carbon response are highly uncertain (Zeng et al., 2004). Our results suggest that the 1998–2002 Midlatitude drought was a response to reduced precipitation and increased temperature, with widespread consequences to the terrestrial ecosystem and the global carbon cycle, highlighted by the anomalous increase in atmospheric CO_2 growth rate in recent years (Jones and Cox, 2005). However, new record of CO_2 emissions from fossil-fuel burning and industrial processes may cloud the contribution from the land-atmosphere carbon flux for the higher CO_2 growth during 2002-2003. Raupach et al. (2007) found that CO_2 emissions have been accelerating at a global scale, with their growth rate increasing from 1.1%/yr for 1990–1999 to >3%/yr for 2000–2004. Further analysis to quantify the contribution of CO_2 emission and biosphere in response to climate variation thus are needed to provide a close accounting for the recent acceleration of CO_2 growth rate.

However, this 1998–2002 Midlatitude drought is unusual. The spatial extension of it has been attributed to a synergy of surface temperature changes across the tropical oceans. In addition to the usual changes associated with a La Niña cold event in the eastern Pacific Ocean, this wide-spread drought was significantly influenced by simultaneous warming in the western Pacific and the Indian Ocean (Hoerling and Kumar, 2003). Although not a perfect analog of global warming, since such conditions may become more likely (Stott et al., 2004), this event provides a

glimpse into the possible future carbon cycle response to climate change.

Chapter 5: How Strong is Carbon Cycle-Climate Feedback under Global Warming?

5.1 Introduction

More than half of the anthropogenic CO_2 emission has been taken up by sinks in the ocean and over land (Prentice et al., 2001). The magnitude of future climate change depends critically on the behavior of these carbon sinks. One major feedback involves the change in these carbon sinks in response to climate change such as changes in temperature and precipitation patterns. Coupled carbon-climate modeling from the Hadley Centre (Cox et al., 2000; Betts et al., 2004) and IPSL (Friedlingstein et al., 2001; Dufresne et al., 2002; Berthelot et al., 2002) which took into account such feedbacks, showed large uncertainties in the predicted strength of carbon-climate feedback and its impact on climate prediction. For instance, changes of the terrestrial carbon pools in these two models differ not only in magnitude but also in the direction. Here we present results from a fully coupled carbon-climate model and discuss the similarities and additional differences from the above two predictions.

5.2 Model and methodology

In Chapters 2, 3 and 4, VEGAS was run in offline mode. In this chapter, we build an Earth system model. It includes two major components: physical climate and carbon cycle (Figure 5.1). The physical climate component of the model usually consists of atmosphere/land/ocean models and the carbon cycle component includes a land/ocean carbon cycle model. Here we focus on the carbon cycle, so the Earth

system model does not have other important biogeochemical cycles, such as Nitrogen, Sulfur, etc. This Earth system model is named UMD in our study. In UMD, the physical climate component consists of a global version of the atmospheric model Quasi-equilibrium Tropical Circulation Model (QTCM) (Neelin and Zeng, 2000; Zeng et al., 2000) and a slab mixed-layer ocean model with Q-flux to represent the effects of ocean dynamics (Hansen et al., 1983). The mixed-layer ocean depth is the annual mean derived from Levitus et al. (2000). QTCM is of intermediate complexity suitable for the modeling of tropical climate and its variability. It occupies a niche among climate models between complex general circulation models and simple models. The primitive-equation-based dynamical framework is constructed using analytical solutions from the quasi-equilibrium convective parameterization as the first basis function of a Galerkin representation of vertical structure. A uniqueness of the QTCM is its balanced treatment of dynamics and physical parameterizations. It includes a linearized longwave radiation scheme, simple cloud prediction and shortwave radiation schemes (http://www.atmos.ucla.edu/~csi/qtcm_frm.html). The land surface model SLand is included in QTCM. UMD's carbon cycle component includes VEGAS and a box ocean carbon model. The box ocean carbon model has 3 ocean carbon pools with different turnover times: upper ocean carbon, deep ocean carbon, and sediment carbon. The ocean-atmosphere carbon flux exchange depends on the sea temperature. However, UMD doesn't consider complicate oceanic biochemical processes which could affect carbon sequestration.

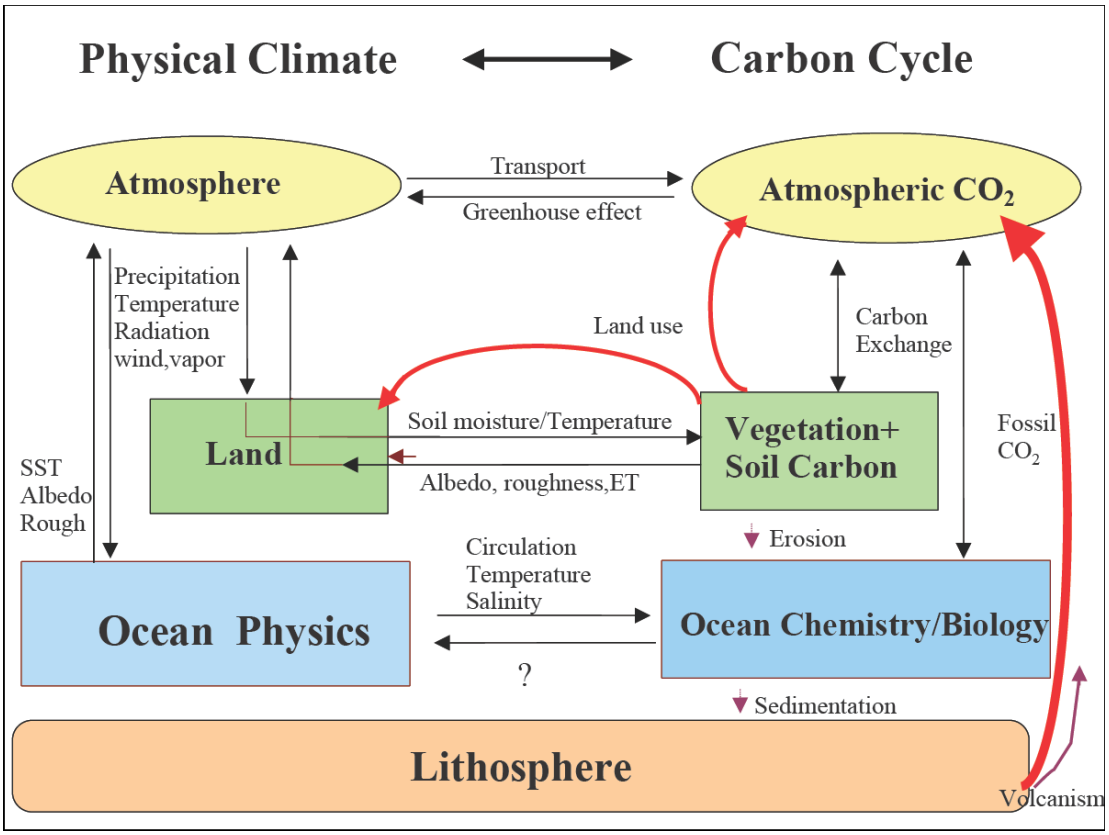

Figure 5.1 A conceptual diagram of the Earth system, divided into components consisting of physical climate and carbon cycle. The arrows indicate the major physical and biological processes, including those affecting carbon. The arrows in red are associated with the human activities for the carbon cycle. In UMD, the physical climate component includes an atmospheric model QTCM, a slab mixed-layer ocean model and the SLand unit, which handles processes such as soil moisture storage, but not carbon. VEGAS and a box ocean carbon model serve as the carbon cycle components.

Experiments conducted with UMD are indicated the in Figure 5.2. The fully coupled carbon-climate model (UMD) was run to a pre-industrial steady state (apart from high frequency internal variability) at year 1790. During this spinup process, the atmospheric CO_2 was nudged to an observed value of 281 ppm so that the carbon pools and climate simulated are close to observations. The model was then run in a freely coupled mode from 1791 to 2100 (results analyzed for 1860–2100), with no other changing external forcing except for the anthropogenic CO_2 emission, taken

from the IPCC-SRES A1B scenario. This run is referred to as the coupled run. In order to delineate the effects of carbon-climate feedback, another run was conducted by using a constant CO_2 level of 281 ppm in the longwave radiation module of the atmospheric model. Thus the carbon model sees a nearly constant climate without global warming, but carbon components are fully interactive including CO_2 fertilization effect and emission. This run is termed as the uncoupled run. Such an experiment has been referred to as an "offline" simulation by Cox et al. (2000), or "prescribed climate" by Dufresne et al. (2002), and uncoupled by Friedlingstein et al. (2003). The difference between the coupled and the uncoupled run is an indicator of the strength of carbon-climate feedback.

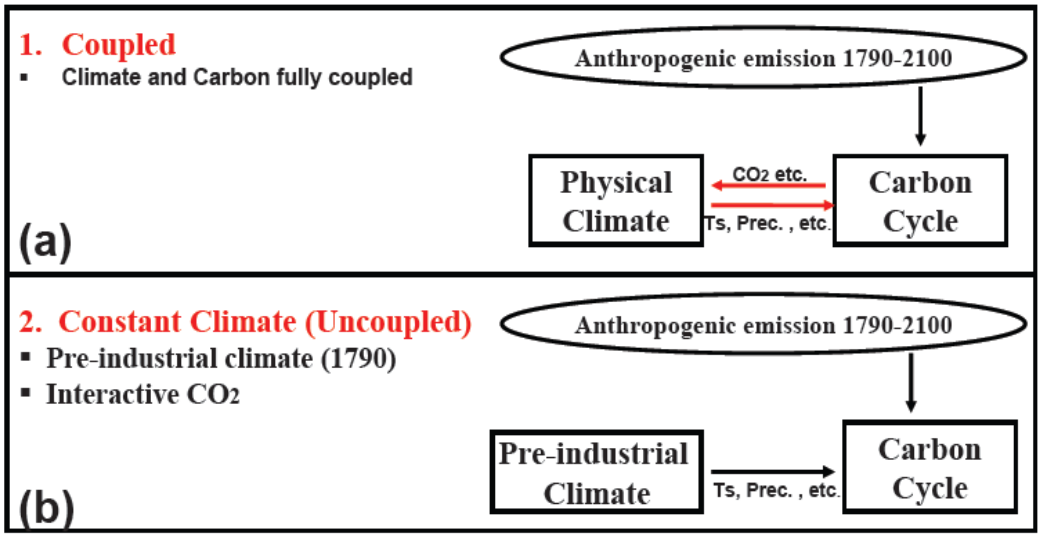

Figure 5.2 Model experiments: (a) Coupled: the physical climate and carbon cycle model are fully coupled from 1791 to 2100, with no other changing external forcing except for the anthropogenic CO_2 emissions. (b) Uncoupled: the carbon model sees a nearly constant climate without global warming, but carbon components are fully interactive including CO_2 fertilization and emission. Then an additional simulation where the CO_2 is from uncoupled run was used to force the physical climate model to calculate the surface temperature increase, similar to conventional GCM global warming simulations. The external anthropogenic emission used IPCC-SRES A1B scenario.

5.3 Carbon cycle-Climate feedback

By year 2000, the UMD coupled run simulated 15 ppm higher CO_2 compared to the observations, while the uncoupled CO_2 is very close to the observation (Figure 5.3a). The surface temperature in the coupled run has risen by about 0.6˚C, comparable to the observed overall warming (Figure 5.3b). Since the multi-decadal surface temperature changes in the 20th century are likely affected by factors not considered here such as solar variability, aerosol and non-CO_2 greenhouse gases (Stott et al., 2000; Jones et al., 2003b), such level of agreement indicates a reasonably good representation of the past climate changes. During this historical period, our uncoupled run simulates a cumulative land sink of 28 PgC and an ocean sink of 178 PgC, which is much stronger than the 100 PgC of the Hadley model (Cox et al., 2000). This strong ocean uptake partly compensates for our weak land sink so that CO_2 level in 2000 is only slightly higher than the observed value.

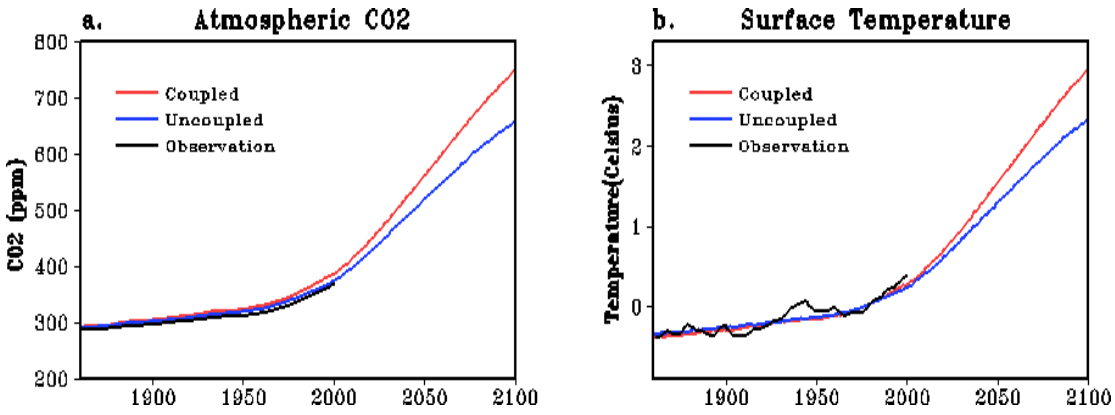

Figure 5.3 (a) Atmospheric CO_2 (ppm) and (b) surface temperature change (˚C) from 1860 to 2100, simulated by the fully coupled carbon cycle-climate model (in red), with constant (pre-industrial) climate (in blue), compared to observations (in black). The surface temperature curve labeled in uncoupled was obtained by an additional simulation where the CO_2 from uncoupled run was used to force the physical climate model, similar to conventional GCM global warming simulations.

By 2100, atmospheric CO_2 reached a level of 658 ppm in the uncoupled run, but the coupled run produced a CO_2 level of 748 ppm, 90 ppm higher. As a result, the coupled run surface temperature is 0.6˚C higher by 2100 (Table 5.1). These results indicate a positive feedback from the interactive response of carbon cycle to climate change, because the only difference in the two runs is the climate forcing for the carbon cycle, thus supporting the results from the Hadley Centre (Cox et al., 2000) and IPSL (Friedlingstein et al., 2001; Dufresne et al., 2002). However, the magnitude of the change differs significantly among the three models (Table 5.1). UMD model predicts about 90 ppm additional CO_2 due to climate impact on the carbon cycle, which implies a 0.6˚C additional warming, while the Hadley model shows 250 ppm more CO_2 and 1.5˚C additional warming. The IPSL model results are more similar to ours in terms of these changes, but other aspects differ greatly (see below).

Table 5.1 Differences of the atmospheric CO_2 (ppm) and surface temperature (˚C) changes from 1860 to 2100 between the coupled run and the uncoupled runs from UMD, Hadley Centre and IPSL.

	ΔCO_2	ΔTs
UMD	90	0.6
Hadley	250	1.5
IPSL	75	0.6

Part of the differences are due to the different climate sensitivity to a given CO_2 change. For instance, our coupled run has a warming of about 3˚C at year 2100, while it is 5.5˚C for the Hadley model and 3˚C for the IPSL model. These numbers are compounded with the strength of the carbon cycle feedback. It should be noted that the IPCC-SRES-A2 scenario used by IPSL has about 300 PgC larger cumulative

emissions than the IPCC-SRES-A1B scenario we used which is more similar to the IS92a used by Hadley. The difference in ocean carbon models are also partly responsible, especially given the simplicity of the box model we used. From 1860 to 2100, ocean in our coupled run absorbs 867 PgC, about 49% of the cumulative 1780 PgC emission, somewhat larger than the 700 PgC of IPSL model, and significantly larger than the 490 PgC of the Hadley model (Table 5.2). This is also in line with the weak land and strong ocean carbon sinks from 1860–2000. An elegant analysis by Friedlingstein et al. (2003) has shown that the major contribution comes from land in the Hadley and IPSL models. The main differences from the UMD model also appear to be on land, which is the focus of the rest of this chapter.

Table 5.2 Change in the carbon pools by 2100 from 1860 in three coupled carbon-climate models:UMD, Hadley Centre, and IPSL. Units in PgC.

	Uncoupled				Coupled				Difference			
	Vege	Soil	Land	Ocean	Vege	Soil	Land	Ocean	Vege	Soil	Land	Ocean
UMD	60	40	100	866	20	-40	-20	867	-40	-80	-120	1
Hadley	220	410	630	370	60	-150	-90	490	-160	-560	-720	120
IPSL	380	300	680	670	310	170	480	700	-70	-130	-200	30

5.4 Uncertainties in land carbon response

Figure 5.4 shows the evolution of the land carbon pool which consists of vegetation and soil carbon. In the uncoupled run, CO_2 fertilization leads to an increase in the net primary production (NPP) and subsequent accumulation of carbon in vegetation biomass. This drives an increase in soil carbon as vegetation-to-soil turnover also increases. The total increase in land carbon from 1860 to 2100 is about 100 PgC with 60 PgC from vegetation, 40 PgC from soil (Table 5.2).

A remarkable reversal of soil carbon uptake is seen in the coupled run where the soil has released 40 PgC by 2100. Although vegetation carbon increased, its storage has saturated at 20 PgC in 2100. The smaller vegetation uptake compared to the uncoupled run is partly due to warming-enhanced maintenance cost (autotrophic respiration), and partly due to the change in precipitation pattern. This modest increase in vegetation carbon (therefore the turnover) is not enough to counteract the enhancement of respiration loss in soil at higher temperature. As a result, land has become a net CO_2 source of 20 PgC to the atmosphere by the end of the simulation.

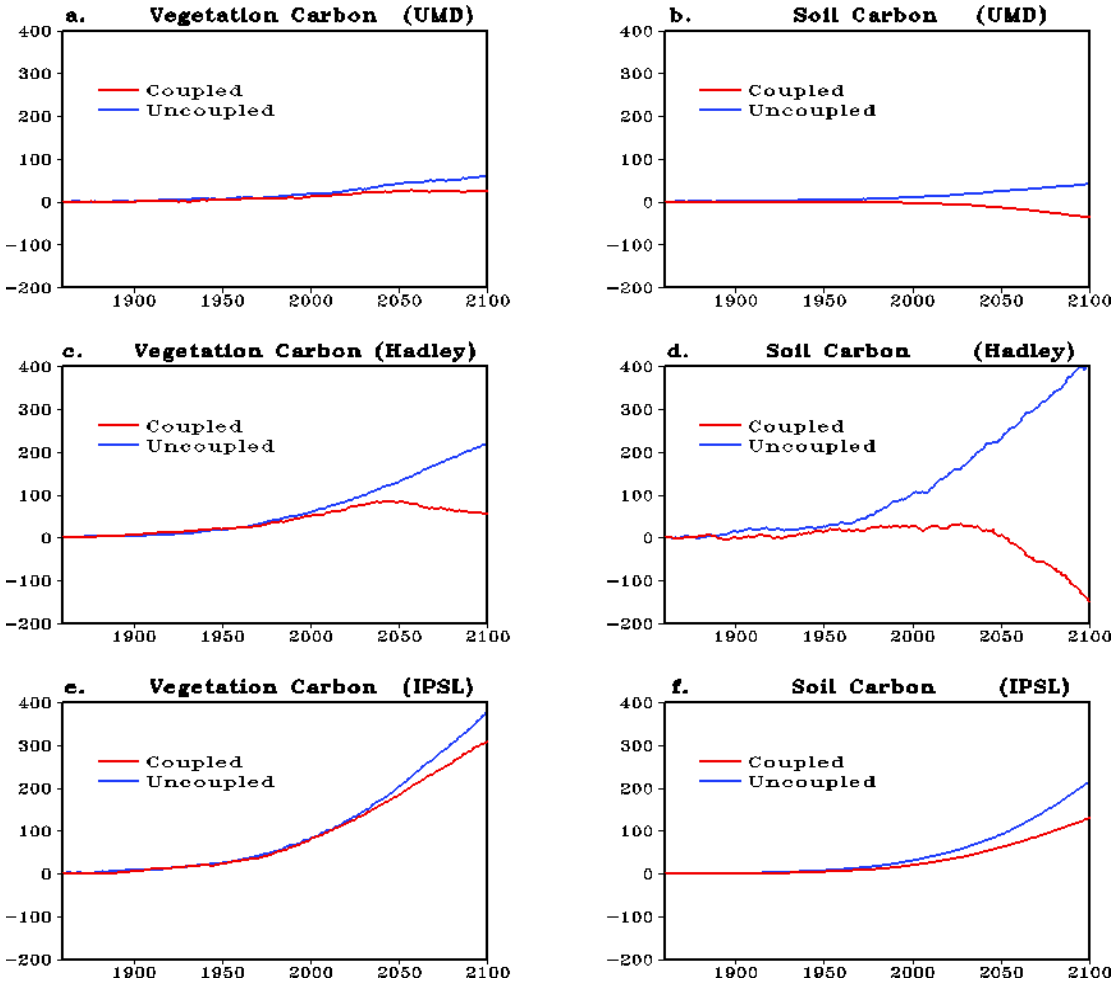

Figure 5.4 Cumulative vegetation and soil carbon changes in PgC since 1860 for the fully coupled run (red) and uncoupled run (blue) from the present model (UMD, upper panels), the Hadley Centre (middle panels), and IPSL (lower panels).

Such a divergence in land carbon response with or without climate-carbon feedback (120 PgC difference in the two runs) is also seen in the Hadley Centre results, but their amplitude is 720 PgC, 6 times larger than ours (Table 5.2). The IPSL difference between the two runs (200 PgC) is more similar to ours, but they differ from ours and Hadley's in that their vegetation growth enhancement significantly outcompetes the climate change impact on respiration rate, so that in the coupled run both soil and vegetation pools continue to increase over time. In coupled run both soil and vegetation pools continue to increase over time.

The spatial pattern of the land carbon change (Figure 5.5) indicates that the UMD uncoupled run has an increase of carbon accumulation everywhere due to CO_2 fertilization effect. The coupled run shows intriguing spatial variations. At high latitude regions in Canada, Scandinavia and northern Siberia, the coupled run shows increase in carbon storage larger than the uncoupled run due to enhanced growth in these currently temperature-limited regions, which locally outcompetes the increased respiration loss at higher temperature. However, at middle and low latitudes, increased soil decomposition and autotrophic respiration at higher temperature dominate over the CO_2 fertilization effect, leading to less carbon storage. This is somewhat complicated by the change in precipitation which tends to have high spatial variation. Increases in precipitation (not shown) are responsible for the carbon increase in regions such as parts of the northern Amazon and West Africa. Such a precipitation pattern is somewhat different from the Hadley Centre model where a perpetual El Niño-like state gave rise to a reduced rainfall and vegetation dieback in the Amazon (Betts et al., 2004). Because the UMD model does not have ocean

dynamics, and climate models also differ widely in their regional responses, such regional comparisons should only be viewed with great caution.

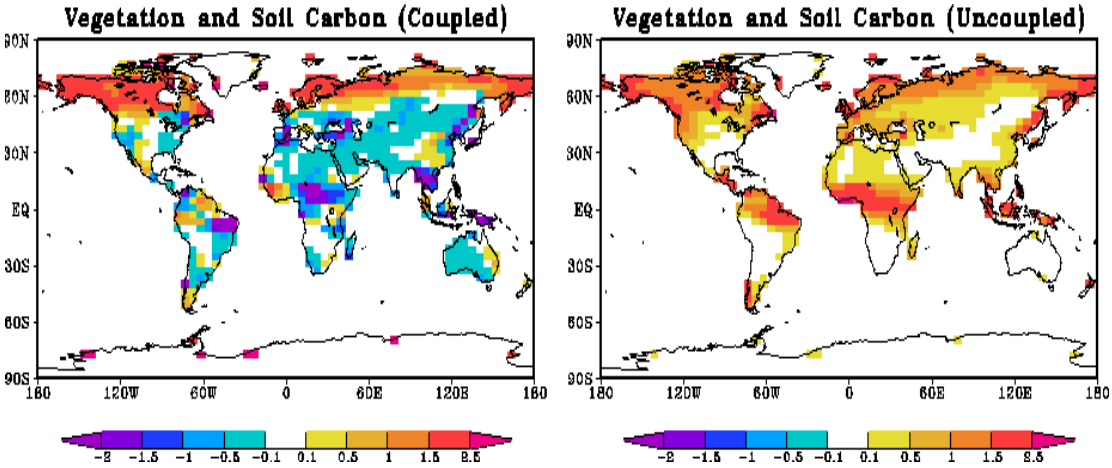

Figure 5.5 Spatial distribution of total land carbon (vegetation + soil) change for the UMD coupled and uncoupled runs. These are the differences between the last 30 years (2071–2100) and the first 30 years (1860–1889), showing different behavior at high latitude and mid-low latitude regions. Units in kgC/m^2.

5.5 Discussion and conclusion

In order to understand the large differences among the three models, we conducted the following three sensitivity experiments with UMD (coupled and uncoupled runs for each individual experiment) with different model parameterizations from the standard run described above: 1. Stronger fertilization; 2. Single soil pool; 3. Higher soil decomposition (Table 5.3). The results from the coupled runs for these three experiments together with the standard run are shown in Figure 5.6. A stronger fertilization effect increases growth significantly so that land is still a sink of 150 PgC by 2100, unlike the 20 PgC source in the standard run. This source-to-sink reversal in the coupled UMD also makes the direction of the carbon changes the same as that of the coupled IPSL result. The coupled single soil pool

experiment shows that land becomes a carbon source of 100 PgC, much larger than the standard run, but similar to the Hadley carbon release under global warming (Jones et al., 2003a). We were thus surprised not to see a similarly high level of sensitivity in the third experiment varying Q_{10} as we did with the previous two model modifications. This is likely because the turnover time in these two pools, especially the slow soil pool, are comparable or longer than the 100 year time scale considered here for global warming, and thus their full potential of carbon release has not been realized by the year 2100. In contrast, the single soil pool experiment has a fast turnover time for all the soil carbon and thus a near-equilibrium response to the warming.

Table 5.3 Three sensitivity experiments with different model parameterizations.

Experiment	Model parameterizations
Stronger CO_2 fertilization	Double the sensitivity of photosynthesis to CO_2 in VEGAS.
One soil pool	Single soil pool by lumping the three soil carbon pools (fast, intermediate and slow) into one, with a turnover time of 25 years at 25˚C, a value somewhat slower than the standard run's fast soil pool, but much faster than the intermediate (80 years) and the slow soil pool (1000 years).
Higher soil decomposition	Higher soil decomposition rate dependence on temperature for the lower two soil layers (Q_{10} = 2.2).

Table 5.4 Difference in total land carbon pool (PgC) between coupled and uncoupled runs at year 2100 for various sensitivity simulations of UMD, Hadley Centre, and IPSL.

UMD Standard	UMD Strong Fertilization	UMD One soil pool	UMD All Q_{10}=2.2	Hadley	IPSL
-120	-80	-260	-130	-720	-200

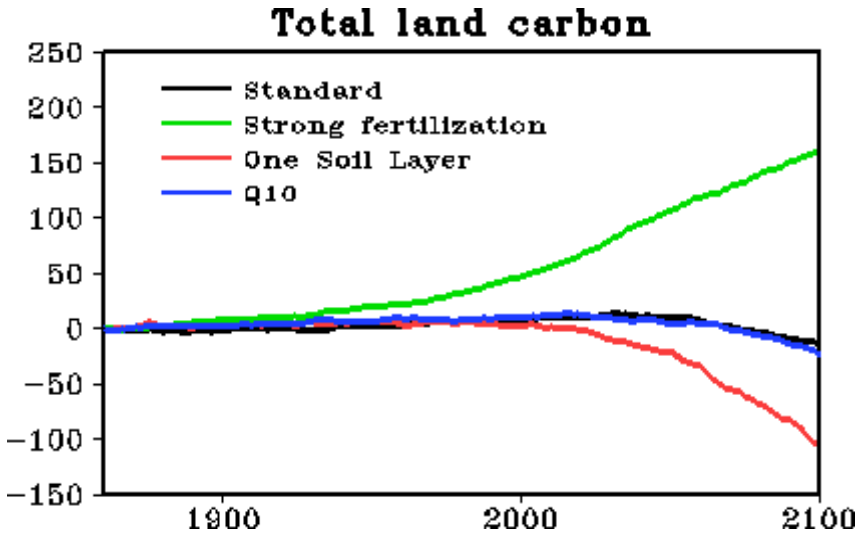

Figure 5.6 Total land carbon change (PgC) since 1860 in four fully coupled runs of UMD: the standard run (same run as in Figure 5.3), and three sensitivity experiments: strong CO_2 fertilization effect, single soil pool, and high soil decomposition rate dependence on temperature (Q_{10} = 2.2 for all soil layers, blue).

Current observations have not converged on the strength of CO_2 fertilization on a global scale (Field, 2001). While models often rely on strong CO_2 fertilization to explain the "missing carbon sink" of 1–2 PgC/yr observed in the 1980–90s (Prentice et al., 2001), the weak dependence in the UMD model produces only a small land CO_2 sink of 0.5 PgC/yr in the uncoupled run, 0.2 PgC/yr in the coupled run (partly due to warming-induced soil carbon release). However, the UMD model, as well as those of Hadley and IPSL, do not consider effects such as land use change and fire suppression, which may be important contributors to be considered in future coupled modeling. In addition, the slower soil pools may not respond to global warming as fast, and their temperature dependence may not be as strong as the surface soil and litter. Our sensitivity experiments suggest a significant impact of these uncertainties.

Although all models agree on a positive carbon cycle feedback as indicated by

the negative values in Table 5.4, the predicted difference between coupled and uncoupled runs for our strong fertilization case is -80 PgC, compared to -120 PgC in the standard case. Both values are modest, but somewhat similar to IPSL (-200 PgC). The biggest difference in the modified coupled runs is the flux of -260 PgC for the one soil pool runs, more than double the flux from the standard case. This is a bit closer to, but still significantly smaller than the Hadley model (-720 PgC). These results suggest that different CO_2 fertilization strengths may explain some part of the UMD-IPSL differences (and the UMD-Hadley difference in the uncoupled runs), and soil decomposition and turnover time may explain partly the UMD-Hadley differences in the coupled runs. Thus, in order to narrow down uncertainties in the prediction of future carbon and climate change in projects such as the Coupled Carbon Cycle Climate Model Intercomparison Project (C4MIP) (Fung et al., 2000), it we urgently need to improve our knowledge of some major issues in the carbon cycle, including the global strength of CO_2 fertilization effect and the turnover and decomposition rates of the slower soil pools.

Chapter 6: Enhanced Terrestrial Carbon uptake in the Northern High Latitudes under Climate Change in the 21st Century from C4MIP Models Projections

6.1 Introduction

Carbon cycle is one of the most important biogeochemical cycles in the climate system because carbon dioxide is a principal greenhouse gas that contributes significantly to global warming (IPCC, 2007). The amount of carbon dioxide in the atmosphere is not only dependent on anthropogenic fossil fuel emission, but also on the exchange of fluxes of carbon between the atmosphere, land, and ocean. Carbon exchange between the atmosphere and ecosystem are in turn highly sensitive to climate change. Therefore, understanding the interaction between climate and carbon cycle is essential for the accurate projection of future climate change.

The terrestrial ecosystem mainly gains carbon from the atmosphere through photosynthesis and loses it primarily through respiration (autotrophic and heterotrophic) (biomass burning is also an important non-biological contributor). During the past decades, Northern High Latitudes (NHL: poleward of 60°N) have witnessed dramatic changes where the annual average temperature increased by 1-2˚C in northern Eurasia and northwestern North America (Arctic Climate Impact Assessment, 2005). This intense warming is much larger than the increase of global average surface temperature of 0.65±0.2˚C over the 20th century (IPCC, 2007). The snow/ice albedo reduction due to warming is traditionally believed to be one of the

main amplifiers of greenhouse warming in the NHL (Holland and Bitz, 2003; Kaplan and New, 2006).

This dramatic climate change affects the two dominant biomes of the NHL: the boreal forests and the tundra (Figure 6.1). Accompanying the accelerating climate change in the NHL, in the past decades, a "greening" of vegetation has been observed in the boreal forests based on satellite data and phenology studies (Keeling et al., 1996; Myneni et al., 1997; Zhou et al., 2001; Tucker et al., 2001; Lucht et al., 2002). Such a "greening" has been associated with a 10 to 20-day lengthening of the growing season (Zhou et al., 2001; Tucker et al., 2001; Linderholm, 2006; Schwartz et al., 2006; Piao et al., 2006; Piao et al., 2007). The increase in photosynthetic activity due to the persistent increase in the length of the growing season may lead to long-term increases in carbon storage and changes in vegetation cover, which in turn affect the climate system. However, Piao et al. (2008) found that there is a net carbon dioxide loss of northern ecosystems in response to autumn warming. This is because the increase in respiration is greater than photosynthesis during autumn warming. On the other hand, frozen soils are prevalent in the tundra with a north-south gradient from continuous-to-discontinuous permafrost. With low ambient temperatures, waterlogged soils, and slow drainage, these ecosystems have been slowly accumulating a large amount of carbon (Sitch et al., 2007). The soil carbon becomes metabolized when the frozen soil begins to melt in response to rising temperatures. This leads to an increase of soil carbon released to the atmosphere. One estimate suggested that global warming could thaw 25% of the permafrost area by 2100, thus rendering about 100 PgC vulnerable to decay (Davidson et al., 2006). To date, such

below-ground processes are poorly understood (Melillo et al., 2002; Bond-Lamberty et al., 2004; Eliasson et al., 2005; Lawrence and Slater, 2005; Bronson et al., 2008). The competition between absorption of carbon due to the greening of the boreal forests and the release of carbon from the soil due to the rising temperatures in the terrestrial biosphere in the NHL therefore will determine whether the NHL becomes a source or sink of carbon in the future.

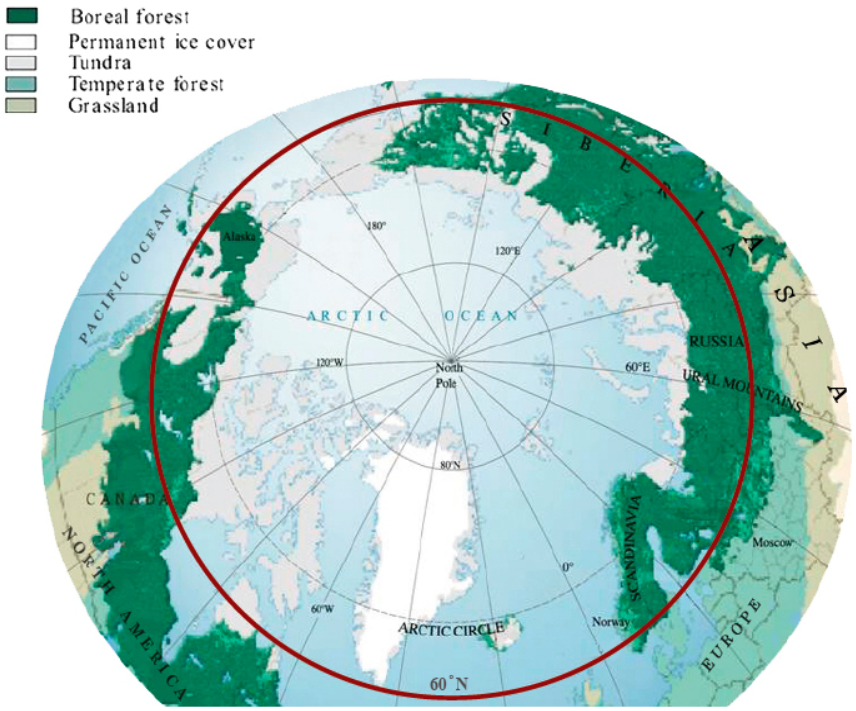

Figure 6.1 Boreal vegetation distribution in the northern high latitudes (modified from Montaigne, 2002). The area poleward of 60˚N (circled in dark brown) is defined as Northern High Latitudes (NHL) in this study.

Several studies have used offline simulations of vegetation-carbon models forced by the IPCC climate projection to investigate the future effects of CO_2 fertilization, climate change, land-use change, and nutrient limitation on the NHL ecosystem (McGuire et al., 2000; Cramer et al., 2001; Schaphoff et al., 2006; Sitch et

al., 2007). However, few studies have considered the carbon cycle-climate coupling in the NHL (McGuire et al., 2006). Fully coupled three-dimensional carbon cycle-climate models have been used to study the interaction between the global carbon cycle and climate (Cox et al., 2000; Friedlingstein et al., 2001; Joos et al., 2001; Zeng et al., 2004; Thompson et al., 2004; Matthews et al., 2005). Albeit uncertain in magnitude, most studies indicate a positive feedback for the carbon cycle. Quantifying and predicting this carbon cycle-climate feedback is difficult because of the limited understanding of the processes by which carbon and the associated nutrients are transformed or recycled within ecosystems, and then exchanged with the overlying atmosphere (Heimann et al., 2008). Large uncertainties from various model parameterizations and modeling protocols have highlighted an urgent need of model intercomparsions to understand the interaction between climate and carbon cycle.

In the Coupled Carbon Cycle Climate Model Intercomparison Project (C4MIP), 11 climate modeling groups have used their fully-coupled carbon cycle-climate models to investigate such interactions, with particular emphasis on the feedback processes involved (Friedlingstein et al., 2006). The modeling protocols used by all the modeling groups were: 1) The same anthropogenic emission of CO_2 Intergovernmental Panel on Climate Change (IPCC) Special Report on Emissions Scenarios (SRES) A2 scenario as the external forcing for each fully coupled carbon cycle-climate model; 2) Two separate simulations: a fully coupled interactive carbon cycle-climate run and a uncoupled run wherein a prescribed climate was used (radiative CO_2 concentration was kept at pre-industrial level), while the vegetation and carbon model can see the increasing CO_2 for photosynthesis. Carbon cycle-

climate feedback is then calculated as the difference between the two simulations. Friedlingstein et al. (2006) indicate a positive carbon cycle-climate feedback from all C4MIP models in the 21st century, on a global scale. Due to this positive feedback, there is an additional 20-200 ppm CO_2 in the atmosphere by 2100, leading to a 0.1-1.5˚C warming in the C4MIP models. A majority of the models indicated a robust reduction of terrestrial carbon uptake in the tropics due to such climate feedback (Figure 6.1 in Friedlingstein et al., 2006).

Climate change during the past decades has been changing the physical, biological, and societal conditions in the NHL. When the interaction between the climate and carbon cycle is included in the climate system, the following questions are still open:

- Will the NHL terrestrial biosphere become a carbon sink or a source in the future? In particular how will the vegetation and soil carbon change in the NHL?
- How do the mechanisms involved in the carbon exchange between the vegetation and the soil affect the individual growth rate of their carbon storage by 2100? In particular what are the effects of CO_2 fertilization and climate change (intense warming in NHL) on vegetation photosynthesis and soil decomposition?
- Is the future projection of terrestrial carbon change by fully coupled carbon cycle-climate simulation, consistent with the current observed "greening" and a northward shift of vegetation distributions over the past decades?

In contrast to previous modeling studies in which projection of future climate solely drives vegetation and carbon models, in this study, we investigated the interaction between climate and carbon cycle in the NHL based on the simulations of fully coupled carbon cycle-climate C4MIP models, with particular emphasis on addressing the above scientific questions. Current NHL "greening" and a northward shift of vegetation distributions have been reported by satellites and land based observations during the past decades. The change in the NHL ecosystem is thus of importance and the interaction between carbon cycle and climate on the future climate system is examined here. If this C4MIP modeling study can provide an insight to assessment of the carbon uptake under global warming, it will be encouraging and of great significance to apply fully coupled models in the projection of future climate in the NHL.

6.2 Data and methodology

The principal focus of our study is to investigate the terrestrial carbon storage change in the high latitude regions poleward of 60˚N in coupled carbon cycle-climate systems. The data used in this study is based on the multi-model simulations provided by C4MIP (http://c4mip.lsce.ipsl.fr/), which is a joint project between the International Geosphere-Biosphere Program (IGBP) and the World Climate Research Program (WCRP). The use of dynamic carbon models in examining future climate has also been highlighted in the 4th Assessment Report of IPCC (IPCC, 2007). The terrestrial carbon model used in the 11 coupled carbon-climate models can be found in Table 6.1 from Friedlingstein et al. (2006), as well as for a detailed description of the models please refer to Friedlingstein et al. (2006). Of those models, HadCM3LC

and UVic use the same land carbon component of Met Office Surface Exchange Scheme (MOSES)/ Top-Down Representation of Interactive Foliage and Flora including Dynamics (TRIFFID), while CLIMBER2-LJP and BERN-CC use the same Lund–Potsdam–Jena (LPJ) vegetation model. These common components provide a good opportunity to examine cases of carbon-climate coupling using the same carbon model but different OAGCMs. All the C4MIP models used the same anthropogenic fossil fuel emissions from Marland et al. (2005) for the pre-industrial period and the IPCC SRES A2 for the 2000-2100 period. The coupled simulation in the C4MIP models, has the climate and the carbon components iteracting freely thus representing a full carbon cycle-climate coupling. The uncoupled simulation treats CO_2 as a non-radiatively active gas (so the carbon cycle experiences no CO_2-induced climate change), while the ecosystem still sees an increasing CO_2. The difference between coupled and uncoupled runs is defined as carbon cycle-climate feedback.

Table 6.1 Major characteristics of the C4MIP models components (adapted from Friedlingtein et al., 2006)

Model	Atmosphere	Ocean	Land Carbon	DGVM* ?	Ocean Carbon
HadCM3LC	HADCM3 (2.5° x 3.75°)	(2.5° x 3.75°), flux adjustment	MOSES/TRIFFID	Yes	HadOCC
IPSL-CM2C	LMD5 (5° x 4°)	OPA-7, (2° x 2°), no flux adjustment	SLAVE	No	NPZD
IPSL-CM4-LOOP	LMDZ-4 (3° x 3°)	ORCA2, (2° x 2°), no flux adjustment	ORCHIDEE	Not here	PISCES
CSM-1	CCM3 T31	NCOM (3.6° x (0.8 -1.8°))	LSM, CASA	No	OCMIP-biotic
MPI	ECHAM5, T63	MPI-OM, 1.5°, no flux adjustment	JSBACH	No	HAMOCC5
LLNL	CCM3, (2.8° x 2.8°)	POP (0.6° x 0.6°)	IBIS,flux adjustment	Yes	OCMIP
FRCGC	CCSR/NIES/FRCGC T42(2.8° x 2.8°)	COCO No flux adjustment, ((0.5°-1.4°) x 1.4°)	Sim-CYCLE	No	NPZD
UMD	QTCM (5.6° x 3.7°)	Slab mixed layer, 5.6°x 3.7°	VEGAS	Yes	Three-box mode
UVic-2.7	EMBM (1.8° x 3.6°)	Mom 2.2, 1.8° x 3.6°, no flux adjustment	MOSES/TRIFFID	Yes	OCMIP Abiotic
CLIMBER2 -LPJ	2.5-D, (10° x 51°) statistical-dynamical	Zonally averaged, 2.5°lat, 3 basins	LPJ	Yes	NPZD
BERN-CC	EBM (2.5° x 3.75°)	HILDA box-diffusion model	LPJ	Yes	Perturbation approach

* DVGM: Dynamic Global Vegetation Model

Currently, each modeling group provided a standard time series of total fossil fuel emissions, simulated global atmospheric CO_2 concentration, surface temperature, terrestrial Net Ecosystem Product (NEP), ocean net CO_2 flux, Net Primary Product (NPP), Heterotrophic respiration (R_h), and vegetation and soil carbon pools storages for the total globe and band-averaged regions: 90˚S-30˚S, 30˚S-0˚S, 0˚N-30˚N, 30˚N-60˚N, 60˚N-90˚N. Our study focuses on the terrestrial regions poleward of 60˚N. In this study, the total global values are used only as a reference for the NHL comparisons. The results will be presented as the individual response of the 11 models or as that of the ensemble mean in the text.

6.3 NHL terrestrial carbon storage in the 21st century

The NHL terrestrial ecosystem stores a large amount of carbon in boreal forest and frozen soil. It is very important to understand the changes in the uptake of carbon under global change. Prior to investigating the 21st century change of the terrestrial carbon storage in the NHL in the C4MIP models, the NHL vegetation and below ground soil carbon in the pre-industrial era in the individual models was examined (Figure 6.2). Figure 6.2a shows the global partitioning of carbon into land and soil. Globally, the C4MIP models simulate a mean total land carbon storage of 2106 PgC, with a range from 1348 PgC to 3089 PgC. The vegetation carbon pool contains 279-937 PgC and the soil contains 999-2152 PgC. Thus, the C4MIP models indicate that the carbon in the soil is about 2.5 times that of vegetation carbon, highlighting the soil as a major carbon reservoir of land carbon. Unlike this general agreement on the global total of land carbon in C4MIP models, there is a large uncertainty in the carbon stored in the NHL (Figure 6.2b). For example, the mean indicates that the NHL

contains about 15% of the total global terrestrial carbon. IPSL-CM4-LOOP, though, has just 65 PgC in NHL land ecosystem, only about 4% of global total, while CLIMER-LPJ has 568 PgC in NHL, about 21% of global total. UMD has the largest percentage, at 30%. While the NHL contains 15% of total global land carbon, the NHL vegetation holds only 5.8% of global total vegetation carbon. Most of the land carbon in NHL is sealed below the ground in frozen soil. The mean NHL soil carbon is about 9.4 times that of the NHL vegetation carbon. Most of the carbon being locked in the soil is due to the low ambient temperature below freezing and is consistent with previous estimates (Post et al., 1982; Chapin and Matthews, 1993, McGuire and Hobbie, 1997). The mean NHL soil holds about 18% of global total carbon, which is lower than the estimate by McGuire and Hobbie (1997). IPSL-CM2C, IPSL-CM4-LOOP, CSM-1 and MPI even have fractions less than 10%. UMD has a percentage of 35%, close to the estimate by McGuire and Hobbie (1997). Examining the total global partitioning of carbon in pre-industrial era between above and below ground carbon, the models that share the same terrestrial carbon models show similarities (between CLIMBER2-LPJ and BERN-CC, and between HadCM3LC and UVic). However, the partitioning in the NHL in between those two carbon models was more different. This reflects the differences in the two vegetation models to differing climatic conditions.

In the past two decades, winter in the Northern High Latitudes has experienced some of the most rapid changes on the Earth, warming almost 2.5 times faster than the global average rate (Liu et al., 2007). Amplification of greenhouse warming in the NHL have been traditionally attributed to snow/ice-albedo reduction,

dynamical feedbacks associated with the poleward heat transport of the oceans and atmosphere (Holland and Bitz, 2003; Alexeev et al., 2005), and internal feedbacks associated with polar processes (Overland et al., 2004).

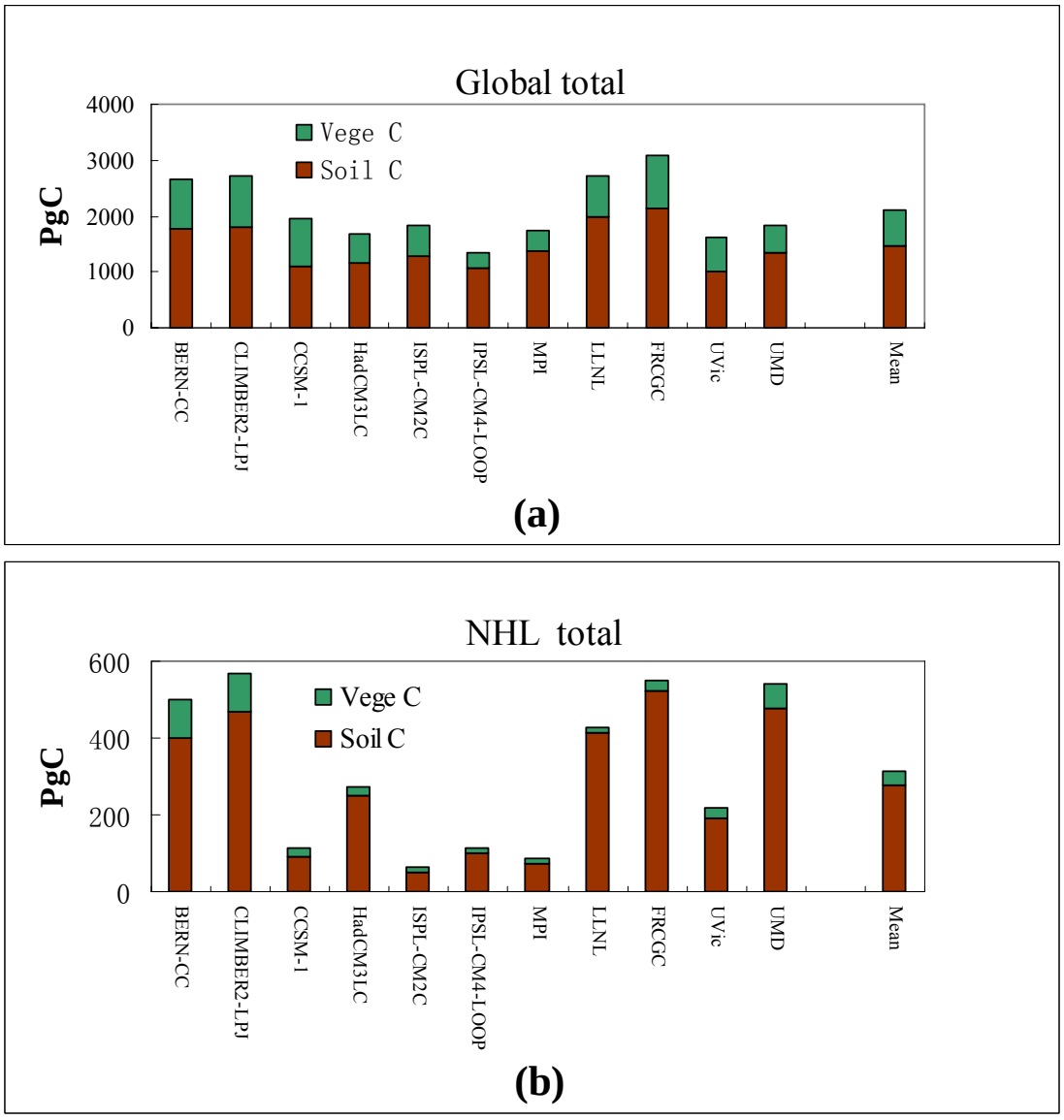

Figure 6.2 Simulated carbon storage for the pre-industrial era in the vegetation and soil by the C4MIP models and model-mean for: (a) Global total; (b) NHL. The stored carbon is calculated based on 1860-1870 for all models except 1870-1880 for LLNL, and 1901-1910 for CLIMBER-LPJ. Soil carbon is indicated in brown, and vegetation in dark green. Most of the carbon is locked in the soil particularly in the NHL. Units of storage are in PgC.

The ocean-atmosphere GCMs indicate that the earth will have warmed by 2˚C relative to pre-industrial temperatures between 2026 and 2060, at which stage the mean annual temperature over the Arctic (60˚N–90˚N) will have increased by between 3.2˚C and 6.6˚C (Kaplan and New, 2006). Consistent with these predictions, the C4MIP models project that by 2100 the mean surface temperature in the NHL will increase by 5.9˚C, in contrast to 3.2˚C for global average (Figure 6.3). Most models show intense warming in NHL, nearly twice the global warming by 2100. The exception is UMD, which does not include a snow/ice scheme at all. LLNL, MPI, FRCGC and IPSL-CM4-LOOP have up to 7-8˚C warming in the NHL.

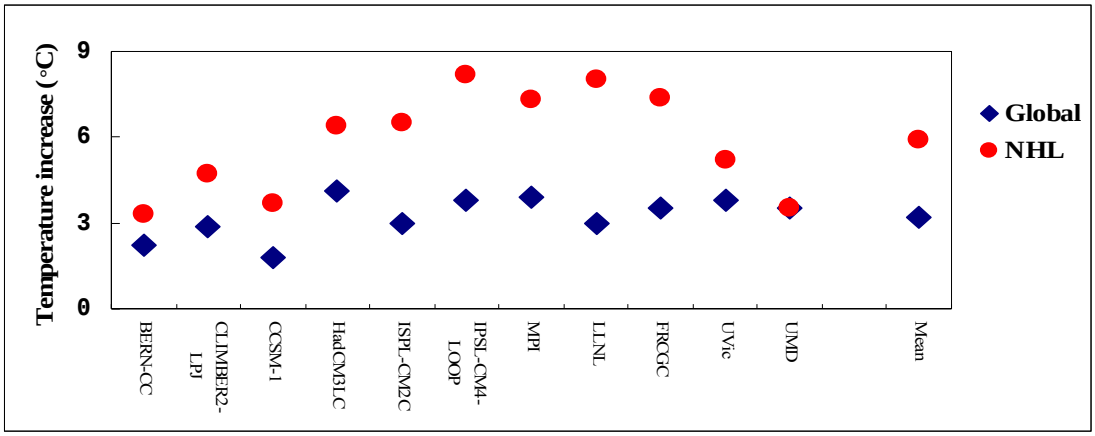

Figure 6.3 Temperature increase from 1860 to 2100 projected by the fully coupled simulations from C4MIP models for global mean (blue diamond) and NHL (red circle) except for LLNL which is from 1870 to 2100, and CLIMBER-LPJ from 1901 to 2100. The multi-model mean is plotted. It is evident that significantly more intense warming is expected in the NHL, compared to global mean. The UMD model is an exception since it does not include a snow/ice albedo scheme.

Though, the "greening" and vegetation migration in NHL during the past decades have been highly correlated to warming (Keeling et al., 1996; Myneni et al., 1997; Zhou et al., 2001; Tucker et al., 2001), the intense warming also accelerates the decay of the organic matter in the soil which will subsequently release CO_2 to the

atmosphere, especially in the NHL, where most of the land carbon is stored in the permafrost soil levels. The increase in vegetation growth due to CO_2 fertilization and warming counteracts the soil decomposition by warming. This difference will determine the change of carbon stored in the terrestrial biosphere in the NHL. Piao et al. (2008) found that there is a trend of net carbon dioxide loss of northern ecosystems in response to autumn warming because of the greater increase in respiration. While such a study by itself does not provide information about how these two highly uncertain competing effects could behave under different future scenarios, it highlights the importance of the effect of temperature on the soil respiration in NHL under global warming.

The C4MIP coupled simulations indicate that by 2100 the NHL is a carbon sink with a mean of 0.4PgC/yr (Figure 6.4a, c). With the exception of FRCGC, the remaining 10 models agree that the NHL ecosystem will absorb carbon from the atmosphere. The range of absorption varies from 0.1 PgC/yr to 1.6 PgC/yr. The inter-model deviation also increases with the time (Figure 6.4c). The model-mean (Figure 6.4c) indicates a tendency of saturation or even a decrease in the carbon uptake by 2060. This saturation tendency is visible in the HadCM3LC, FRCGC and BERN-CC models. The integration of this land-atmosphere carbon exchange indicates the amount of carbon land will absorb. The mean uptake of terrestrial carbon by 2100 is 40 PgC while the range is from 17 to 82 PgC in the C4MIP models (Figure 6.4b, d). LLNL is an exception with a strong carbon source during the first century which switches to a sink in the 1970's and ends as the largest carbon sink with 1.6 PgC/yr by 2100. A possible reason could be a global mean surface temperature drift of -0.15

K and a 15 % increase in ice area in the 1900's, which causes a regional decrease in ecosystem productivity in LLNL (Bala et al., 2006). The differences in trajectories between the models that share the same vegetation models are as large as the remaining inter-model deviations themselves. So, no similarities are identifiable on a regionally averaged scale.

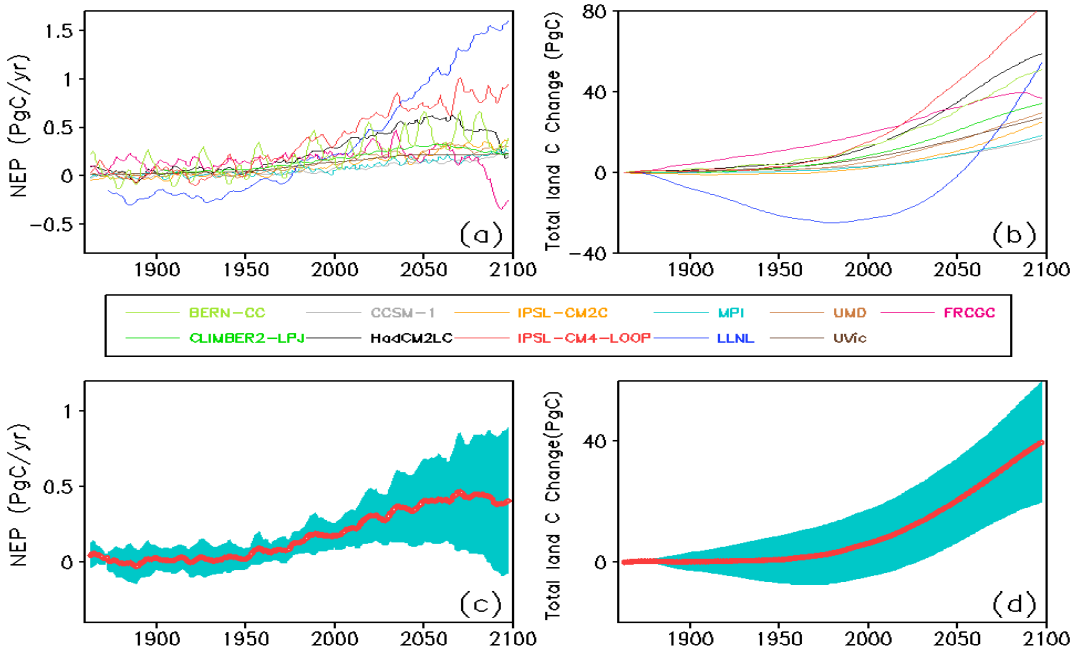

Figure 6.4 Changes of NEP and total land carbon in the NHL during 1860-2100 in C4MIP coupled simulations. (a) NEP; (b) Total land carbon change. Colored lines in the (a) (b) are for individual C4MIP models; (c) (d) the multi-model mean (red solid line) and the 1-σ spread (blue shading) are indicated. The change in total land carbon is indicated relative to 1860, except for LLNL and CLIMBER-LPJ where it is relative to 1870 and 1901 respectively. A 6-year running mean filter is applied to all the curves. Unit for NEP is PgC/yr and for land carbon change is PgC.

The changes in the vegetation and the soil carbon are indicated in Figure 6.5a and 6.5b. The mean of the C4MIP models will gain18 PgC in above ground vegetation and 22 PgC in soil by 2100 compared to the late 18th century. The increment of vegetation carbon stored is a little smaller than the increase of soil carbon pool. However, this is a significant increase in the vegetation carbon. The

NHL vegetation contains about 10% of NHL land carbon, but this carbon storage increases from 38 PgC in the 1860s to 56 PgC by 2100, about 47%. The soil carbon increases only 8%, from 276 PgC to 298 PgC from 1860-2100. Contrary to the estimates of Davidson et al. (2006), our analysis of the C4MIP models indicates that at least in the 21st century, the soil in the NHL will not lose carbon to the atmosphere. Soil carbon, protected from release to the atmosphere by cold and waterlogged conditions in NHL, was thought to be highly susceptible to changes in temperature and permafrost thawing in the 21st century. This dilemma calls for a quantitative analysis of the processes involved that suppresses the effect of the intense warming on soil decomposition in the NHL.

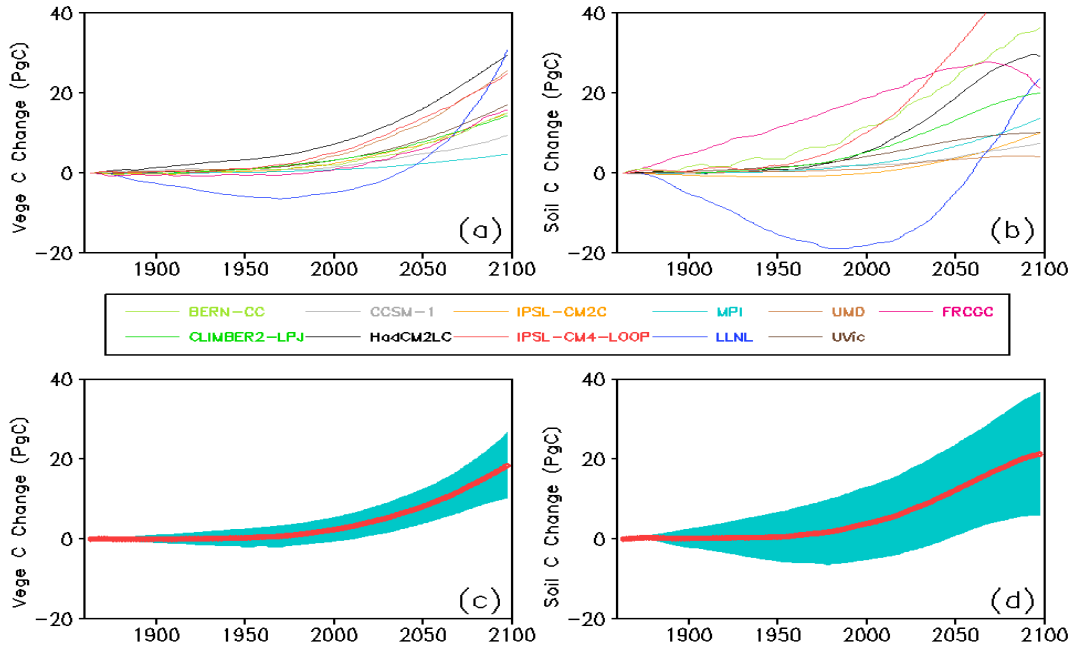

Figure 6.5 Changes of vegetation and soil carbon in the NHL in C4MIP couple simulations: (a, c) Vegetation carbon; (b, d) Soil carbon. Colored lines in the (a) and (b) are for individual C4MIP models; (c) and (d) show the multi-model mean (red solid line) and the 1-σ spread (blue shading) are indicated. All changes are relative to the year of 1860 except for LLNL with 1870, and CLIMBER-LPJ with 1901. A 6-year running mean filter is applied to all the curves. Units are in PgC.

To explore this, the carbon budget of the above-ground vegetation and soil are examined separately. Though NEP reflects changes of the ecosystem carbon exchange, NPP has been used as an indicator of the vegetation activity; these variables do not directly measure the change of vegetation and soil carbon storage. Examination of the mechanisms controlling the vegetation and soil carbon exchange processes involves the following variables: (1) Vegetation (biomass) turnover into soil; (2) Growth rate of vegetation carbon; (3) Growth rate of soil carbon. To date, little attention has been paid to vegetation turnover; however, it is an important bridge for vegetation and soil carbon exchange. The difference between NPP and vegetation turnover is defined as the net growth rate of vegetation carbon. The difference between the vegetation turnover and soil decomposition indicates the net growth of soil carbon.

Most vegetation carbon models constrain the total global NPP within a contain range. However C4MIP models differ a lot in the magnitude of the NHL NPP. It varies from 1.1 PgC/yr in IPCC-CM4-LOOP to 6.8 PgC/yr in UMD in 1860, with the percentage dependence on the global total ranging from 2% to 13% (not shown). In the NHL, the mean of C4MIP models indicates that NPP increases from 3.3 PgC/yr to 6.3 PgC/yr by 2100, nearly 90% more of vegetation activity (Figure 6.6a). IPSL-CM4-LOOP even simulates more than a 400% increase in the NHL NPP (not shown). This robust vegetation increase also reflects the importance of albedo feedback. About 2.7 PgC/yr of biomass will turn over into the soil in the NHL (Figure 6.6b). Higher biomass turnover is normally expected following more vegetation productivity. The difference of about 0.3 PgC/yr remains in the vegetation and is

reflected as the net growth rate of vegetation carbon (Figure 6.6c). This is consistent with the sink of 18 PgC that will accumulate in the vegetation by 2100 as discussed before (Figure 6.5c). The assumption that the biomass turnover is mostly proportional to NPP is reasonable because it is evident that more productivity can produce more biomass turnover over long-time periods in observations.

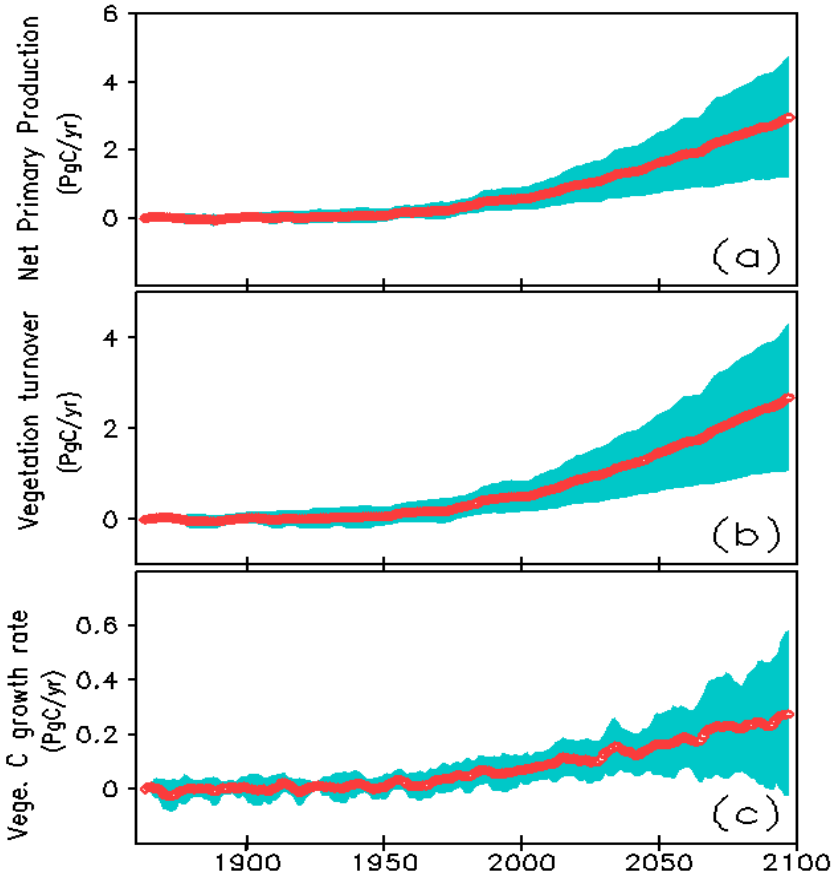

Figure 6.6 The multi-model mean and 1-δ spread of carbon fluxes in vegetation in the NHL in the C4MIP coupled simulations for: (a) Net Primary Product; (b) Vegetation turnover; (c) Vegetation carbon growth rate. The changes are relative to the values in the late 18th century; a 6-year running mean filter is applied to all the curves. Units are PgC/yr for all three panels.

The growth of soil carbon content is determined as a difference between vegetation turnover and soil decomposition. The mean of C4MIP models for these two factors is shown in Figure 6.7. Below the ground, the NHL soil decomposition is

greatly enhanced from 3.3 PgC/yr to 5.9PgC/yr by the intense warming (Figure 6.7a); however, soil decomposition is smaller than biomass turnover, and the residual is locked in the soil as the growth rate of soil carbon (Figure 6.7b). The C4MIP mean-model shows that the growth rate of soil carbon increases up to 2060 after which it decreases until 2100. A possible mechanism is that the soil decomposition increases dramatically after 2060, and quickly catches up with biomass turnover input by 2100. As the warming intensifies, there is a possibility that the NHL soil may lose carbon after 2100 from C4MIP, rather than in the 21st century in the previous estimate. Our study based on C4MIP model results indicates that the vegetation biomass turnover is of utmost significance in understanding the processes that control the changes of vegetation and soil carbon in the NHL.

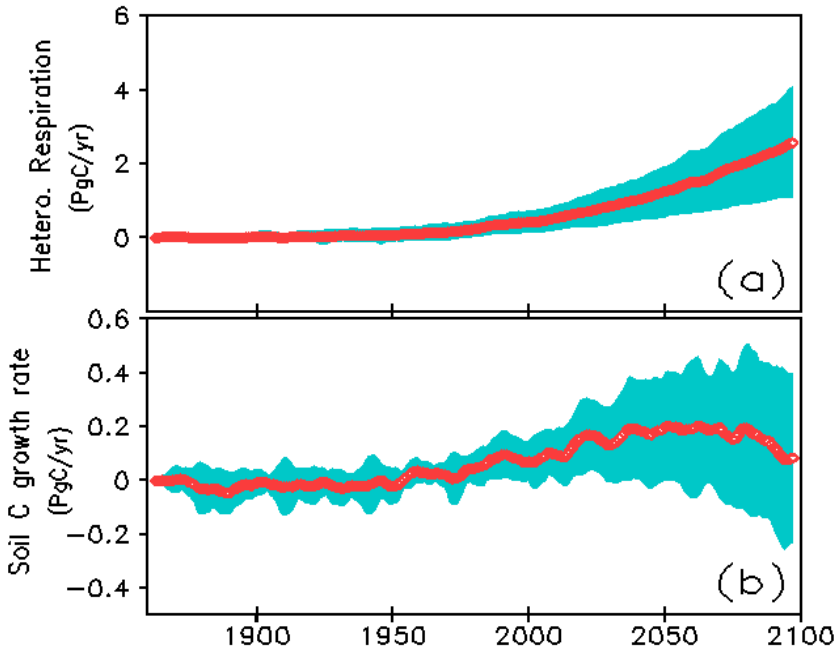

Figure 6.7 Same as Figure 6.6 but for the changes of carbon fluxes in soil for: (a) Heterotrophic Respiration; (b) Soil carbon growth rate. Units are PgC/yr.

6.4 CO_2 fertilization and climate change effects in NHL carbon cycle-climate coupling

The terrestrial carbon sink in the 21st century in the NHL, identified in the previous section using C4MIP coupled simulations, is attributable to CO_2 fertilization and climate change. These two factors play an important role in controlling the carbon stored in the NHL terrestrial system (McGuire et al., 2000; Cramer et al., 2001; Schaphoff et al., 2006; Sitch et al., 2007) and will be the focus of this section. In addition to the coupled simulation, C4MIP provides uncoupled simulation, in which the models do not see the effect of change in temperature due to increase of CO_2 while allowing for CO_2 fertilization with increasing CO_2. The difference between the coupled and uncoupled runs is defined as the carbon cycle-climate feedback (Friedlingstein et al., 2006).

This carbon cycle-climate feedback discussed by Friedlinstein et al. (2006) includes mostly the effect of climate change and a small additional effect because of CO_2 fertilization, due to CO_2 concentration from the coupled run being considerably higher than that of the uncoupled run by 2100[1]. The combination of these two effects indicates the carbon cycle-climate coupling. The changes of vegetation and soil carbon in the NHL, as well as that for the whole globe are indicated in Figure 6.8. Contrary to the negative climate feedback on the global scale in which the land reduces its capacity for the uptake of carbon (Figure 6.8a), most models simulate that land carbon uptake in the NHL will increase slightly in the future due to carbon cycle-climate coupling (Figure 6.8b). All models show a robust increase in the

[1] [1]In C4MIP "uncoupled" runs, the climate is kept constant while the CO_2 level for vegetation photosynthesis is still increasing. This enables use to easily calculate the terrestrial carbon sensitivity to CO_2 fertilization without contamination from the climate change.

vegetation carbon pool size (Figure 6.8d) in the NHL.

Contrary to the robust soil carbon loss due to carbon cycle-climate feedback on the global scale in all C4MIP models (Figure 6.8e) because of enhanced soil decomposition, the NHL soil carbon response to climate feedback varied substantially in the models (Figure 6.8f). However, the robust increase of NHL vegetation carbon largely dominates the terrestrial carbon change. Some models simulate a reduction in soil carbon in the NHL, but the robust carbon increase from vegetation compensates for the carbon loss from soil in most models (apart from CLIMBER, which has a tiny net carbon loss, and FRCGC which has a large net carbon loss), resulting in a general net increase in the terrestrial pool in NHL. Further analysis indicated that this small carbon increase between coupled and uncoupled cases is caused by the higher increase of vegetation growth than soil decomposition due to carbon-climate feedback (not shown). Our analysis indicates that the global and the northern high latitude regions have quite different underlying mechanisms that control the terrestrial carbon storage changes. An interesting point that is elucidated from the coupled climate feedback analysis is that soil carbon plays a key role in the global carbon pool (Figure 6.8e), while robust vegetation growth is the dominant factor in the high latitudes (Figure 6.8d) in the 21st century. Though the magnitude of the NHL terrestrial carbon and its change are much smaller than that of the global scale, this is of great significance because potentially dramatic impacts of climate changes on the NHL terrestrial ecosystem.

Besides CO_2 fertilization, the NHL carbon cycle-climate coupling has a potential to stimulate the vegetation activity in the future due to the feedback of

warming and higher CO_2 concentrations (Figure 6.9b, d). This is in contrast to a negative effect of carbon cycle-climate feedback on vegetation activities on a global scale reported by Friedlingstein et al. 2006 (Figure 6.9a, b).

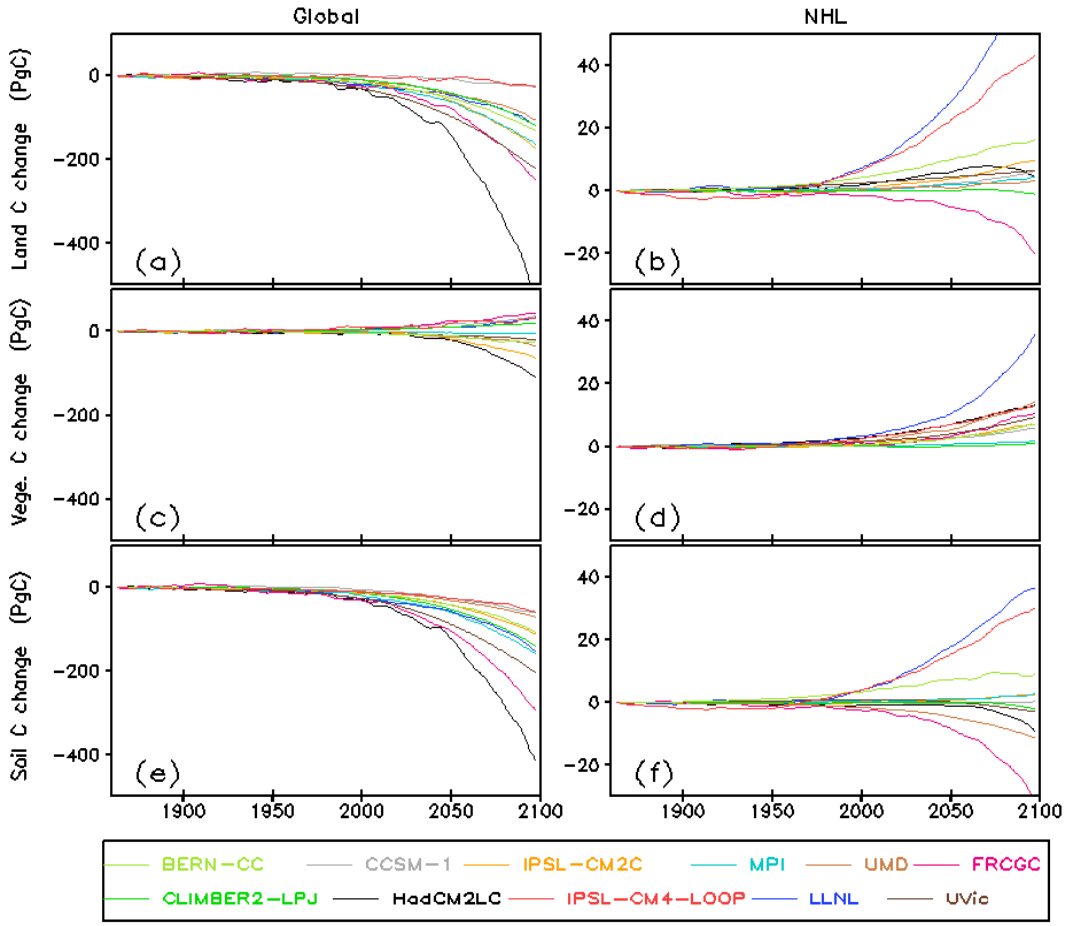

Figure 6.8 Changes in carbon storage during the 1860-2100 period due to carbon cycle-climate feedback (coupled–uncoupled simulation) for the 11 C4MIP members for the globe (a, c, e) and the NHL (b, d, f) for: (a, b) Total land carbon. (c, d) Vegetation carbon; (e, f) Soil carbon; All values are relative to the year of 1860 except for LLNL and CLIMBER-LPJ, which have the beginning years of 1860 and 1901 respectively. A 6-year running mean filter is applied to all the curves.

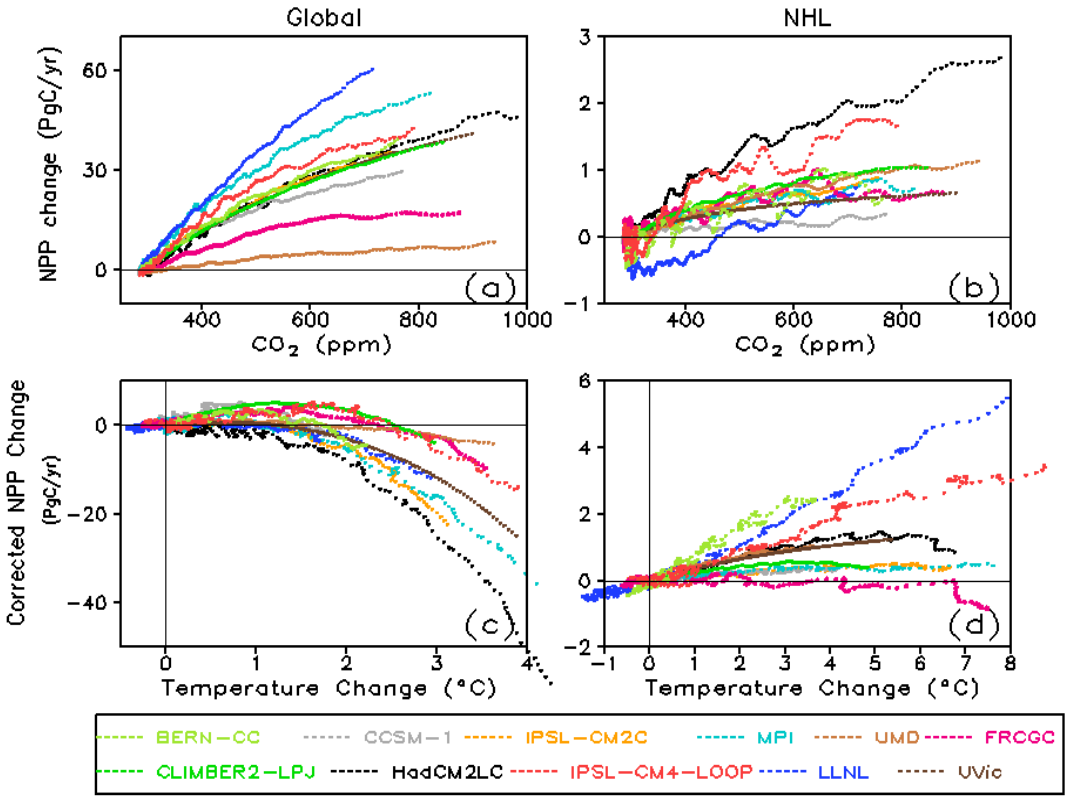

Figure 6.9 The sensitivity of NPP to CO_2 fertilization and temperature change for the whole globe (a, c) and the NHL (b, d) during 1860-2100 for the 11 C4MIP members. The NPP sensitivity to CO_2 fertilization (a, b) is calculated directly from the C4MIP uncoupled simulations, in which the constant climate is prescribed while CO_2 increases for photosynthesis. Then NPP sensitivity to CO_2 fertilization at 2 x CO_2 is used in the coupled simulations to isolate the NPP sensitivity to temperature increase. The NPP sensitivity to temperature (b, d) thus is not the direct NPP from C4MIP coupled simulation. It has been corrected using the sensitivity of NPP to CO_2 fertilization based on uncoupled simulation. For details of this calculation, refer to Friedlingstein et al. (2006). It indicates that NPP sensitivity to temperature change in the NHL is different from the one of global scale. The panels on the left (a, c) are the same as Figure 3a, b in Friedlingstein et al. (2006), and are used here only for comparison to the NHL result.

6.5 Discussion and conclusion

The terrestrial ecosystem in NHL covers 13% of the total global land area, mainly with boreal forests and the tundra. The boreal forest in Northern Hemisphere makes up one-third of the global woodland (Montaigne, 2002). With low ambient temperatures, waterlogged soils, and slow drainage, the NHL ecosystem has been slowly accumulating large amounts of carbon in the soil in the past. The Arctic tundra contains 30-40% of terrestrial soil carbon in the permafrost and peatland at an annual mean surface temperature of -10˚C (Schimel, 1995, Melillo et al., 1995; McGuire and Hobbie, 1997, New et al., 1999). The climate change in the past decades in the NHL has changed the spatio-temporal patterns of terrestrial ecosystem. In the next century, coniferous forests are projected to expand northward and the area of the present tundra coverage could be halved (e.g., see Arctic Climate Impact Assessment, 2005). Changes and potential future changes in the carbon storage and uptake in the high latitudes are important and this work underscores the importance of understanding the underlying mechanisms.

For this purpose, a suite of 11 fully coupled carbon climate simulations from C4MIP were studied to investigate the NHL carbon uptake through 2100. Unlike many modeling studies using climate projections to force carbon cycle models offline (e.g., McGuire et al., 2000; Cramer et al., 2001), the C4MIP coupled simulations consider the interactions between the carbon cycle and the climate. In the pre-industrial period, the mean of the C4MIP models indicates that the NHL soil contained about 18% of global total soil carbon, while the vegetation contained only 5.8% of its global vegetation carbon.

By the end of the 21st century, the mean of the 11 models suggests a 5.9˚C warming in the NHL, in contrast to a 3.2˚C increase for the global mean temperature. The NHL terrestrial carbon changes under the intense high latitude warming and increasing CO_2 in the 21st century can be summarized in a schematic (Fig. 6.10). Our analysis based on C4MIP simulations suggest that the NHL will be a carbon sink with a mean of 0.4 PgC yr-1 through 2100, with an increase of about 40 PgC in land carbon in the C4MIP coupled simulations. Of this, the vegetation carbon increases by about 18 PgC, and the soil carbon increases by about 22 PgC. Though the magnitude of the increment in vegetation carbon is a little smaller, it is robust with a 47% increase, and is of significance to the NHL land carbon budget in the future. In contrast, the increase in soil carbon amounts to only an 8% rise over pre-industrial levels .

Our analysis of the C4MIP models confirms the enhanced vegetation growth ongoing in recent decades as well as projected under future climate change, as described by many previous studies. However, it also reveals a rarely highlighted mechanism, namely, the increased vegetation turnover input to soil carbon that drives an increase in the soil carbon pool. This runs counter to the better-known prediction of loss of soil carbon in response to warming. In contrast to previous estimates that the future NHL soil will lose carbon due to warming (e.g., Davidson et al., 2006), our analysis of the C4MIP models indicate that the NHL soil can still continue to be a carbon sink through 2100. We estimated that the NPP will increase by about 90% by 2100 in NHL. The warming in the NHL region projected from C4MIP models does enhance soil decomposition and drain soil carbon; however, high turnover from the

high productive vegetation provides input to the soil and cancels this soil decomposition in the early 21st century. Davidson et al. (2006) discussed that terrestrial carbon models mostly use Q_{10} or Arrhenius equation for their soil decomposition dependence on temperature. In both parameterizations, decomposition rates have an exponential dependence on temperature, and this is probably why heterotrophic respiration is projected to accelerate at higher temperature. Nevertheless, after 2060, the growth rate of NHL soil carbon begins to decrease because the soil decomposition accelerates at higher temperatures and catches up with the biomass turnover input. Thus, there is a possibility that the NHL soil may lose carbon by intense warming after 2100, rather than in 21st century. The vegetation biomass turnover is of great importance in linking vegetation and soil carbon change.

Further examination of the effects of CO_2 fertilization and climate change in the carbon climate feedback context of C4MIP suggests that besides CO_2 fertilization, the warming in NHL tends to stimulate vegetation productivity to an even greater degree. In contrast to the robust global land carbon loss due to climate-carbon feedback, our analysis suggests that the intense warming in the NHL may help to enhance the terrestrial carbon sink there. The loss of global carbon is dominated by the soil decomposition in the tropics, while the gain in the NHL is dominated by the vegetation growth. This is consistent with current 'greening' and a northward shift of vegetation distributions in the NHL. Such insight into biomass exchanges between the vegetation and soil in the NHL highlights the critical role of carbon cycle-climate interaction under global warming.

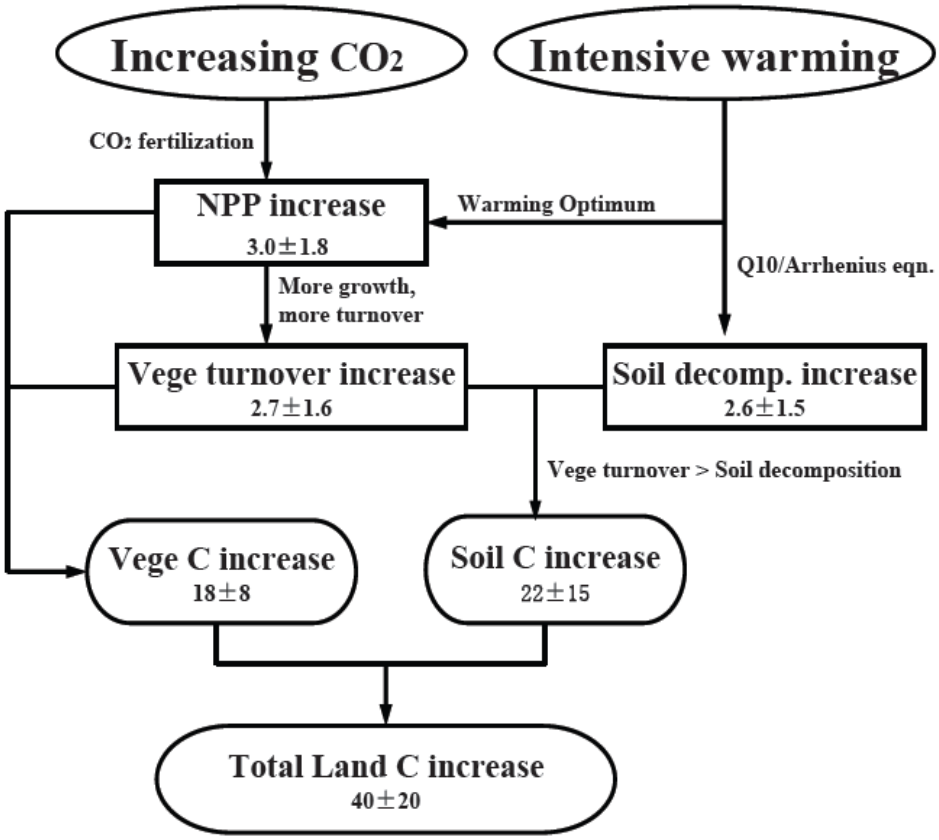

Figure 6.10 The conceptual diagram to show effects CO_2 fertilization and intense warming in NHL on the changes of carbon fluxes and storages by 2100 from C4MIP coupled simulation. The multi-model mean and one standard deviation are provided to indicate the relative magnitudes of these changes. All changes are relative to 1860. Unit for carbon flux is PgC/yr and PgC for carbon storage.

A major caveat to the C4MIP simulations, and therefore to our conclusion predicting an increasing NHL soil carbon pool, is that permafrost and peatland carbon pools are not explicitly represented in these models. When the top soil layer of permafrost thaws, much of the large substrate pool is likely to decompose quickly, and large amounts of otherwise mostly unprotected carbon become available for decomposition (Goulden et al., 1998; Serreze et al., 2000). As the NHL warms significantly, the warming-induced deepening of the layer of seasonal biological activity may cause a net loss of deep soil carbon in the boreal forest and tundra. We

are unfortunately limited to the currently available C4MIP model results, and such possibilities can only be fully addressed in future models/projects that better represent/report these processes.

Another effect that may be of major importance is the change in the hydrological cycle, as precipitation is expected to increase and soil hydrology changes dramatically as permafrost thaws. Angert et al. (2005) studied the NDVI and climate data and reported that drier summers in mid and high latitudes can cancel out the CO_2 uptake enhancement induced by warmer springs, demonstrating that a warming climate does not necessarily lead to higher CO_2 growing-season uptake. Unfortunately, this study could not investigate the effect of soil moisture on NHL ecosystems because no information on precipitation and soil content from C4MIP is provided by the standard output. Soil moisture has been suggested to play an important role for constraining rates of decomposition (Post et al., 1982, Qian et al. 2008), though this effect may be small compared to the intense warming in NHL. Also soil decomposition is known to depend on soil carbon pool size change. We excluded this effect in our analysis because the NHL soil pool only increases by about 8%, compared to the 78% increase of heterotrophic respiration. What is more, the NHL warming has been suggested to have the potential to lengthen the fire season and increase the probability of fires in boreal ecosystems (Randerson et al., 2006; Bond-Lamberty et al., 2007). Land use change could also have a important role in the carbon storage in the NHL (McGuire et al., 2001; Cramer et al., 2001). All of these processes are still poorly understood and need to be addressed in greater depth in future research.

Chapter 7: Conclusion and Future Directions

7.1 Summary

The overall focus of this dissertation was to investigate the variability of the terrestrial carbon cycle and its interaction with climate over a wide range of temporal and spatial scales. The core of my research was based on the terrestrial vegetation and carbon cycle model VEGAS. Using this model, we designed sensitivity simulations with different purposes to explore the scientific questions, and have obtained encouraging results.

7.1.1 Evaluation of VEGAS

We used observed climate forcing to drive VEGAS from 1901-2006. With this offline simulation, we have evaluated VEGAS against FLUXNET observations. In general, VEGAS was able to capture the interannual variation of the land-atmosphere carbon flux against the observations. However, we found that VEGAS simulated the seasonal cycle with the correct amplitude but opposite phase at the Tapajos FLUXNET station site, similar to other state-of-the art models, such as TEM and IBIS. The cause of this behaviour in these models may be the lack of inclusion of some physical processes currently, such as "hydraulic" adaptive process for tree growth during the dry season, as suggested by Saleska et al. (2003). However, these processes are still not well understood. The extent to which, soil moisture, temperature or both, control the heterotrophic respiration, is still an ongoing debate.

Observational stations in the tropical forests are still very sparse and observational records are short. In the meantime, it is encouraging to note that, VEGAS is able to capture a large part of the interannual variation of the land-atmosphere carbon flux compared to the observations there. In the boreal forest of North America, VEGAS can reproduce phenology of the vegetation growth, respiration and land-atmosphere carbon flux at the station site. Despite the deficiency of the seasonal cycle simulated by VEGAS in the tropics, VEGAS captures the variability in both locations on the interannual timescale. This evaluation of VEGAS against FLUXNET observations encourages the application of process-based modeling in studying the response of the terrestrial cycle to climate variation. At the same time, it calls for the model development and improvement, not only for VEGAS, but for other vegetation and carbon cycle models. More observation sites spanning the globe is needed in the future.

7.1.2 Terrestrial carbon cycle in response to ENSO

The interannual variability of atmospheric CO_2 shows an association with ENSO cycle. It can change by as much as 4-5 PgC/yr during ENSO years. Because CO_2 emissions from fossil fuel burning and land use change increase slowly with small year-to-year variation, understanding the mechanism of variability of the terrestrial carbon ecosystem in response to climate variation is of significance for the atmospheric CO_2 growth rate. With this goal, we used offline simulations of VEGAS and studied the responses of the terrestrial carbon ecosystem to the physical climate variations. We isolated those climatic effects of temperature and precipitation. In

particular, this was done to examine the role of soil moisture in the terrestrial ecosystem associated with ENSO.

Our analysis indicates that the simulated global total land-atmosphere carbon flux of VEGAS agrees well on interannual timescales with the results of an inversion model used by Rödenbeck et al. (2003), especially in the tropics. Both models are in agreement with the atmospheric CO_2 growth rate variation at MLO. An evaluation of VEGAS against observations shows that the simulated LAI by VEGAS has better correlation with observed NDVI in the extratropics than the tropics. Our simulation shows that the land-atmosphere carbon flux in the tropics has a similar magnitude as the global total, confirming the dominant role of the tropics on the interannual timescale. This underscores the importance of extending the observational network in the tropics in the future.

Further study of terrestrial timing with respect to ENSO evolution indicates that in the tropics VEGAS simulates a robust signal of F_{ta} with a 6-month lag of ENSO cycle during 1980-2000. This is largely caused by the suppression of vegetation and enhancement of soil decomposition, as suggested by the "conspiracy" theory of Zeng et al. (2005a). Though the anomalous precipitation lags ENSO cycle by 1-2 months, the vegetation-dependent soil moisture takes about 5 months to respond due to soil memory. Less precipitation, with higher temperature drains the soil moisture and results in drought conditions unfavorable for vegetation growth. This results in a 6-month lag of the NPP from El Niño. Simultaneously, higher temperature directly enhances soil decomposition. As a result, reduction of NPP and

enhancement of R_h contribute in same direction, and provide a large amount of carbon release to the atmosphere.

The precipitation and temperature have very different mechanisms in regulating the above variation of vegetation growth and soil decomposition during ENSO events. In total, precipitation variations contributes about 56% of the F_{ta} anomaly, mostly through soil wetness in the photosynthesis process, while temperature accounts for 44%, which includes 25% from direct effect on soil decomposition, 7% from its direct effect on vegetation respiration, and 12% from its indirect effect on the photosynthesis through soil wetness. Such an indirect effect, though significant, has not been studied in the past. The unique design and analysis of the appropriate sensitivity simulations in this study helped delineate the indirect effect of temperature affecting photosynthesis through its effect on soil wetness. The experimental results thus indicate that in the tropics vegetation activity suppression (NPP) contributes 68% of variation to F_{ta}, with the remaining 32% coming from soil decomposition under warmer and drier conditions. Within, the total land-atmosphere carbon flux, about 25% is due to fire burning, which is included in the vegetation and soil respiration. The additive responses to temperature and precipitation forcing observed in the tropics helped quantify the mechanisms through which each forcing affects the carbon flux directly and indirectly, thus highlighting the critical role of soil moisture in the ecosystem and carbon cycle. This is critical, as soil wetness is a poorly constrained factor, observationally.

7.1.3 Impact of Midlatitude drought on the terrestrial ecosystem

The above study illustrates the canonical tropical dominance of the terrestrial carbon flux in response to ENSO. It quantifies the mechanisms through which precipitation and temperature affect the carbon flux directly and indirectly, highlighting the importance of soil moisture on tropical terrestrial ecosystems. Changes in the carbon sources and sinks in Midlatitude regions often tend to cancel each other, so the overall variability is weakly correlated with ENSO and it contributes only to a small fraction of the interannual variability in atmospheric CO_2. However, during 1998-2002 the Northern Hemisphere Midlatitudes were undergoing a long-term drought, with the most severity in the regions of the western US, southern Europe, Southwest Asia, eastern Asia and Siberia (Waple et al., 2002; Hoerling and Kumar, 2003). During 2002-2003, the MLO station witnessed an unprecedented growth rate of over 2 ppm/yr. Based on our VEGAS offline simulation, we have established a relationship between this drought and the sustained CO_2 growth rate during 2002–2003. The 1998–2002 Midlatitude drought was characterized by reduced precipitation and increased temperature. The anomalous climate caused widespread consequences to the terrestrial ecosystem there. Our results suggest that during 1998-2002, the Northern Hemisphere land between 20˚N and 50˚N was a nearly constant source releasing 1.3 PgC/yr more relative to the 1980-98 average, consistent with the similar trend found from the inversion modeling by Rödenbeck et al. (2003). In VEGAS, an enlarged spatial extent of semi-arid regions with reduced NPP followed the precipitation changes in the Midlatitudes during 1998-2002. Meanwhile, the long-term warming trend during that period led to yet more respiration. As a result, the

Northern Hemisphere Midlatitude was predominantly a CO_2 source to the atmosphere during 1998 –2002 with a spatial extent larger than merely the area affected by reduced precipitation.

7.1.4 Carbon cycle-climate feedback

The magnitude of future climate change for a given anthropogenic fossil fuel emission depends critically on the efficiency of carbon uptake by land and ocean. There are large uncertainties in the predicted strength of carbon-climate feedback and its impact on climate prediction. Using a fully coupled carbon-climate model (UMD) we conducted experiments to investigate the feedback on future climate change and compared this with the modeling results of the Hadley and IPSL models.

Our results indicate a positive feedback from the interactive response of the carbon cycle to climate change. Due to this feedback, there is about 90 ppm additional CO_2 by 2100, which implies a 0.6˚C additional warming in UMD, compared to the Hadley model with 250 ppm more CO_2 and a 1.5˚C additional warming. The IPSL model results are more similar to ours in terms of the CO_2 increase and warming. However, the terrestrial carbon uptake change due to the carbon cycle differs significantly among the three models. UMD predicts that the land will be a carbon source of size 20 PgC (1860-2100 cumulative) in coupled mode, which is the same direction as the Hadley model. However, the Hadley model simulated a much more robust land carbon loss due to positive carbon cycle-climate feedbacks, and their amplitude is 720 PgC, 6 times larger than ours. The IPSL (200 PgC) model released a similar amount of carbon from the land to the atmosphere as ours, but their results differ from ours and the Hadley Center's in that both the soil

and vegetation pools continue to increase over time, in contrast to the reduction of the soil carbon pool storage in the Hadley and UMD models. Our sensitivity experiments show that if a stronger CO_2 fertilization is applied in UMD, there will be a land carbon sink of 150 PgC in 2100, comarped to a 20 PgC source in the standard run. This modification forces UMD in the direction of the IPSL result. In a separate scheme using only a single soil pool, UMD was highly sensitized to warming and had a cumulative land carbon source of 100 PgC through year 2100, more similar to the Hadley model. These sensitivity experiments have helped to understand how large differences among the three models can arise.

7.1.5 Future carbon uptake in Northern High Latitudes

These large differences among the models call for intensive investigative projects like C4MIP. Based on the results from C4MIP, Friedlingstein et al. (2006) indicate a positive carbon cycle-climate feedback from all C4MIP models in the 21st century, which causes an additional 20-200 ppm CO_2 to be injected into the atmosphere by 2100, leading to 0.1-1.5˚C additional warming, globally. During the past decades, Northern High Latitudes (NHL: poleward of 60°N) have witnessed dramatic changes where the annual average temperatures increased by 1-2˚C in northern Eurasia and northwestern North America, changes much larger than the increase of global average surface temperature of 0.65±0.2˚C over the 20th century (IPCC, 2007). The ongoing and continued projected rapid Arctic warming has been changing the physical, biological, and societal conditions in the NHL via “greening” and northward shifts of the vegetation distribution.

On one hand, warming and higher CO_2 stimulate vegetation growth wherein

tundra transitions to boreal forests, thus taking up CO_2. On the other hand, warming accelerates decomposition of dead organic matter, thus losing soil carbon to the atmosphere. The resulting net land-atmosphere CO_2 flux is important for future carbon cycle-climate feedback and the degree of climate change. NHL stores a large amount of carbon in the permafrost and peatland under conditions of -10˚C annual mean surface temperature. This sealed carbon is potentially vulnerable to release under future intense warming in the NHL. Using the C4MIP model results, we have investigated the future carbon uptake scenario by 2100 in Northern High Latitudes poleward of 60˚N. C4MIP models project an intense warming in the NHL with the ensemble mean warming there of 5.9˚C, in contrast to 3.2˚C for the global mean increase in temperature. Our analysis based on the C4MIP simulations indicates that the NHL is likely to be a carbon sink with a mean of 0.4 PgC/yr by 2100, with a cumulative increase of about 40 PgC land carbon in the C4MIP coupled simulations. Of this, the vegetation carbon increases by about 18 PgC, and the soil carbon increases by about 22 PgC. Though the magnitude of the increment in vegetation carbon is slightly smaller, it is robust - a 47% increase. This is of significance to the NHL land carbon budget in the future, when compared to the only 8% increase in soil carbon. In contrast to previous estimates that future NHL soil will lose carbon due to intense warming, our analysis indicates that the NHL soil can still continue to be a carbon sink by 2100. The intense warming in the NHL region does enhance soil decomposition and thereby drain some soil carbon; however, the NPP will increase by about 88% by 2100 in the NHL, and this leads to a high vegetation turnover and overall carbon input to the soil. We project that this fertilization will cancel the soil

decomposition effects in the early 21st century. Nevertheless, after 2060, the growth rate of NHL soil carbon begins to decrease because the soil decomposition begins to accelerate under intense warming. Eventually, decomposition should catch up with the increased biomass fertilization and turnover, sometime after 2100.

Another interesting point is that in contrast to the robust global land carbon loss due to climate-carbon feedback discussed by Friedlingtein et al. (2006), our analysis suggests that the intense warming in the NHL may help to enhance the terrestrial carbon sink there. The loss of global carbon is dominated by enhanced soil decomposition in the tropics, while the gain in the NHL is dominated by the vegetation growth. Besides CO_2 fertilization, the intense warming in the NHL tends to stimulate vegetation productivity. Our results show that the future NHL carbon storage change by 2100 is consistent with current "greening" and a northward shift of vegetation distributions in the NHL, reported from the observations. Such insight into biomass exchanges between the vegetation and soil in the NHL highlights the critical role of carbon cycle-climate interactions for carbon uptake under global warming.

7.2 Future directions

7.2.1 Multi-decadal variability of terrestrial carbon

On decadal time scales, variations of atmospheric CO_2 growth rate are related to the variability of the carbon absorption by land and ocean, land use change, and change in fossil fuel emissions, etc. The simulation of terrestrial carbon of the last century implies a relationship between the multi-decadal variability of global total terrestrial carbon flux with climate decadal variation, such as the PDO (Pacific

Decadal Oscillation) (Figure 7.1). The examination and quantification of decadal variability of global and regional average terrestrial carbon would help us to understand the pathway of carbon destinations, such as the difference of land carbon sinks between the 1980s and the 1990s (IPCC, 2001; House et al., 2003).

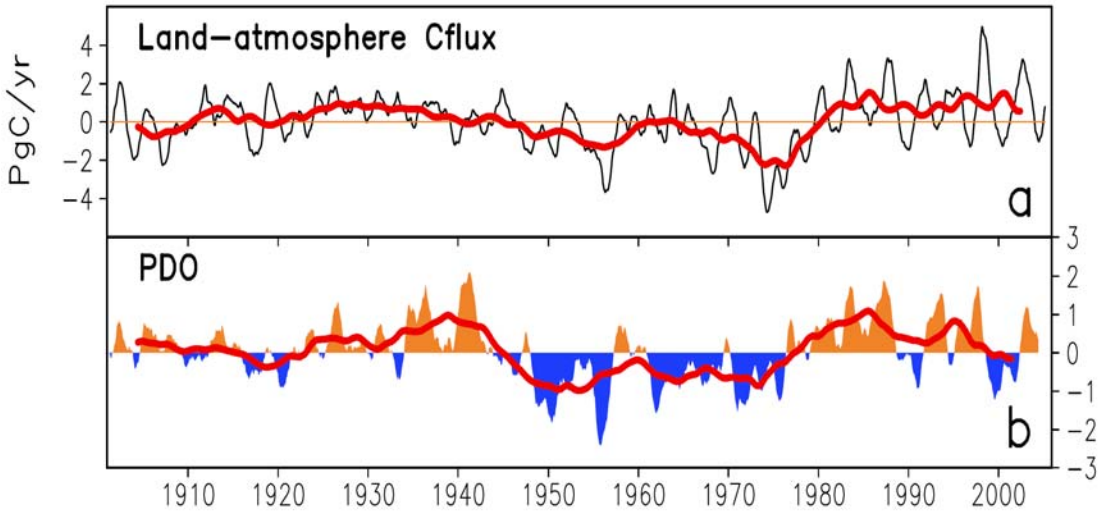

Figure 7.1 (a) Land-atmosphere carbon flux of 1901-2004 from VEGAS offline simulation; (b) Pacific Decadal Oscillation (PDO) Index of 1901-2004. 6-year running mean applied to smooth the curves to extract the low frequency signal (red).

7.2.2 Soil moisture effect on the vegetation growth and soil respiration

In Chapter 3, we highlighted the importance of soil moisture on the vegetation growth, in particular temperature's indirect effect on the vegetation growth via changes in soil moisture. The role of soil moisture on vegetation growth is, however, potentially very model-dependent. I will extend this work with the aid of other vegetation-carbon models to better quantify this effect. Moreover, the conclusions were entirely based on our analysis for tropical land. The extratropics, especially the semi-arid areas in the Midlatitudes, are important cropland and agriculture regions.

Water availability there plays an important role for crop growth. The regional scale of soil moisture's effect on vegetation growth in the Midlatitudes is, thus, of interest. Soil temperature and moisture are two of the most important environmental parameters controlling variations in soil CO_2 flux; however, the relationship between soil respiration and soil moisture is still not well understood. In Figure 3.9, our result shows that VEGAS simulates a relatively small effect of soil moisture on the soil respiration; however, Saleska et al. (2003) suggested that the soil wetness, rather than temperature, plays a more important role on the soil decomposition during the wet season at Tapajos. Mechanisms by which water content can influence soil respiration are by way of the influence of soil moisture on dissolved organic matter content loading, on soil aeration, and on the energy allocation of microbes and plants. Thus, further study on relationship between soil respiration and water content will focus on discerning potential effects of water distribution changes on the pattern of soil respiration in terrestrial ecosystem along with global change.

7.2.3 Improvement of VEGAS

The development and improvement of VEGAS is a pathway for our better understanding of natural physical processes. Though we have encouraging results from modeling interannual variability of the terrestrial carbon cycle, we are currently developing a new version of VEGAS with a better seasonal cycle, and incorporating land use change into VEGAS to examine the carbon change due to historical land use change.

Appendices

A.1 Vegetation carbon dynamics in VEGAS

In VEGAS, the gross photosynthetic rate Ag is a function of, temperature, soil moisture, light and atmospheric CO_2 concentration:

$$A_g = G\{\alpha(T), \beta(W), \gamma(PAR, LAI, H), \theta(CO_2)\} A_{g0} \quad \text{(A.1)}$$

where $\alpha(T)$ is a temperature dependent (Figure A.1), $\beta(W)$ is soil moisture dependent, $\gamma(PAR, LAI, H)$ is light dependent (Figure A.2) and $\theta(CO_2)$ is CO_2 dependent growth factor (Figure A.3), and function G is a co-limiting function. $\beta(W)$ uses a linear function of soil moisture. Vegetation parameters used in VEGAS can be found in Table A.1. A_{g0} is the maximum carbon assimilation rate, taken as 5.5 KgC/m^2/yr. γ is a function of Photosynthetically Active Radiation (*PAR*), Leaf Area Index (*LAI*), and vegetation Height (*H*). The PFT-dependent height and *LAI* determine the relative competitive advantage of trees vs. grasses, as well as young and old trees. The gross carbon assimilation is partly used for vegetation growth, so that the net assimilation is:

$$A = A_g - r_{grow} A_g \quad \text{(A.2)}$$

Where r_{grow} is the growth respiration fraction, taken as 0.3.

The change of vegetation leaf, wood and root carbon pools are:

$$\frac{dC_l}{dt} = f_l A - (R_l + T_l + S_l + F_l) \quad \text{(A.3)}$$

$$\frac{dC_r}{dt} = (1 - f_l) f_r A - (R_r + T_r + S_r) \quad \text{(A.4)}$$

$$\frac{dCw}{dt} = (1 - f_l)(1 - f_r) A - (R_w + T_w + S_w + F_w) \quad \text{(A.5)}$$

where C_l, C_r, C_w are the leaf, root and wood carbon pools, with subscript *l*, *r*, *w* representing leaf, root and wood, respectively. The loss terms are proportional to the respective carbon pool, such as $R_l = r_l f_{Tl}(T_{air}) C_l$, $T_l = t_l C_l$ and so on, where r_l is the rate of carbon loss; and this applies to R, T, S for *l*, *r*, *w*. R is respiration, T is turnover, S is drought and cold stress turnover. F is carbon loss due to fire, only for vegetation leaf and wood. The leaf carbon pool gets a fraction of the total assimilation carbon at an allocation factor $f_l = f_l(LAI, H)$ which is a function of *LAI* and vegetation height *H*, and f_r is a root allocation factor, and the rest goes into the wood carbon pool.

Tree height is a function of wood mass using the bolometric function:

$$H^k = H^k_{\max}[1 - \exp(-C_w / C^k_{ws})] \quad \text{(A.6)}$$

Where $H_{\max}$ is maximum height and C_{ws} is a wood mass scaling factor and k refers to the different 4 PFTs in VEGAS.

The light extinction coefficient is a function of vegetation height:

$$\lambda = \lambda_{\max} - (\lambda_{\max} - \lambda_{\min}) \exp(-H^k / H_s) \quad \text{(A.7)}$$

Where lambda is light extinction coefficient and H_s is the tree height scalar. The fraction allocated to leaf is initially large, but decreases as the plant grows

$$f_l = \exp[-0.15 \frac{\lambda_{\max}}{\lambda} L] \quad \text{(A.8)}$$

Where L is Leaf Area Index (LAI). The fraction of the rest which is allocated to roots f_r is 0.3 for trees and 0.8 for grasses. The remainder goes to the wood carbon pool.

The light dependent growth rate is

$$\gamma = \gamma_0 \{1 - \exp[-0.15 \frac{\gamma}{\gamma_{\max}} [L + L_{\min}]\} \quad \text{(A.9)}$$

Where γ_0 is the normalized PAR at the top of the vegetation canopy and the term in the braces is a shading factor related to canopy structure. This is modified from Sellers (1991) such that given the same LAI, taller plants are better at trapping light because of their three-dimensional structure.

The competition between the PFTs depends on their fractional cover of each PFT. It is simply proportional to tree height:

$$\delta = \frac{H^k}{\sum_k H^k} \quad \text{(A.10)}$$

Since tree height is the result of the balance between growth and loss, this deceptively simple competition rule actually includes a major factor. For instance, grasses would grow faster than tree initially as they allocate more resources to grow leaves. But since grasses have smaller maximum height they would be eventually out competed by trees (Eq. A.10).

The temperature dependence of respiration is:

$$f_T = \exp[-k(T - 25)] \quad \text{(A.11)}$$

For leaf and wood: k = 0.08 (Q_{10} = 2.2), root and fast soil pool: k = 0.045 (Q_{10} =1.5) intermediate soil pool: k = 0.03 (Q_{10} =1.35) and slow soil pool: k = 0.01(Q_{10} =1.105), where Q_{10} is the ratio of temperature dependence of respiration function f_T with 10˚C temperature change to the original one at 25˚C. Leaves are subject to additional cold

and drought stress under which leaves are removed at a rate more rapid than merely represented by the imbalance of reduced photosynthesis and normal respiration and turnover loss:

$$S_l = S_l \{\exp[0.1(T_c - T_{cod}) + \exp[w_s(0.2 - \beta)]\} \quad \text{(A.12)}$$

Where T_{cod} = min (T_{air} , 5) such that there is no stress over 5˚C ; T_c is a critical temperature and T_c = 5, -45, -5, 5 for the 4 PFTs; w_s is a drought resistant factor.

Table A.1 Vegetation parameters used in VEGAS for 4 different Plant Functional Types (PFTs), namely, broadleaf tree, needle leaf tree, cold grass and warm grass. In the following chart, PFT1 means broadleaf tree, PFT2 for needle leaf tree, PFT3 for cold grass, and PFT4 for warm grass.

Parameters	Physical name	Value		Unit
A_{g0}	Max carbon assimilation rate	5.5		KgC m^{-2} yr^{-1}
r_{grow}	Growth respiration fraction	0.3		
H_{max}	Max tree/grass height	PFT1	50	m
		PFT2	50	
		PFT3	2	
		PFT4	2	
C_{ws}	Wood mass scalar	PFT1	20	Kg
		PFT2	20	
		PFT3	0.1	
		PFT4	0.1	
H_s	Tree height scalar	10.0		m
λ_{max}	Max light extinction coefficient	0.8		
λ_{min}	Min light extinction coefficient	0.3		
R_l	Leaf respiration rate	1		yr^{-1}
R_w	Sapwood respiration rate	1/10		yr^{-1}
R_r	Root respiration rate	1/2		yr^{-1}
T_l	Leaf turnover rate	1		yr^{-1}
T_w	Sapwood turnover rate	1/30		yr^{-1}
T_r	Root turnover rate	1/2		yr^{-1}
S_l	Leaf drought and cold stress rate	1/2		yr^{-1}
S_w	Sapwood drought and cold stress rate	1/100		yr^{-1}
S_r	Root drought and cold stress rate	1/100		yr^{-1}
T_{cod}	Critical temperature for the cold stress	PFT1	5.0	°C
		PFT2	-45.0	
		PFT3	-5.0	
		PFT4	5.0	
W_s	Water stress coefficient	10.0		
Q_{10}	Temperature dependent for respiration	Leaf and wood: 2.2 root: 1.5		

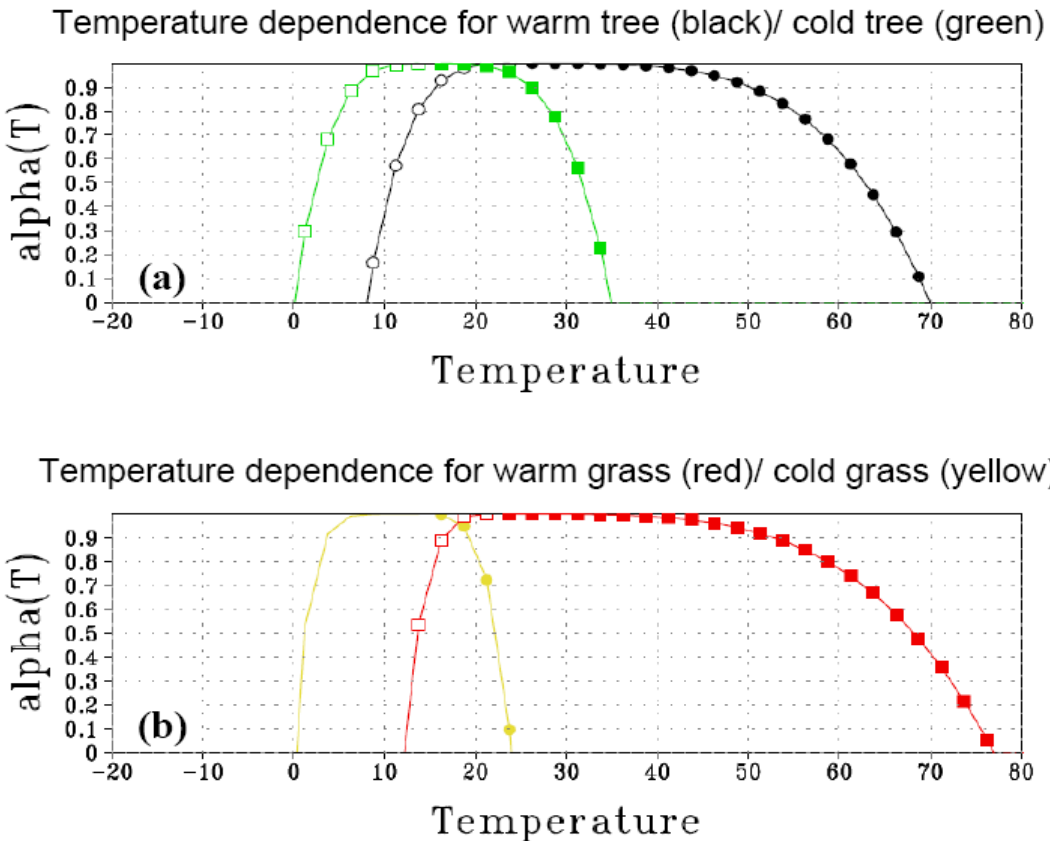

Figure A.1 The temperature dependent function $\alpha(T)$ for 4 PFTs in VEGAS. (a) Warm tree and cold tree; (b) Warm grass (C4) and cold grass (C3).

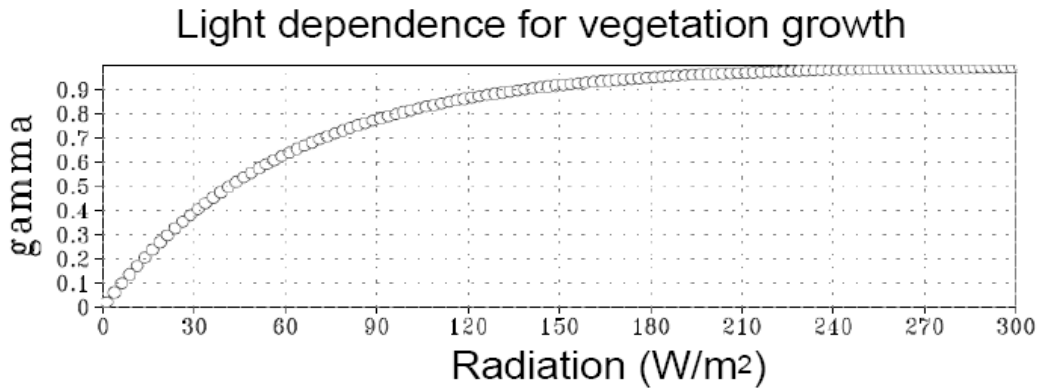

Figure A.2 The light dependent $\gamma(PAR, LAI, H)$ on the radiation in VEGAS.

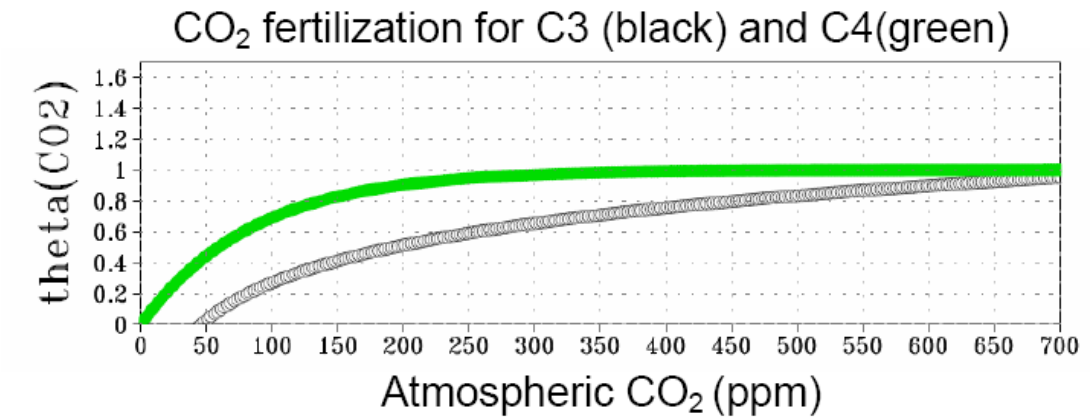

Figure A.3 The CO_2 dependent growth factor $\theta(CO_2)$ for C3 (warm/cold tree and cold grass) and C4 (warm grass) in VEGAS.

A.2 Soil carbon dynamics in VEGAS

The total turnover from vegetation biomass $T_v = T_l + T_r + T_w + S_l + S_r + S_w +$ F_{vt} is the input for the first soil pool C_{sf} (litter-fall):

$$\frac{dC_{sf}}{dt} = T_v - (R_f + T_f + E_f + b_f F_f) \qquad \text{(A.13)}$$

The carbon is lost through respiration $R_f = r_f f_{Tf}(T_{soil}) C_{sf}$, and turnover to the intermediate soil pool $T_f = t_f C_{sf}$, and erosion $E_f = e_f C_{sf}$. F_{vt} Is the turnover from the dead vegetation due to fire. $b_f F_f$ is the flux of fast soil pool due to fire (see the following section of fire module). The intermediate (C_{sm}) and slow (C_{ss}) soil pools are modeled similarly as the fast soil except that there is no turnover for the slow soil pool (end of cascade). The soil parameters used in VEGAS can be found in Table A.2.

$$\frac{dC_{sm}}{dt} = T_f - (R_m + T_m + E_m) \qquad \text{(A.14)}$$

$$\frac{dC_{ss}}{dt} = T_m - (R_s + E_s) \qquad \text{(A.15)}$$

Table A.2 Soil parameters used in VEGAS for three soil carbon pools: fast soil, intermediate soil and slow soil carbon pool.

Parameters	Physical name	Value	Unit
R_f	Fast soil pool respiration rate	1/2	yr^{-1}
R_m	Intermediate soil pool respiration rate	1/100	yr^{-1}
R_s	Slow soil pool respiration rate	1/1000	yr^{-1}
T_f	Fast soil pool turnover rate	1/80	yr^{-1}
T_m	intermediate soil pool turnover rate	1/1000	yr^{-1}
E_l	Fast soil pool erosion rate	1/400	yr^{-1}
E_w	Intermediate ast soil pool erosion rate	1/5000	yr^{-1}
E_r	Slow soil pool erosion rate	1/50000	yr^{-1}
Q_{10}	Temperature dependence of respiration	Fast soil: 1.5 Intermediate: 1.35 Slow soil: 1.105	

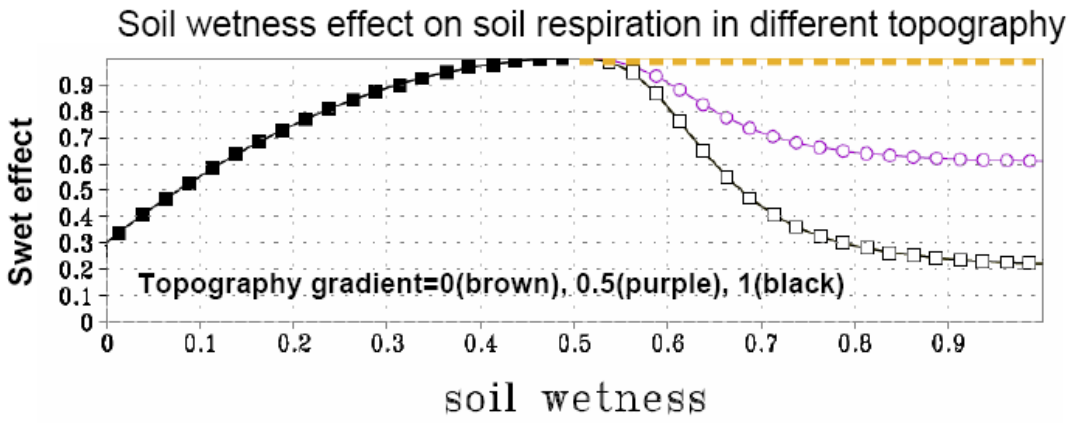

Figure A.4 Soil wetness effect on the soil respiration in VEGAS with different topography. The topography information is scaled to the topography gradient in VEGAS and doesn't change in modeling with time. The plot indicates that at a higher soil wetness condition, the respiration tends to be reduced somewhat (e.g., wetland) by the topographic effects.

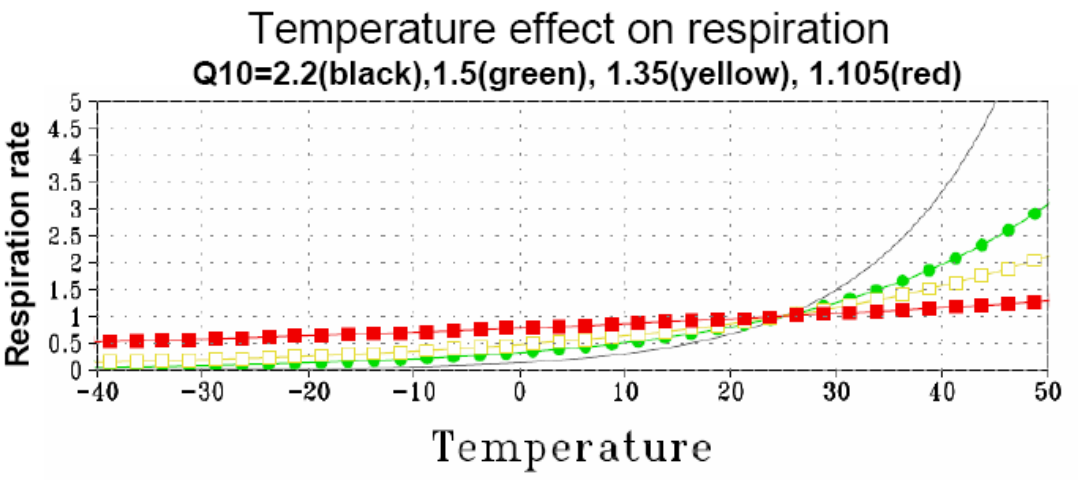

Figure A.5 Temperature effect Q_{10} on the respiration in VEGAS. Q_{10} =2.2 for leaf and wood, 1.5 for the root and fast soil, 1.35 for the intermediate soil and 1.105 for the slow soil carbon pool.

A.3 Fire module in VEGAS

VEGAS has a fire module which calculates the land-atmosphere carbon flux due to biomass burning based on the effects of moisture availability, fuel load and PFT dependent resistance (Eq. A.16). When fire occurs in VEGAS, leaves suitable as fuel load burns completely, while wood and fast soil carbon get only partly combusted. The rest of dead vegetation is a turnover going into the fast soil pool that is decomposed later according to local soil and climate condition (indirect fire carbon flux) (Eq. A.17)

$$CF_{ire} = b_l F_l + b_w F_w + b_f F_f \tag{A.16}$$

$$F_{vt} = (1 - b_l) F_l + (1 - b_w) F_w \tag{A.17}$$

Where b_l, b_w and b_f are the fractions of leaf, wood and surface soil pool suitable to burn completely into the atmosphere. b_l = 1 (all leaves are burned), b_w = 0.2,0.5,0.9 for broadleaf tree, needle leaf tree and grasses, respectively, b_f =0.2 is for the surface soil pool (our fast soil pool includes litter-fall). Needle leaf tree has a higher burnt

fraction because of the more flammable material (sap etc.) such as the boreal forests in Canada and Siberia.

$$F_l = r_{fire} P_{fire} C_l \tag{A.18}$$

$$F_w = r_{fire} P_{fire} C_w \tag{A.19}$$

$$F_f = r_{fire} \overline{P_{fire}} C_f \tag{A.20}$$

Where the r_{fire} is a unit loss rate and P_{fire} is the probability of fire occurrence. $\overline{P_{fire}}$ is a PFT weighted average of P_{fire}.

The probability of fire occurrence is predicted as:

$$P_{fire} = P_{swet} P_{temp} P_{fuel} \tag{A.21}$$

Where the soil dependence P_{swet} is as:

$$P_{swet} = \exp(-swet / 0.1) \tag{A.22}$$

And the temperature dependence is not used, i. e. P_{temp}=1. The fuel load dependence requires a minimum fuel load of 0.2 kg/m^2 in order for fire to become self-sustainable and increases linearly afterwards:

$$P_{fuel} = (C_{fuel} - 0.2) / 1.0 \tag{A.23}$$

Where C_{fuel} is the fuel load for PFT type, k dependent:

$$C_{fuel} = b_l C_l + b_w C_w + b_f C_{sf} \tag{A.24}$$

In VEGAS, CF_{ire} is included in the vegetation and soil respiration (R_a and R_h). The carbon flux associated with biomass burning of vegetation leaf/wood is included in the vegetation respiration of vegetation (R_a) and the part of fast soil pool due to fire is included in soil decomposition (R_h). The dead vegetation due to fire turnover into fast soil pool, is an indirect part of fire, which is much smaller with respect to the

total vegetation turnover. We estimate that 83% of the carbon fluxes due to biomass burning is included in the R_a and the remaining 17% is included in R_h.

Often observationally available is fire recurrence interval (FRI) which can be diagnosed as:

$$FRI = \frac{1}{r_{fire}\overline{P_{fire}}} \tag{A.25}$$

And $r_{fire}\overline{P_{fire}}$ is the probability of fire per unit time.

Table A.3 Parameters used in the fire module in VEGAS.

Parameters	Physical name	Value		Unit
r_{fire}	A unit loss rate	1/2.0		yr^{-1}
b_l	Fraction of leaf suitable to burn completely	1.0		
b_w	Fraction of wood suitable to burn completely	PFT1	0.2	
		PFT2	0.5	
		PFT3	0.9	
		PFT4	0.9	
b_f	Fraction of fast soil pool suitable to burn completely	0.2		

A.4 Carbon fluxes at steady stage in VEGAS

At steady state in the VEGAS offline simulation (see the Chapter 2 for the description of offline simulation), the global total GPP is 124 PgC/yr with NPP of 61 PgC/yr, and vegetation and soil carbon pools contain 641 PgC, 1848 PgC, respectively. In vegetation, leaf contains 15 PgC, wood has 615 PgC and the root has 21 PgC. As for the three soil carbon pools, the fast soil carbon pool contains 307 PgC, 610 PgC in intermediate pool and 910 PgC in the slow soil carbon pool. The following figure (Figure A.7b) indicates the magnitude of the individual carbon fluxes in VEGAS.

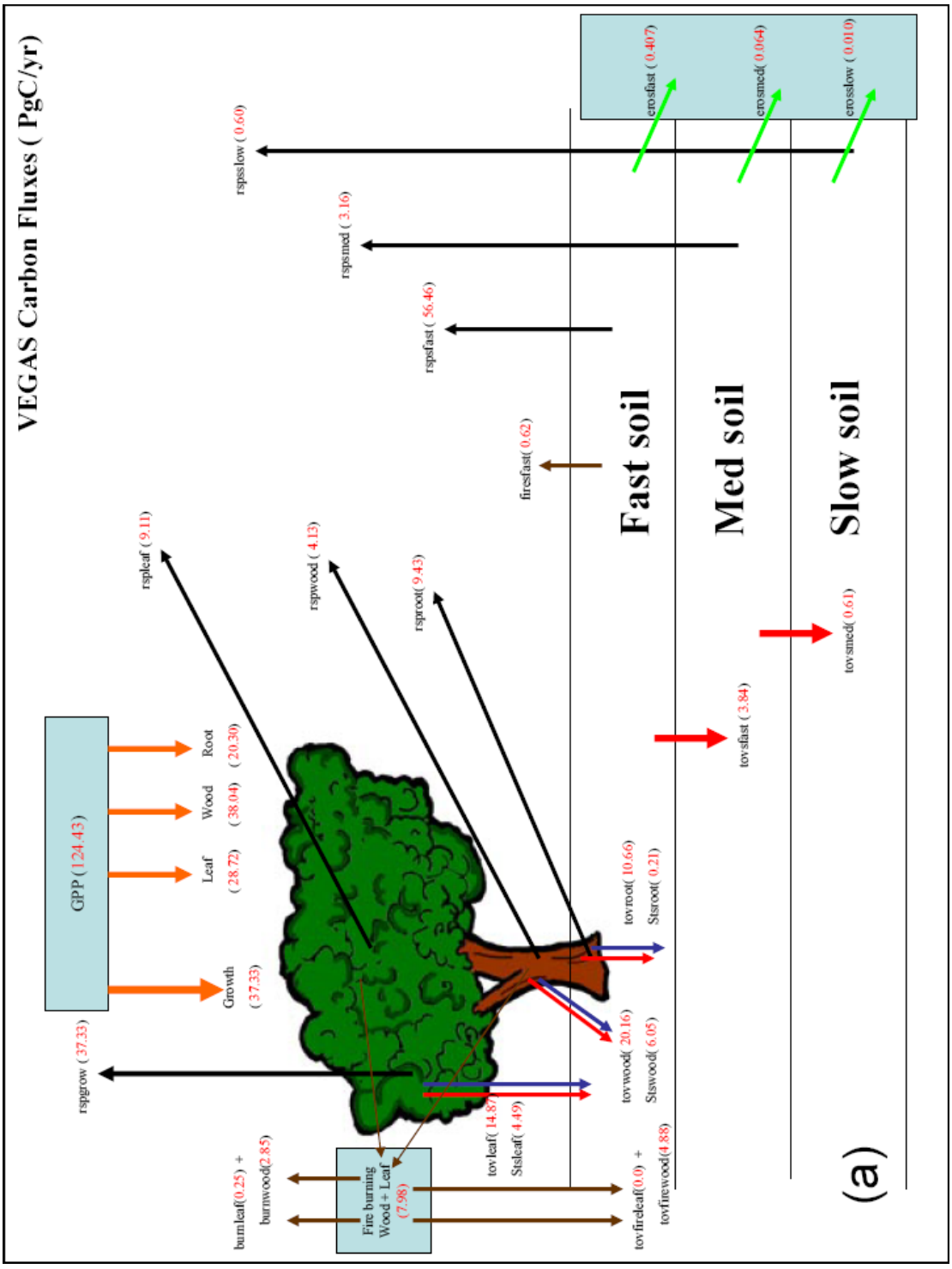
VEGAS Carbon Fluxes (PgC/yr)
GPP (124.43)
Leaf (28.72)
Wood (38.04)
Root (20.30)
Growth (37.33)
rspgrow (37.33)
rspleaf (9.11)
rspwood (4.13)
rsproot(9.43)
rspsslow (0.60)
rspsmed (3.16)
rspsfast (56.46)
firesfast(0.62)
Fast soil
Med soil
Slow soil
erosfast (0.407)
erosmed(0.064)
erosslow (0.010)
tovsmed(0.61)
tovsfast (3.84)
tovroot(10.66)
Stsroot(0.21)
tovwood(20.16)
Stswood(6.05)
tovleaf(14.87)
Stsleaf(4.49)
tovfireleaf(0.0) +
tovfirewood(4.88)
Fire burning
Wood + Leaf
(7.98)
burnleaf(0.25) +
burnwood(2.85)
(a)

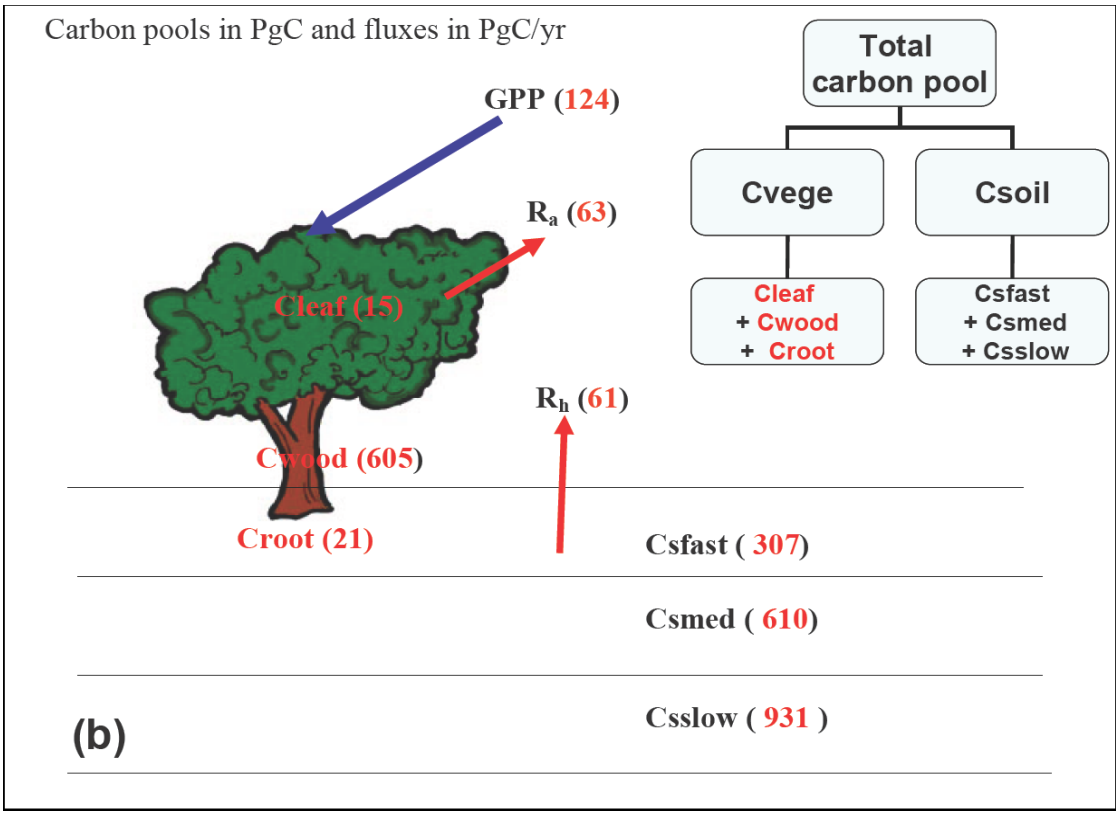

Figure A.6 (a) Annual mean of carbon fluxes (PgC/yr) in VEGAS. The figure indicates the magnitude of the individual carbon fluxes in VEGAS. The values in red in parenthesis are calculated at steady state of offline VEGAS simulation. The arrows in colors are used to indicate different biological processes. (b) Annual mean of GPP, Ra and Rh (PgC/yr) and individual carbon pool (PgC) of vegetation and soil in VEGAS. The physical meaning of these variables in this figure with respect to their names in Appendices can be found in the following table:

Variable in the Appendices	Variables in Figure 6	Physical meaning of variables
A	GPP	Gross Primary Productivity
	Growth	Fraction of GPP into vegetation growth
$f_l A$	leaf	Fraction of GPP into vegetation leaf
$(1-f_l)(1-f_r)A$	wood	Fraction of GPP into vegetation wood
$(1-f_l)f_r A$	root	Fraction of GPP into vegetation root
$r_{grow} A_g$	rspgrow	Growth respiration
R_l	rspleaf	Vegetation leaf respiration
R_w	rspwood	Vegetation wood respiration
R_r	rsproot	Vegetation root respiraiton
T_l	tovleaf	Vegetation leaf turnover into soil
T_w	tovwood	Vegetation wood turnover into soil
T_r	tovroot	Vegetation root turnover into soil
S_l	Stsleaf	Vegetation leaf stress into soil
S_w	Stswood	Vegetation wood stress into soil
S_r	Stsroot	Vegetation root stress into soil
$b_l F_l$	burnleaf	Vegetation leaf burnt into atmosphere
$b_w F_w$	burnwood	Vegetation wood burnt into atmosphere
F_l+F_w	Biomass burning	Vegetation wood/leaf suitable for burning
$(1-b_l) F_l$	tovfireleaf	Vegetation dead leaf after biomass burning into soil
$(1-b_w)F_w$	tovfirewood	Vegetation dead wood after biomass burning into soil
$b_f F_f$	firesfast	Fast soil pool burnt into atmosphere
R_f	rspsfast	Fast soil respiration
R_m	rspsmed	Intermediate soil respiration
R_s	rspsslow	Slow soil respiration
T_f	tovfast	Fast soil turnover
T_m	tovmed	Intermediate soil turnover
E_f	erosfast	Fast soil erosion
E_m	erosmed	Intermediate soil erosion
E_s	erosslow	Slow soil erosion
NPP		Net Primary Productivity, GPP-R_a
R_a	R_a	Autotrophic respiration or plant respiration
R_h	R_h	Heterotrophic respiration or soil decomposition
NEE		Net Ecosystem Exchane
C_l	Cleaf	Vegetation leaf carbon pool
C_w	Cwood	Vegetation wood carbon pool
C_r	Croot	Vegetation root carbon pool
C_{sf}	Csfast	Fast soil carbon pool
C_{sm}	Csmed	Intermediate soil carbon pool
C_{ss}	Csslow	Slow soil carbon pool

A.5 Variables used in the carbon research community

The most important common variables used by the carbon research community are as follows:

$$GPP = A_g \tag{A.26}$$

$$NPP = GPP - R_a \tag{A.27}$$

$$NEP = NPP - R_h \tag{A.28}$$

$$NEE = -NEP \tag{A.29}$$

Where *GPP* (Gross Primary Production) is the difference of total photosynthetic carbon and growth respiration. *NPP* denotes net primary production, R_a is autotrophic respiration, *NEP* is net ecosystem product, and R_h is heterotrophic respiration. *NEE* is the land-atmosphere carbon flux.

Glossary

AVHRR	Advanced Very High Resolution Radiometer
C4MIP	Coupled Carbon Cycle Climate Model Inter-comparison Project
CASA	Carnegie-Ames-Stanford Approach
CCMLP	Carbon Cycle Model Linkage Project
CMDL	Climate Monitoring & Diagnostics Laboratory
CRU	Climate Research Unit
CO_2	Carbon Dioxide
DGVM	Dynamics Global Vegetation Model
ENSO	El Niño-Southern Oscillation
ESM	Earth System Model
gCO_2	CO_2 growth rate, time derivative of the CO_2 concentration of Mauna Loa Observatory in this thesis
EVI	Enhanced Vegetation Index
GIMMS	Global Inventory Monitoring and Modeling Studies
GPP	Gross Primary Production
GRACE	Gravity Recovery and Climate Experiment
FLUXNET	A global network of micro-meteorological tower sites with CO_2 flux
F_{ta}	Land-atmosphere carbon flux, same as NEE
GISS	Goddard Institute for Space Studies
IBIS	Integrated Biosphere Simulator

IGBP	International Geosphere-Biosphere Programme
IPCC	Intergovernmental Panel on Climate Change
IPSL	Institut Pierre Simon Laplace, France
LAI	Leaf Area Index
MEI	Multivariate ENSO Index
MLO	Mauna Loa Observatory
MODIS	Moderate Resolution Imaging Spectroradiometer
NASA	National Aeronautics and Space Administration
NDVI	Normalized Difference Vegetation Index
NEE	Land-atmosphere carbon flux; -NEP
NEP	Net Ecosystem Production
NHL	Northern High Latitudes poleward of 60°N in this thesis
NPP	Net Primary Production
NOAA	National Oceanic and Atmospheric Administration
OAGCMs	Coupled atmosphere-ocean general circulation models
PDO	Pacific Decadal Oscillation
PER	Precipitation-Evaporation-and-Runoff
PFT	Plant Functional Types
PgC	petagrams of carbon, 1 PgC = 10^{15} gram carbon
ppm	parts per million by volume
Q_{10}	Function of the temperature dependence of soil respiration, this factor represents the difference in respiration rates over a 10˚C interval
QTCM	Quasi-equilibrium Tropical Circulation Model

R_a	Autotrophic Respiration
R_e	Total Ecosystem Respiration
R_h	Heterotrophic Respiration
SLand	Simple Land surface Model
SOI	Southern Oscillation Index
SST	Sea Surface Temperature
Swet	Soil wetness
TEMs	Terrestrial Ecosystem Model
UMD	University of Maryland
VEGAS	VEgetation-Global-Atmosphere-Soil
WCRP	World Climate Research Programme

Bibliography

Alexeev, V.A., P. L. Langen, and J. R. Bates, 2005: Polar amplification of surface warming on an aquaplanet in "ghost forcing" experiments without sea ice feedbacks. *Climate Dynamics*, **24**, 655–666.

Arctic climate impact assessment. 2005: Lead authors, Jim Berner and others. Carolyn Symon, Lelani Arris, and Bill Heal, editors. pp. 101-144. *Cambridge University Press.*

Angert, A., S. Biraud, C. Bonfils, W. Buermann, and I. Fung, 2004: CO_2 seasonality indicates origins of post-Pinatubo sink. *Geophys. Res. Lett.,* **31**, L11103, doi:10.1029/2004GL019760.

Angert, A., S. Biraud, C. Bonfils, C. C. Henning, W. Buermann, J. Pinzon, C. J. Tucker, and I. Fung, 2005: Drier summers cancel out the CO_2 uptake enhancement induced by warmer springs. *Proc. Natl. Acad. Sci. U.S.A.*, **102(31)**, 10,823–10,827.

Bacastow, B. R., 1976: Modulation of atmospheric carbon dioxide by the Southern Oscillation. *Nature*, **261**, 116–118.

Bala, G., K.Caldeira, A. Mirin, M. Wickett, C. Delire, and T. J. Phillips, 2006: Biogeophysical effects of CO_2-fertilization on global climate. *Tellus B*, **58**, 620–27.

Baker, D. F., R. Law, K. Gurney, P. Rayner, P. Peylin, A. Denning, P. Bousquet, L. Bruhwiler, Y-H. Chen, P. Ciais, I. Fung, M. Heimann, J. John, T. Maki, S. Maksyutov, K. Masarie, M. Prather, B. Pak, S. Taguchi, and Z. Zhu, 2006: Transcom 3 inversion intercomparison: Impact of transport model errors on the interannual variability of regional CO_2 fluxes, 1988-2003. *Global Biogeochem. Cycles*, **20**, GB1002, doi:10.1029/2004GB002439.

Berthelot, M., P. Friedlingstein, P. Ciais, P. Monfray, J. L. Dufresne, H. Le Treut, and L. Fairhead, 2002: Global response of the terrestrial biosphere to CO_2 and climate change using a coupled climate-carbon cycle model. *Global Biogeochem. Cycles*, **16**, 1084, doi:10.1029/2001GB001827.

Betts, R., P. Cox, S. Lee, and F. Woodward, 1997: Contrasting physiological and structural vegetation feedbacks in climate change simulations. *Nature*, **387**, 796–799.

Betts, R. A, 2004: Global vegetation and climate: self-beneficial effects, climate forcings and climate feedbacks. *Journal de Physique,* **IV 121**, 37–60.

Bond-Lamberty, B., C. K. Wang, and S. T. Gower, 2004: Contribution of root respiration to soil surface CO_2 flux in a boreal black spruce chronosequence. *Tree Physiol.*, **24(12)**, 1387–1395.

Bond-Lamberty, B. S. D. Peckham, D. E. Ahl S. T. Gower, 2007: Fire as the dominant driver of central Canadian boreal forest carbon balance. *Nature*, **450**, 89-92.

Bousquet, P., P. Peylin, P. Ciais, C. Le, Quere, P. Friedlingstein, and P. Tans, 2000: Regional changes in carbon dioxide fluxes of land and oceans since 1980. *Science*, **290**, 1342–1346.

Braswell, B., D. Schimel, E. Linder, and B. Moore, 1997: The response of global terrestrial ecosystems to interannual temperature variability. *Science*, **278**, 870–872.

Bronson, D.R., S. Gower, M. Tanner, S. Linder, and Van Herk, 2008: Response of soil surface CO_2 flux in a boreal forest to ecosystem warming. *Global Change Biol.*, **14**, 856-867.

Budyko, M. I., 1974: Climate and life, *Academic*, New York.

Buermann, W., B. Anderson, and C. Tucker, R. Dickinson, W. Lucht, C. Potter, and R. Myneni, 2003: Interannual covariability in northern hemisphere air temperatures and greenness associated with El Niño-Southern Oscillation and the Arctic Oscillation. *J. Geophys. Res.*, **108(D13)**, 4396, doi:10.1029/2002JD 002630.

Cao, M., and F. Woodward, 1998: Dynamic responses of terrestrial ecosystem carbon cycling to global climate change. *Nature*, **393**, 249–252.

Chapin, F. S., and E. Matthews, 1993: Boreal carbon pools: approaches and constraints in global extrapolations. In: Vinson, T. S. and Kolchugina, T. P.

(Eds) Carbon Cycling in Boreal Forest and Sub-Arctic Ecosystems, pp. 9-20. Proceedings International Workshop, EPA 600/R-93/084.

Cook, B., N. Zeng, and J-H. Yoon, 2008: Future drying of the southern Amazon and central Brazil. *Submitted to Proc. Natl. Acad. Sci.*

Cox, P. M., R. A. Betts, C. D. Jones, S. A. Spall, and I. J. Totterdell, 2000: Acceleration of global warming due to carbon-cycle feedbacks in a coupled climate model. *Nature*, **408**, 184–187.

Cox, P. M., R. A. Betts, M. Collins, P. P. Harris, C. Huntingford, and C. D. Jones, 2004: Amazonian forest diaback under climate-carbon projections for the 21st century. *Theor. Appl. Climatol.,* **78**, 137–156.

Cramer, W., D. W. Kicklighter, A. Bondeau, B. Moore, C. Churkina, B. Nemry, A. Ruimy, and A. L. Schloss, 1999. Comparing global models of terrestrial net primary productivity (NPP): overview and key results. *Global Change Biol.* **5**, 1–15, Suppl. 1.

Cramer, W., A. Bondeau, F. Woodward, I. Prentice, R. Betts, V. Brovkin, P. Cox, V. Fisher, J. Foley, A. Friend, C. Kucharik, M. Lomas, N. Ramankutty, S. Sitch, B Smith, A. White, and C. Young-Molling, 2001: Global response of terrestrial ecosystem structure and function to CO_2 and climate change: results from six dynamic global vegetation models. *Global Change Biol.* **7(4)**, 357–373.

Dargaville, R., M. Heimann, A. McGuire, I. Prentice, D. Kicklighter, F. Joos, J. Clein, G. Esser, J. Foley, J. Kaplan, R. Meier, J. Melillo, B. Moore, N. Ramankuty, T. Reichenau, A. Schloss, S. Sitch, H. Tian, L. Williams, and U. Wittenberg, 2002: Evaluation of terrestrial carbon cycle models with atmospheric CO_2 measurements: Results from transient simulations considering increasing CO_2, climate, and land-use effects. *Global Biogeochem. Cycles*, **16(4)**, 1092, doi:10.1029/2001GB001426.

Davidson, E. A., I. A. Janssens, and Y. Luo, 2006: On the variability of respiration in terrestrial ecosystems: Moving beyond Q_{10}. *Global Change Biol.*, **12**, 154–164.

DeFries, R. S., R. A. Houghton, M. C. Hansen, C. B. Field, D. Skole, and J. Townshend, 2002: Carbon emissions from tropical deforestation and regrowth

based on satellite observations for the 1980s and 1990s. *Proc. Natl. Acad. Sci.*, **99**(22), 14,256–14,261.

Dufresne, J., P. Friedlingstein, M. Berthelot, L. Bopp, P. Ciais, L. Fairhead, H. Le, Treut, and P. Monfray, 2002: On the magnitude of positive feedback between future climate change and the carbon cycle. *Geophys. Res. Lett.,* **29(10)**, 1405, doi:10.1029/2001GL013777.

Eliasson, P. E., R. E. McMurtrie, D. A. Pepper, M. Stömgren, S. Linder, and G. I. Ågren, 2005: The response of heterotrophic CO_2 flux to soil warming. *Global Change Biol.,* **11**, 167–181.

Feely, R., J. Boutin, C. Cosca, Y. Dandonneau, J. Etcheto, H. Inoue, M. Ishii, C. Le Quere, D. Mackey, M. McPhaden, N. Metzl, A. Poisson, and R. Wanninkhof, 2002: Seasonal and interannual variability of CO_2 in the equatorial pacific. *Deep Sea Res. Part II*, **49**, 2443–2469.

Field, C. B., 2001: Plant physiology of the "missing" carbon sink. *Plant Physiol.,* **125**, 25– 28.

Friedlingstein, P., L. Bopp, P. Ciais, J. Dufresne, L. Fairhead, H. LeTreut, P. Monfray, and J. Orr, 2001: Positive feedback between future climate change and the carbon cycle. *Geophys. Res. Lett.,* **28 (8)**, 1543–1546.

Friedlingstein, P., J. Dufresne, P. Cox, and P. Rayner, 2003: How positive is the feedback between climate change and the carbon cycle? *Tellus B*, **55**, 692–700.

Friedlingstein, P., P. Cox, R. Betts, L. Bopp, W. von Bloh, V. Brovkin, S. Doney, M. Eby, I. Fung, B. Govindasamy, J. John, C. Jones, F. Joos, T. Kato, M. Kawamiya, W. Knorr, K. Lindsay, H. D. Matthews, T. Raddatz, P. Rayner, C. Reick, E. Roeckner, K.-G. Schnitzler, R. Schnur, K. Strassmann, S. Thompson, A. J. Weaver, C. Yoshikawa, and N. Zeng, 2006: Climate-carbon cycle feedback analysis: Results from the C4MIP model intercomparison, *J. Clim.,* **19(14)**, 3337–3353.

Fung, I., 2000: *IGBP NEWS*, **41**.

Fung, I., S. Doney, K. Lindsay, and J. John, 2005: Evolution of carbon sinks in a changing climate. *Proc. Natl. Acad. Sci.* **102(32)**, 11,201–11,206.

Goulden, M. L., S. C. Wofsy, J. W. Harden, S. E. Trumbore, P. M. Crill, S. T. Gower, T. Fries, B. C. Daube, S.-M. Fan, D. J. Sutton, A. Bazzaz, and J. W. Munger, 1998: Sensitivity of boreal forest carbon balance to soil thaw. *Science*, **279**, 214–221.

Gu, L. H., D. D. Baldocchi, S. C. Wofsy, J. W. Munger, J. J. Michalsky, S. P. Urbanski, and T. A. Boden, 2003: Response of a deciduous forest to the Mount Pinatubo eruption: Enhanced photosynthesis. *Science*, **299**, 2035–2038.

Gurney, K., R. Law, A. Denning, P. Rayner, D. Baker, P. Bousquet, L. Bruhwiler, Y. Chen, P. Ciais, S. Fan, I. Fung, M. Gloor, M. Heimann, K. Higuchi, J. John, T. Maki, S. Maksyutov, K. Masarie, P. Peylin, M. Prather, B. Pak, J. Randerson, J. Sarmiento, S. Taguchi, T. Takahashi, and C. Yuen, 2002: Towards robust regional estimates of CO_2 sources and sinks using atmospheric transport models. *Nature*, **415**, 626–630.

Hansen, J., A. Lacis, D. Rind, G. Russell, P. Stone, I. Fung, R. Ruedy, and J. Lerner, 1983: Climate sensitivity: Analysis of feedback mechanisms in climate processes and climate sensitivity, in Climate Processes and Climate Sensitivity. *Geophys. Monogr. Ser.*, vol. **29**, pp. 130– 163, AGU, Washington, D. C.

Hansen, J., E. R. Ruedy, J. Glascoe, and M. Sato, 1999: GISS analysis of surface temperature change. *J. Geophys. Res.,* **104**, 30997–31022.

Hashimoto, H., R. Nemani, M. White, W. Jolly, S. Piper, C. Keeling, R. Myneni, and S. Running, 2004: El Niño-Southern Oscillation-induced variability in terrestrial carbon cycling. *J. Geophys. Res.*, **109**, D23110, doi:10.1029/2004JD04959.

Heimann, M., and M. Reichstein, 2008: Terrestrial ecosystem carbon dynamics and climate feedbacks. *Nature*, **451**, 289-292.

Heimann, M., G. Esser, and A. Haxeltine, 1998: Evaluation of terrestrial carbon cycle models through simulations of the seasonal cycle of atmospheric CO_2: First results of a model intercomparison study. *Global Biogeochem. Cycles*, **12(1)**, 1–24.

Hoerling, M., and A. Kumar, 2003: The perfect ocean for drought. *Science*, **299**, 691–694.

Holland, M. M., and C. M. Bitz, 2003: Polar amplification of climate change in coupled models. *Climate Dynamics*, **21**, 221–232.

Houghton, R. A., 1999: The annual net flux of carbon to the atmosphere from changes in land use 1850–1990. *Tellus*, **51B**, 298–313.

Houghton, R. A., J. L. Hackler, and K. T. Lawrence, 1999: The US carbon budget: Contributions from land-use change. *Science*, **285**, 574–578.

Houghton, R. A., 2000: Interannual variability in the global carbon cycle. *J. Geophys. Res.,* **105**, 20,121–20,130.

Houghton, R. A., 2003a: Revised estimates of the annual net flux of carbon to the atmosphere from changes in land use and land management 1850–2000, *Tellus*, *Ser. B*, **55**, 378–390.

Houghton, R. A., 2003b: Why are estimates of the terrestrial carbon balance so different?, *Global Change Biol.,* **9**, 500–509.

House, J. I., I. C. Prentice, N. Ramankutty, R. A. Houghton, and M. Heimann, 2003: Reconciling apparent inconsistencies in estimates of terrestrial CO_2 sources and sinks. Tellus, Ser. B, **55(2)**, 345–363.

Huete, A., K. Didan, Y. Shimabukuro, P. Ratana, S. Saleska, L. Hutyra, W. Yang, R. Nemani, and R. Myneni, 2006: Amazon rain forests green-up with sunlight in dry season. *Geophys. Res. Lett.,* **33**, L06405, doi:10.1029/2005GL025583

Ichii, K., H. Hashimoto, R. Nemani, and M. White, 2005: Modeling the interannual variability and trends in gross and net primary productivity of tropical forests from 1982 to 1999. *Global Planet. Change,* **48**, 274–286.

IPCC (2007) Climate change 2007: the physical science basis. Contribution of Working Group I. In: Fourth Assessment Report of the Intergovernmental Panel on Climate Change (eds Solomon S, Qin D, Manning M, Chen Z, Marquis M, Averyt KB, Tignor M, Miller HL), Cambridge University Press, Cambridge, 996pp.

Jones, C. D. and P. M. Cox, 2001: Modeling the volcanic signal in the atmospheric CO_2 record. *Global Biogeochem. Cycles*, **15(2)**, 453–465.

Jones, C., M. Collins, P. Cox, and S. Spall, 2001: The carbon cycle response to ENSO: A coupled climate-carbon cycle model study. *J. Climate*, **14**, 4113–4129.

Jones, C. D., P. Cox, and C. Huntingford, 2003a: Uncertainty in climate carbon-cycle projections associated with the sensitivity of soil respiration to temperature, *Tellus, Ser. B*, **55(2)**, 642–648.

Jones, C. D., P. M. Cox, R. L. H. Essery, D. L. Roberts, and M. J. Woodage, 2003b: Strong carbon cycle feedbacks in a climate model with interactive CO_2 and sulphate aerosols. *Geophys. Res. Lett.,* **30(9)**, 1479, doi:10.1029/2003GL016867.

Jones, C., and P. Cox, 2005: On the significance of atmospheric CO_2 growth rate anomalies in 2002–2003. *Geophys. Res. Lett.,* **32**, L14816, doi:10.1029/2005GL023027.

Joos, F., I. C. Prentice, S. Sitch, R. Meyer, G. Hooss, G. Plattner, S. Gerber, and K. Hasselmann, 2001: Global warming feedbacks on terrestrial carbon uptake under the Intergovernmental Panel on Climate Change (IPCC) emission scenarios. *Global Biogeochem. Cycles*, **15**, 891–908.

Kaplan, J. O., and M. New, 2006: Arctic climate change with a 2°C global warming: Timing, climate patterns and vegetation change. *Clim. Change*, **79**, 213–241, doi: 10.1007/s10584-006-9113-7.

Keeling, D. C., and R. Revelle, 1985: Effects of ENSO on the atmospheric content of CO_2. *Meteroritics*, **20**, 437–450.

Keeling, C., J. Chin, and T. Whorf, 1996: Increased activity of northern vegetation inferred from atmospheric CO_2 measurements. *Nature*, **384**, 146–149.

Kindermann, J., G. Wurth, G. Kohlmaier, and B. FW, 1996: Interannual variation of carbon exchange fluxes in terrestrial ecosystems. *Global Biogeochem. Cycles*, **10**, 737–755.

Knorr, W., 2000: Annual and interannual CO_2 exchanges of the terrestrial biosphere: process-based simulations and uncertainties. *Global Ecol. Biogeogr.,* **9(3)**, 225–252.

Knyazikhin, Y., J. V. Martonchik, D.J. Diner, R. B. Myneni, M. Verstraete, B. Pinty, and N. Gobron, 1998: Estimation of vegetation canopy leaf area index and fraction of absorbed photosynthetically activeradiation from atmosphere-corrected MISR data. *J. Geophys. Res.,* **103**, 32239–32256.

Langenfelds, R. L., R. J. Francey, B. C. Pak, L. P. Steele, J. Lloyd, C. M. Trudinger, and C. E. Allison, 2002: Interannual growth rate variations of atmospheric CO_2 and its δ13C, H2, CH4, and CO between 1992 and 1999 linked to biomass burning. *Global Biogeochem. Cycles*, **16(3)**, 1048, doi:10.1029/2001GB001466.

Lawrence, D. M., and A. G. Slater, 2005: A projection of severe near surface permafrost degradation during the 21st century. *Geophys. Res. Lett.*, **32**, L24401, doi:10.1029/2005GL025080.

Le Quere, C., O. Aumont, L. Bopp, P. Bousquet, P. Ciais, R. Francey, M. Heimann, C. Keeling, R. Keeling, H. Kheshgi, P. Peylin, S. Piper, I. Prentice, and P. Rayner, 2003: Two decades of ocean CO_2 sink and variability. *Tellus B*, **55**, 649–656.

Levitus, S., J. I. Antonov, T. P. Boyer, and C. Stephens, 2000: Warming of the world ocean. *Science*, **287**, 2225–2229.

Linderholm, H.W., 2006: Growing season changes in the last century. *Agricultural and Forest Meteorology*, **137**, 1–14.

Liu, J., J. A. Curry, Y. Dai, and R. Horton, 2007: Causes of the northern high-latitude land surface winter climate change. *Geophys. Res. Lett.*, **34**, L14702, doi:10.1029/2007GL030196.

Lotsch, A., M. A. Friedl, B. T. Anderson, and C. J. Tucker, 2005: Response of terrestrial ecosystems to recent Northern Hemispheric drought. *Geophys. Res. Lett.,* **32**, L06705, doi:10.1029/2004GL022043.

Lucht, W., I. Prentice, R. Myneni, S. Sitch, P. Friedlingstein, W. Cramer, P. Bousquet, W. Buermann, and B. Smith, 2002: Climatic control of the high-latitude vegetation greening trend and pinatubo effect. *Science*, **296**, 1687–1689.

Lucht, W., S. Schaphoff, T. Erbrecht, U. Heyder, and W. Cramer, 2006: Terrestrial vegetation redistribution and carbon balance under climate change. *Carbon Balance Manage.*, **1(6)**, doi:10.1186/1750-0680-1-6.

Marland, G., T. A. Boden, and R. J. Andres, 2005: Global, regional, and national CO_2 emissions. Trends: A compendium of data on global change, Carbon Dioxide Information Analysis Center, Oak Ridge National Laboratory, U.S. Department of Energy, Oak Ridge, TN.

Markgraf, V., and H. F. Diaz, 2000: The past ENSO record: A synthesis. In El Niño and the Southern Oscillation: Multiscale Variability and Global and Regional Impacts, Diaz, H. F., and Markgraf, V. (Eds.), Cambridge University Press, 465-488.

Matthews, H. D., M. Eby, A. J. Weaver, and B. J. Hawkins, 2005: Primary productivity control of simulated carbon cycle-climate feedbacks. *Geophys. Res. Lett.,* **32**, L14708, doi:10.1029/2005GL022941.

McGuire, A. D., and J. E. Hobbie, 1997: Global climate change and the equilibrium responses of carbon storage in arctic and subarctic regions. pp. 47-48. IN: Arctic System Science Modeling Workshop Report. The Arctic Research Consortium of the United States. Fairbanks, Alaska.

McGuire, A. D., J. S. Clein, J. Melillo, D. Kicklighter, R. Meier, C. Vorosmarty, and M. Serreze, 2000: Modeling carbon responses of tundra ecosystems to historical and projected climate: sensitivity of pan-Arctic carbon storage to temporal and spatial variation in climate. *Global Change Biol.,* **6**, 141– 159.

McGuire, A., S. Sitch, J. Clein, R. Dargaville, G. Esser, J. Foley, M. Heimann. F. Joos, J. Kaplan, D. Kicklighter, R. Meier, J. Melillo, B. Moore, I. Prentice, N. Ramankutty, T. Reichenau, A. Schloss, H. Tian, L. Williams, and U. Wittenberg, 2001: Carbon balance of the terrestrial biosphere in the twentieth century: Analyses of CO_2, climate and land use effects with four process-based ecosystem models. *Global Biogeochem. Cycles*, **15**, 183–206.

McGuire, A.D., F. Chapin, J. Walsh, and C. Wirth, 2006: Integrated regional changes in arctic climate feedbacks: implications for the global climate system. *Annual Review of Environment and Resources*, **31**, 61–91.

Melillo, J. M., P. A. Steudler, J. D. Aber, K. Newkirk, H. Lux, F. P. Bowles, C. Catricala, A. Magill, T. Ahrens, and S. Morrisseau1, 2002: Soil warming and carbon-cycle feedbacks to the climate system. *Science*, **298**, 2173–2176.

Melillo J. M., D. W. Kicklighter, A. D. McGuire, W. T. Peterjohn, K. M. Newkirk, 1995: Global change and its effects on soil organic carbon stocks. In: Role of Nonliving Organic Matter in the Earth's Carbon Cycle (eds Zepp RG, Sonntag Ch), pp.175-189. John Wiley & Sons Ltd.

Mitchell, T. D., and P. D. Jones, 2005: An improved method of constructing a database of monthly climate observations and associated high-resolution grids. *Int. J. Climatol.*, **25**, 693–712.

Montaigne, F., 2002: The Great Northern Forest: Boreal. *National Geographic*, **201**, 42–65.

Myneni, R., C. Keeling, C. Tucker, G. Asrar, and R. Nemani, 1997: Increased plant growth in the northern high latitudes from 1981 to 1991. *Nature*, **386**, 698–702.

Myneni, R. B., C. J. Tucker, G. Asrar, and C. D. Keeling, 1998: Interannual variations in satellite-sensed vegetation index data from 1981 to 1991. *J. Geophys. Res.*, **103(D6)**, 6145–6160.

Neelin, J., and N. Zeng, 2000: The first quasi-equilibrium tropical circulation model formulation. *J. Atmos. Sci.,* **57**, 1741–1766.

Nemani, R., C. D. Keeling, H. Hashimoto, W. M. Jolly, S. C. Piper, C. J. Tucker, R. B. Myneni, and S. W. Running, 2003: Climate-driven increases in global terrestrial net primary production from 1982 to 1999. *Science*, **300**, 1560–1563.

Nemani, R. R., and S. W. Running, 1989: Testing a theoretical climate-soil-leaf area hydrologic equilibrium of forests using satellite data and ecosystem simulation. *Agric. For. Meteorol.,* **44**, 245-260.

Nemry, B., L. Francois, J. Gerard, A. Bondeau, and M. Heiman, 1999: Comparing global models of terrestrial net primary productivity (NPP): analysis of the seasonal atmospheric CO_2 signal. *Global Change Biol.,* **5**, 65–76 Suppl. 1.

New, M. G., M. Hulme, and P. D. Jones, 1999: Representing 20^{th} century space-time climate variability. I. Development of a 1961–1999 mean monthly terrestrial climatology. *J. Climate*, **12**, 829–865.

Oliveira, R., T. Dawson, S. Burgess, and D. Nepstad, 2005: Hydraulic redistribution in three Amazonian trees. *Oecologia*, **145**, 354–363.

Overland, J. E., M. C. Spillane and N. N. Soreide, 2004: Integrated analysis of physical and biological Pan-Arctic change. *Clim. Change*, **63**, 291–322.

Page, S. E., F. Siegert, J. O. Rieley, H. Boehm, A. Jaya, and S. Limin, 2002: The amount of carbon released from peat and forest fires in Indonesia during 1997. *Nature*, **420**, 61–65.

Piao, S. L., P. Ciais, P. Friedlingstein, P. Peylin, M. Reichstein, S. Luyssaert, H. Margolis, J. Y. Fang, A. Barr, A. P. Chen AP, A. Grelle, D. Y. Hollinger, T. Laurila, A. Lindroth, A. D. Richardson, T. Vesala, 2008: Net carbon dioxide losses of northern ecosystems in response to autumn warming. *Nature* **451**, 49–53.

Piao, S. L., P. Friedlingstein, O. Ciais, L. M. Zhou, and A. P. Chen, 2006: The effect of climate and CO_2 changes on the greening of the Northern Hemisphere over the past two decades. *Geophys. Res. Lett.*, **33**, L23402, doi:10.1029/2006GL 028205.

Piao, S. L., P. Friedlingstein, P. Ciais, N. Viovy, and J. Demarty, 2007: Growing season extension and its impact on terrestrial carbon cycle in the Northern Hemisphere over the past 2 decades. *Global Biogeochem. Cycles*, VOL. 21, GB3018, doi:10.1029/2006GB002888.

Plattner, G., F. Joos, and T. Stocker, 2002: Revision of the global carbon budget due to changing air-sea oxygen fluxes. *Global Biogeochem. Cycles*, **16(4)**, 1096, doi:10.1029/2001GB001746.

Post, W. M., W. R. Emanuel, P. J. Zinke, and A. G. Strangenberger, 1982: Soil carbon pools and world life zones. *Nature*, **298**, 156–159.

Potter, C., S. Klooster, M. Steinbach, P. Tan, V. Kumar, S. Shekhar, R. Nemani, and R. Myneni, 2003: Global teleconnections of climate to terrestrial carbon flux. *J. Geophys. Res.,* **108(D17)**, 4556, doi:10.1029/2002JD002979

Prentice, I. C. et al., 2001: The carbon cycle and atmospheric CO_2, in The Intergovernmental Panel on Climate Change (IPCC) Third Assessment Report, edited by J. T. Houghton and D. Yihui, chap. 3, pp. 185–237, Cambridge Univ. Press, New York.

Qian, H., R. Joseph, and N. Zeng, 2008: Carbon uptake by the Northern High Latitude Terrestrial Biosphere under Climate Change in the 21st Century in C4MIP models. *Submitted to Global change boil.*

Qian, H., R. Joseph, and N. Zeng, 2008: Response of the Terrestrial Carbon Cycle to the El Niño-Southern Oscillation, *Tellus B*, doi: 10.1111/j.1600-0889.2008.00360.x.

Randerson, J., C. Field, I. Fung, and P. Tans, 1999: Increases in early season ecosystem uptake explain recent changes in the seasonal cycle of atmospheric CO_2 at high northern latitudes. *Geophys. Res. Lett.,* **26**, 2765–2768.

Rasmusson, E. M. and T. H. Carpenter, 1982: Variations in tropical sea surface temperature and surface wind fields associated with the Southern Oscillation / El. Niño. *Mon. Wea. Rev,* **110**, 354-384.

Raupach, M., G. Marland, P. Ciais, C. L. Quéré, J. G. Canadell, G. Klepper, and C. Field, 2007: Global and regional drivers of accelerating CO_2 emissions. *Proc. Natl. Acad. Sci. U.S.A.,* **104**, 10,288–10,293.

Rayner, P., R. Law, and R. Dargaville, 1999: The relationship between tropical CO_2 fluxes and the El Niño-Southern Oscillation. *Geophys. Res. Lett.,* **26**, 493–496.

Reichstein, M., D. Papale, R. Valentini, M. Aubinet, C. Bernhofer, A. Knohl, T. Laurila, A. Lindroth, E. Moors, K. Pilegaard, and G. Seufert, 2007: Determinants of terrestrial ecosystem carbon balance inferred from European eddy covariance flux sites. *Geophys. Res. Lett.,* **34**, L01402; doi:10.1029/2006GL027880.

Rödenbeck, C., S. Houweling, M. Gloor, and M. Heimann, 2003: CO_2 flux history 1982-2001 inferred from atmospheric data using a global inversion of atmospheric transport. *Atmos. Chem. Phys.,* **3**, 1919–1964.

Ropelewski, C. F., and M. S. Halpert, 1987: Global and regional scale precipitation patterns associated with the El-Nino Southern Oscillation. *Mon. Weather Rev.,* **115**, 1606–1626.

Russell, J. L., and J. M. Wallace, 2004: Annual carbon dioxide drawdown and the Northern Annular Mode. *Global Biogeochem. Cycles,* **18**, GB1012, doi:10.1029/2003GB002044.

Saleska, S., S. Miller, D. Matross, M. Goulden, S. Wofsy, H. da Rocha, P. de Camargo, P. Crill, B. Daube, H. de Freitas, L. Hutyra, M. Keller, V. Kirchhoff, M. Menton, J. Munger, E. Pyle, A. Rice, and H. Silva, 2003: Carbon in Amazon forests: Unexpected seasonal fluxes and disturbance-induced losses. *Science*, **302**, 1554–1557.

Saleska, S., K. Didan, A. Huete, H. da Rocha, 2007: Amazon Forests green-up during 2005 drought. *Science*, doi: 10.1126/science.1146663.

Schaphoff, S., W. Lucht, D. Gerten, S. Sitch, W. Cramer, and I. C. Prentice, 2006: Terrestrial biosphere carbon storage under alternative climate projections. *Clim. Change*, **74**, doi:10.1007/s10584-005-9002-5.

Schimel, D. S., 1995: Terrestrial ecosystems and the carbon cycle. G*lobal Change Biol.*, **1**, 77–91.

Schlesinger, W., 1991: Biogeochemistry: An Analysis of Global Change. *Academic Press*, San Diego.

Schwartz, M. D., R. Ahas, and A. Aasa, 2006: Onset of spring starting earlier across the Northern Hemisphere. *Global Change Biol.,* **12**, 343–351.

Sellers, P. J., 1991: Modeling and observing land–surface–atmosphere interactions on large scales. In: Wood, E.F. (Ed.), Land–Surface–Atmosphere Interactions for Climate Modeling: Observations, Models and Analysis. Kluwer Academic Publishers, Dordrecht.

Serreze, M. C., J. E. Walsh, F. S. Chapin III, T. Osterkamp, M. Dyurgerov, V. Romanovsky, W. C. Oechel, J. Morison, T. Zhang and R. G. Barry, 2000: Observational evidence of recent change in the northern high-latitude environment. *Clim. Change*, **46**, 159-207.

Siegenthaler, U., T. F. Stocker, E. Monnin, D. Luthi, J. Schwander, B. Stauffer, D, Raynaud, J.M. Barnola, H. Fischer, V. Masson-Delmotte, and J. Jouzel, 2005: Stable carbon cycle-climate relationship during the late Pleistocene. *Science*, **310**, 1313–1317.

Sitch, S., A. D. McGuire, J. Kimball, N. Gedney, J. Gamon, R. Engstrom, A. Wolf, Q. Zhuang, J. Clein, and K. McDonald, 2007: Assessing the carbon balance of

circumpolar arctic tundra using remote sensing and process modeling. *Ecological Application,* **17**, 213–234.

Spahni, R., J. Chappellaz, T. F. Stocker, L. Loulergue, G. Hausammann, K. Kawamura, J. Flückiger, J. Schwander, D. Raynaud, V. Masson-Delmotte, and J. Jouzel, 2005: Atmospheric methane and nitrous oxide of the late Pleistocene from Antarctic ice cores. *Science*, **310**, 1317-1321.

Stott, P. A., D. A. Stone, and M. R. Allen, 2004: Human contribution to the European heatwave of 2003. *Nature*, **432**, 610– 614.

Thompson, M. V., J. T. Randerson, C. M. Malmström, and C. B. Field, 1996: Change in net primary production and heterotrophic respiration: How much is necessary to sustain the terrestrial carbon sink? *Global Biogeochem. Cycles,* **10(4)**, 711–726.

Thompson, S. L., B. Govindasamy, A. Mirin, K. Caldeira, C. Delire, J. Milovich, M. Wickett, and D. Erickson, 2004: Quantifying the effects of CO_2-fertilized vegetation on future global climate and carbon dynamics. *Geophys. Res. Lett.*, **31**, L23211, doi:10.1029/2004GL021239.

Tian, H. Q., J. M. Melillo, D. W. Kicklighter, A. D. McGuire, J. V. K. Helfrich, B. Moore, and C. J. Vorosmarty, 1998: Effect of interannual climate variability on carbon storage in Amazonian ecosystems. *Nature*, **396**, 664–667.

Trenberth, K. E., 1997: The definition of El Niño. *Bull. Am. Meteorol. Soc.,* **78**, 2771–2777.

Trenberth, K. E., Branstator, G. W., Karoly, D., Kumar, A., Lau, N. C. and C. Ropelewski, 1998: Progress during TOGA in understanding and modeling global teleconnections associated with tropical sea surface temperatures. *J. Geophys. Res.,* **103**, 14291–14324.

Tucker, C. J., D. A. Slayback, J. E. Pinzon, S. O. Los, R. B. Myneni, and M. G. Taylor, 2001: Higher northern latitude normalized difference vegetation index and growing season trends from 1982 to 1999. *Int. J. Biometeorol.*, **45**, 184–190.

Tucker, C. J., J. E. Pinzon, M. E. Brown, D. Slayback, E. W. Pak, R. V. E. Mahoney, and N. El Saleous, 2005: An extended AVHRR 8-km NDVI data set compatible

with MODIS and SPOT vegetation NDVI data. *Int. J. Remote Sens.,* **26(20)**, 4485–4498.

Van der Werf, G. R., J. T. Randerson, G. J. Collatz, L. Giglio, P. S. Kasibhatla, A. F. Arellano, S. C. Olsen, and E. S. Kasischke, 2004: Continental-scale partitioning of fire emissions during the 1997 to 2001 El Niño/La Niña period. *Science*, **303**, 73–76.

Waple, A. M., J. H. Lawrimoreb, M. S. Halpertc, G. D. Bellc, W. Higginsc, B. Lyond, M. J. Mennee, K. L. Gleasone, R. C. Schnellf, J. R. Christyg, W. Thiawh, W. J. Wrighti, M. J. Salingerj, L. Alexanderk, R. S. Stonel, and S. J. Camargom, 2002: Climate assessment for 2001. *Bull. Am.Meteorol. Soc.*, **83**, S1– S62.

Wardley, N. W., and P. J.Curran, 1984: The estimation of green leaf area index from remotely sensed airborne multiespectral scanner data. *Int. J. Remote Sens.,,* **5(4)**, 671-679.

Wetherald, R. T., and S. Manabe, 1995: The mechanisms of summer dryness induced by greenhouse warming. *J. Clim.,* **12**, 3096– 3108.

Winguth, A. M. E., M. Heimann, K. D. Kurz, E. Maier-Reimer, U. Mikolajewicz, and J. Segschneider, 1994: El Niño–Southern Oscillation related fluctuations of the marine carbon cycle. *Global Biogeochem. Cycles*, **8**, 39–64.

Wittenberg, U., M. Heimann, G. Esser, A. McGuire, and W. Sauf, 1998: On the influence of biomass burning on the seasonal CO_2 signal as observed at monitoring stations. *Global Biogeochem. Cycles*, **12(3)**, 531–544.

Wolter, K., and M. S. Timlin, 1998: Measuring the strength of ENSO events-how does 1997/98 rank? *Weather*, **53**, 315-324.

Xiao, X., Q. Zhang, S. Saleska, L. Hutyra, P. de Camargo, S. Wofsy, S. Frolking, S. Boles, M. Keller, and B. Moore, 2005: Satellite-based modeling of gross primary production in a seasonally moist tropical evergreen forest. *Remote Sens. Environ.,* **94**, 105–122

Xie, P., and P. Arkin, 1996: Analyses of global monthly precipitation using gauge observations, satellite estimates, and numerical model. *J. Climate*, **9**, 840–858.

Zeng, N., J. Neelin, K. Lau, and C. Tucker, 1999: Enhancement of interdecadal climate variability in the Sahel by vegetation interaction. *Science*, **286**, 1537–1540.

Zeng, N., J. D. Neelin, and C. Chou, 2000: A quasi-equilibrium tropical circulation model: Implementation and simulation. *J. Atmos. Sci.,* **57**, 1767– 1796.

Zeng, N., 2003: Glacial-interglacial atmospheric CO_2 change-The glacial burial hypothesis. *Adv. Atmos. Sci.,* **20**, 677–693.

Zeng, N., H. Qian, E. Munoz, and R. Iacono, 2004: How strong is carbon cycle-climate feedback under global warming?. *Geophys. Res. Lett.*, **31**, L20203, doi: 10.1029/2004GL020904.

Zeng, N., A. Mariotti, and P. Wetzel, 2005a: Terrestrial mechanisms of interannual CO_2 variability. *Global Biogeochem. Cycles*, **19**, GB1016, doi:10.1029/2004GB 002273.

Zeng, N., H. Qian, C. Rödenbeck, and M. Heimann, 2005b: Impact of 1998-2002 Midlatitude drought and warming on terrestrial ecosystem and the global carbon cycle. *Geophys. Res. Lett.,* **32**(22),L22709, doi:10.1029/2005GL024607.

Zeng, N., J-H Yoon, A. Mariotti, and S. Swenson, 2008: Long-term soil moisture variability from a new P-E water budget method. *J. Climate*, **15**, 248-265.

Zhou, L., C. J. Tucker, R. B. Myneni, R. K. Kaufmann, D. Slayback, N. V. Shabanov, and R. B. Myneni, 2001: Variations in northern vegetation activity inferred from satellite data of vegetation index during 1981 to 1999. *J. Geophys. Res.*, **106**, 20069–20083.

Zhuang, Q., V. E. Romanovsky, and A. D. McGuire, 2001: Incorporation of a permafrost model into a large-scale ecosystem model: Evaluation of temporal and spatial scaling issues in simulating soil thermal dynamics. *J. Geophys. Res.,* **106**, 33,649–33,670.